# EXPLORING SOLITON AND SIMILARITON FORMATION IN RESONANT OPTICAL MEDIA

by

Soodeh Haghgoo Poorvali

Submitted in partial fulfillment of the
requirements for the degree of
Doctor of Philosophy

at

Dalhousie University
Halifax, Nova Scotia
September 2012

DALHOUSIE UNIVERSITY

DEPARTMENT OF ELECTRICAL AND COMPUTER ENGINEERING

The undersigned hereby certify that they have read and recommend to the Faculty of Graduate Studies for acceptance a thesis entitled "EXPLORING SOLITON AND SIMILARITON FORMATION IN RESONANT OPTICAL MEDIA" by Soodeh Haghgoo Poorvali in partial fulfillment of the requirements for the degree of Doctor of Philosophy.

Dated: September 14, 2012

External Examiner: _____

Research Supervisor: _____

Examining Committee: _____

_____

Departmental Representative: _____

DALHOUSIE UNIVERSITY

DATE: September 14, 2012

AUTHOR: Soodeh Haghgoo Poorvali

TITLE: EXPLORING SOLITON AND SIMILARITON FORMATION IN RESONANT OPTICAL MEDIA

DEPARTMENT OR SCHOOL: Department of Electrical and Computer Engineering

DEGREE: Ph.D. CONVOCATION: May YEAR: 2013



Signature of Author

*Dedication*

*This thesis is dedicated to my parents, Ashraf & Ahmad, who have never failed to give me support while I am abroad, and my sister Samira. To the little baby I am going to give birth to. I also lovingly dedicate this thesis to my soul mate; my beloved husband Saeed, who supported me each step of the way, for filling my life with his endless love and encouragement.*

# Table of Contents

# List of Figures

## Abstract

Investigating the behavior of an atom in response to the applied electric field when the latter frequency is in resonance with the natural frequency of the atom is an interesting subject. Near resonance, some of the most interesting optical phenomena such as dispersion, and absorption are more pronounced. Moreover, considering resonant and near resonant interaction of light with two-level atoms, uncovers fascinating physical phenomena such as area theorem and self-induced transparency describing stable pulse propagation regimes in which the pulses maintain their identity. Existence of these optical structures in on-resonance optical media has not been investigated in detail. In this thesis, the on-resonance interaction of optical field with atoms is considered and the formation of several novel self-similar and kink waves in linear and nonlinear resonant media is discovered and theoretically explored.

First, self-similar pulse formation in homogeneous broadened linear amplifiers in a vicinity of an optical resonance is analyzed. It is demonstrated that the self-similar pulses serve as universal asymptotics of any near resonance short pulses propagating in coherent linear amplifiers. Second, ultrashort self-similar pulse propagation in coherent linear absorbers near optical resonance is investigated. Third, existence of self-similar optical waves with kink structure in resonant optical systems is discovered. Fourth, it is found that self-induced transparency quadratic solitons are realizable in the media with quadratic optical nonlinearities, doped with resonant impurities. Finally, stable spatial similaritons supported by homogeneous conservative optical media with quintic nonlinearities are explored.

To experimentally realize the presented results, physical models are presented for all systems under consideration. The stability of the proposed near resonance optical systems is demonstrated through a series of numerical case studies.

## List of Abbreviations and Symbols Used

| | |
|---|---|
| CW | Continuous wave |
| *Im* | Imaginary part |
| *Re* | Real part |
| QD | Quantum dots |
| QS | Quadratic solitons |
| FW | Fundamental wave |
| SH | Second harmonic |
| GVD | group-velocity dispersion |
| GVM | group-velocity mismatch |
| SIT | Self-induced transparency |
| SPM | Self-phase modulation |
| $e$ | Excited state |
| $g$ | Ground state |
| $\omega_0$ | Resonance frequency |
| $\omega$ | Angular optical frequency |
| $\gamma$ | Nonlinear parameter |
| $\Delta$ | Frequency detuning |
| $\rho$ | Density matrix |
| $T_\perp$ | Transverse relaxation time |
| $T_\parallel$ | Energy relaxation time |
| $\gamma_\perp$ | Transverse relaxation rate |
| $\gamma_\parallel$ | Energy relaxation rate |
| $w$ | Single-atom inversion |
| $u$ | In-phase component of the dipole moment |
| $v$ | In-quadrature component of the dipole moment |
| $\theta$ | Field area |
| $\chi'$ | Real part of electric susceptibility |
| $\chi''$ | Imaginary part of electric susceptibility |

| | |
|---|---|
| $k$ | Propagation constant |
| $n_0$ | Linear refractive index |
| $n_2$ | Cubic nonlinear refractive index coefficient |
| $n_4$ | Quintic nonlinear refractive index coefficient |
| $\alpha$ | Linear absorption coefficient |
| $I$ | Light intensity |
| $d_{eg}$ | Dipole matrix element |
| $\kappa$ | Coupling constant |
| $\varepsilon_0$ | Free space permittivity |
| $I_0$ | Modified Bessel function of zero order |
| $\sigma$ | Atomic dipole moment envelope |
| $\delta$ | Width of inhomogeneous broadening |
| c | Speed of light in vacuum |
| $\chi^{(2)}$ | Second-order nonlinear electric susceptibility |
| $\chi^{(3)}$ | Third-order nonlinear electric susceptibility |
| $\Delta k$ | Wave number mismatch |
| $\lambda$ | Wavelength |
| $C$ | Phase chirp |
| $\hbar$ | Reduced Planck constant |
| $v_g$ | Group velocity |

## Acknowledgements

I would like to express my sincere gratitude to my supervisor Dr. Sergey Ponomarenko for the continuous support of my Ph.D study and research, for his patience, motivation, and immense knowledge. His guidance helped me in all the time of research and writing of this thesis.

It is a pleasure to thank the rest of my thesis committee: Dr. Govind Agrawal, Dr. Zhizhang (David) Chen, and Dr. Kimberley Hall, for reading the thesis, and their useful comments and recommendations.

Finally, my sincere love goes to my family: my parents Ahmad and Ashraf. They gave birth to me, raised me, supported me, and loved me. Lastly, and most importantly, I wish to thank my beloved ones; my husband Saeed for providing a loving environment for me, and my unborn baby. To them I dedicate this thesis.

# Chapter 1

# Introduction

## 1.1 Preface

In writing this thesis our intention has been to concentrate on the physics of resonant light-matter interactions. This chapter presents the main theme of the thesis. The historical overview of the resonant and near-resonant interaction of light with matter is reviewed. After that, thesis motivations and objectives are introduced. Finally, thesis outline is presented.

## 1.2 Historical Preamble and Theme of the Thesis

The first comprehensive classical theory of linear interaction of light with matter was developed by Lorentz. Based on this theory, optical phenomena can be described by the interaction of elementary charges and dipoles with the electromagnetic field [1]. The classical Lorentzian theory describes most physical phenomena near resonance and requires modifications only in some circumstances. The weakpoint of this theory is that it just deals with the linear interactions when the field intensity is weak. However, for fields which are so intense as to excite atomic nonlinearities there should be departures from Lorentz theory. Some optical phenomena such as lasing, self-phase modulation, and self-induced transparency appearing in high intensity field interactions with atoms and the corresponding nonlinear regimes cannot be expressed by the predictions of the classical Lorentz theory. Therefore, the detailed theory of the interaction of field and matter required the extension to quantum optics. Although the discovery of quantum mechanics has changed the definition of light nature, it has not contradicted the previous theories.

Later in 1958, a new subfield of optics arose when Schawlow, Townes, and Prokhorov discovered that a laser could be operated at optical frequencies [2]. Since then, many intensive investigations were done on diverse subjects in both semiclassical and quantum optics. The experimental examination was carried out with the development of practical

methods for producing both high intensity and shorter pulses. In 1960, Maiman constructed the first laser called the ruby laser [3].

In the middle of the second decade of laser physics, dye laser, one of the most important advances, was developed in 1966 offering high power and narrow bandwidth anywhere in the optical spectrum [4]. After that, the need to investigate any optical resonance at very narrow spectral range arose. However, many effects, especially those involved in the propagation of intense pulses, need departure from the classical models. Fortunately, near resonance behavior can be described by the semiclassical models or mix of both classical and quantum models. For example, the quantum mechanical optical Bloch equations along with the classical Maxwell wave equations for the electric field are entirely sufficient to explore the response of near resonant atoms to an applied electric field.

On the other hand, absorption near resonance is very large implying that the atoms take more energy from the field. Using short pulses reduces the time for the atoms to interact with the field and take energy from it. In general, generation of ultrashort pulses is a key to explore the dynamic behavior of matter interacting with the electric field on ultrashort timescales. Developments in laser and need for large bandwidth pulses also require using short pulses. Nowadays, ultrashort pulses in femtosecond and even attosecond ranges have been generated. In 1974, Shank and Ippen generated subpicosecond pulses (0.5-1.0 psec) by passive mode locking of a composite medium dye laser [5]. Later in 2001, by spectral broadening from 600 to 1200 nm generating from a Kerr-lens mode-locked Ti:sapphire laser 5-fs pulses were produced. These spectra were the broadest ever generated directly from a laser oscillator [6]. In 2001, the attosecond ($1as = 10^{-18}s$) pulses were generated in order to find the attosecond response of the atomic system [7].

In this thesis, we have restricted our attention to the resonant and near resonant interaction of light with atoms. By applying the on-resonance limit, the two-level model for atoms can be adopted. In other words, light interaction involves only one transition in the atom that means the atom has only two energy levels. Based on the Lorentz theory, one should consider the motion of dipoles which are free to respond to the electromagnetic field of light waves in order to study the interaction of light with matter. Bloch and Maxwell equations faithfully describe the response of near resonant atoms to an applied electric field in a wide range of absorption and amplification regimes. With the two-level system assumption, we devote the following section to a review of general terms and definitions used in this thesis

repeatedly.

## 1.3 General Terms Definition

### 1.3.1 Two-Level Atoms

Atoms in gases and some solid-state laser media have line spectra, and the spectral lines are associated with transitions between adjacent energy eigenstates. In general, there is an infinite number of energy eigenstates in an atomic, molecular or solid-state medium. In a near resonant situation, it is sufficient to consider only two of the possible energy eigenstates. This simple model is called a two-level atom. The interaction of the two-level atom with the electric field is described by the Bloch equations.

In this thesis, for both analytical and numerical calculations, the medium will be considered as a two-level system. In Fig. 1.1 a schematic of two-level atoms is presented. Atom has only two energy levels, excited and ground states and the difference between these two levels is the resonance frequency $\omega_0$, while $\omega$ is the applied light frequency. The difference between these two frequencies is called detuning $\Delta$. In this thesis more attention is devoted to the regimes where the detuning is zero, $\Delta = 0$ (on-resonance), or where $|\Delta| << \omega_0$ (near resonance). If a population inversion between the levels $a$ and $b$ is established, such a medium can amplify light in a frequency band around the separation of the levels.

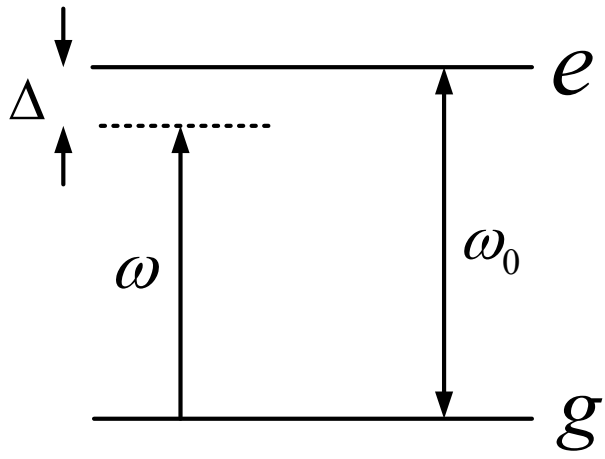


Figure 1.1: Schematic of a two-level atom system.

If the atom couples to an external heat bath, there are incoherent relaxation processes other than the spontaneous decay [8]. To study the interaction of an open atom with light,

the state of a two-level atom is represented by means of a $2 \times 2$ density matrix $\rho$

$$\rho(t) \equiv \begin{pmatrix} \rho_{gg} & \rho_{ge} \\ \rho_{eg} & \rho_{ee} \end{pmatrix} = \begin{pmatrix} c_g c_g^* & c_g c_e^* \\ c_e c_g^* & c_e c_e^* \end{pmatrix}. \tag{1.1}$$

In a two-level system, each element of the density matrix corresponds to a physical quantity. The off-diagonal elements are related to the atomic dipole moment, while the diagonal elements give the population probabilities for the atom to be in a state $e$ or $g$. To describe the decay of the levels and the damping of the atomic dipole moment, a damping constant is introduced, $\gamma_e$, with the assumption that in the two-level atoms system, the ground state is a true ground state. In the absence of an electric field, the probability amplitude for finding an atom in the excited state, $c_e$, decays exponentially as

$$c_e(t) = c_{e0} e^{-\frac{1}{2}\gamma_e t}, \tag{1.2}$$

so, $\rho_{ee}$ and $\rho_{ge}$, have decay constants $\gamma_e = \gamma_\parallel$ and $\gamma_\perp$ such that $\gamma_\perp = \frac{1}{2}\gamma_e$. $\gamma_\perp$ represents the decay constant for the dipole moment of the atom. $1/\gamma_\perp$ is related to the time of atomic phase memory or coherence. The spectral linewidth $\gamma_\perp$ is called homogeneous.

When there is an ensemble of atoms, an additional broadening is obtained. In solids the atoms may have different resonance frequencies due to inhomogeneities in the crystal environment. In gases various atomic velocities cause the same effect called Doppler broadening. The average over resonance frequencies leads to a decay of the polarization or an inhomogeneous broadening. In this thesis, the definitions $\gamma_\perp = \frac{1}{T_\perp}$, $\gamma_\parallel = \gamma_e = \frac{1}{T_\parallel}$ are considered. $T_\perp$ and $T_\parallel$ are called the transverse or phase relaxation time, and the longitudinal or energy relaxation time, respectively. Atoms in a medium do not only interact with the field, they might collide with each other especially in gases. All these processes must be taken into account when determining the energy and phase relaxation rates. Some of these processes only affect the phase, but do not cause an energy loss in the system. As a result, the processes reduce $T_\perp$ but have no effect on $T_\parallel$. In most real systems the phase relaxation time is much shorter than twice the energy relaxation time.

The inversion $w$ of the atom is defined as

$$w = |c_e|^2 - |c_g|^2, \tag{1.3}$$

where $|c_e|^2$ and $|c_g|^2$ are the probabilities for finding the atom in the excited state or ground state. The inversion always has an equilibrium value, corresponding to the system in a thermal equilibrium. The inversion goes back into equilibrium with a time constant, if it deviates from its equilibrium value. For all temperature the inversion is negative, so all the atoms rest in the ground state and the lower level is stronger populated than the upper level.

### 1.3.2 Framework for Analysis and Bloch Equations

The sequence to study the interaction between the matter and the electric field is that the electric field $\vec{E}(r,t)$ polarizes the atoms of the medium according to the Bloch equations. The atomic dipole moments add up to a macroscopic polarization $\vec{P}(r,t)$, which in turn enters Maxwell equations as a source term and drives the electric field.

In order to define the behavior of the atom when applying an electric field, consider the density matrix as [8]

$$\rho(t) = \frac{1}{2}\begin{pmatrix} 1+w & u-iv \\ u+iv & 1-w \end{pmatrix}. \tag{1.4}$$

The components $u$, $v$, and $w$ are atomic variables and are solutions to the reduced Bloch equations [8]

$$\dot{u} = -\Delta v, \tag{1.5}$$

$$\dot{v} = \Delta u + \kappa \mathscr{E} w, \tag{1.6}$$

$$\dot{w} = -\kappa \mathscr{E} v. \tag{1.7}$$

where $u$ and $v$ are the components of the atomic dipole moment envelope in-phase and in-quadrature with the field, $\Delta = \omega_0 - \omega$ is the detuning, $\kappa = \frac{2d_{eg}}{\hbar}$, $\mathscr{E}$ is the electric field amplitude, and $w$ is the single atom population difference, which is called one-atom inversion. Considering the total dynamics of the two-level system including the (possibly) incoherent pumping and incoherent relaxation processes, the complete Bloch equations are given by [8]

$$\dot{u} = -\Delta v - \frac{u}{T_\perp}, \tag{1.8}$$

$$\dot{v} = \Delta u - \frac{v}{T_\perp} + \kappa \mathscr{E} w, \tag{1.9}$$

$$\dot{w} = -\frac{w - w_{eq}}{T_\parallel} - \kappa \mathscr{E} v, \tag{1.10}$$

where $w_{eq}$ is a value of the one-atom inversion in the absence of the field (equilibrium). $w$ is related to the internal energy of the atom, while $v$ and $u$ are absorptive and dispersive components of the dipole moment, respectively. In these equations, the electric field amplitude $\mathscr{E}$ is unchirped and as a result it has a real value. If the electric field is chirped, its amplitude is complex. Therefore, the complex Rabi frequency which is the electric field amplitude $\mathscr{E}$ in frequency units is defined as $\Omega = 2d_{eg}\mathscr{E}/\hbar = \kappa\mathscr{E}$. By considering the dipole moment envelope $\sigma = u - iv$, the Bloch equations are given by

$$\dot{\sigma} = -(\gamma_\perp + i\Delta)\sigma - i\Omega w, \tag{1.11}$$

$$\dot{w} = -\gamma_\parallel (w - w_{eq}) - \tfrac{i}{2}(\Omega^* \sigma - \Omega \sigma^*). \tag{1.12}$$

The probability conservation implies that $u^2 + v^2 + w^2 = 1$ if damping can be ignored. It means the Bloch vector $(u, v, w)$ trajectories lie on a unit sphere. This sphere which is called the Bloch sphere corresponds to solutions to the Bloch equations. In Fig. 1.2 the Bloch vector evolution on the Bloch sphere for different values of detuning is shown. Bloch equations together with Maxwell's equations are equations built the Maxwell-Bloch equations, a system of equations which describes the dynamics of interaction between atoms and the electromagnetic field.

### 1.3.3 Area Theorem and Self-Induced Transparency

Area theorem expresses the fact that the change of area $\theta = \kappa \int_{-\infty}^{+\infty} \mathscr{E}(t', z)\, dt'$ depends on initial $\theta$ alone and in not affected by the shape of the field envelope $\mathscr{E}$. To interpret the area theorem consider an arbitrary input pulse with an arbitrary area $\theta(0)$ at $z = 0$. Over long propagation distances the area will have reached an integral multiple of $\pi$. The area theorem for amplifiers is sketched in Fig. 1.3 [9]. It can be seen in the figure that in amplifiers, pulses with odd multiple of $\pi$ area are stable while pulses with even multiple of

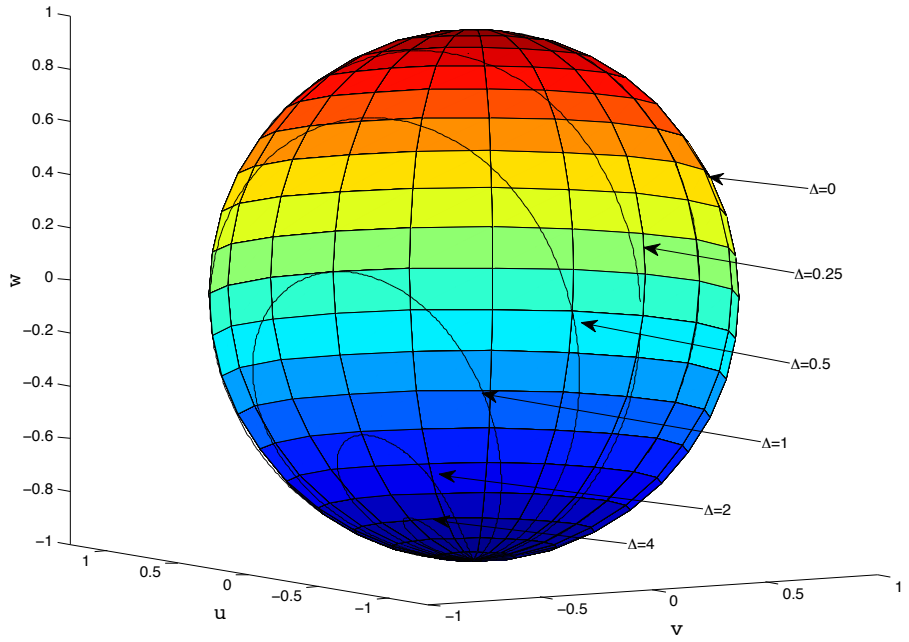


Figure 1.2: Bloch vector trajectories on the unit sphere (Bloch sphere) corresponding to the solutions to the reduced Bloch equations for different values of detuning Δ. In every case the atom is being driven by a $2\pi$ sech pulse, $2\text{sech}(t)$.

$\pi$ area are unstable.

The area theorem for a medium with atoms initially in the ground state (an absorber) is shown in Fig. 1.4 [9]. For an initial pulse area $\theta_0 < \pi$ the total area decays to zero on the basis of the area theorem. As it can be seen, for the initial area $\pi < \theta_0 < 3\pi$ the pulse evolves into a $2\pi$ pulse. Unlike amplifiers, in absorbers $2n\pi$ pulses are more stable than those that are odd multiples. McCall and Hahn observed that not only the area of the pulse with area equal to an integer multiple of $2\pi$ is stable but also the shape is stable, which means the pulse will not decay over long distances [10, 11]. This pulse behaves as if the medium is transparent, so this effect was called the self-induced transparency which is illustrated in Fig. 1.5 [8]. The self-induced transparency causes soliton formation for long propagation distances.

### 1.3.4 Lorentz Oscillator Model

The classic harmonic oscillator model is applicable in absorptive media when the optical field is near resonance and its area is small such that $\theta << \pi$. The atom in this model is assumed to act like a damped harmonic oscillator with the natural frequency $\omega_0$ and a

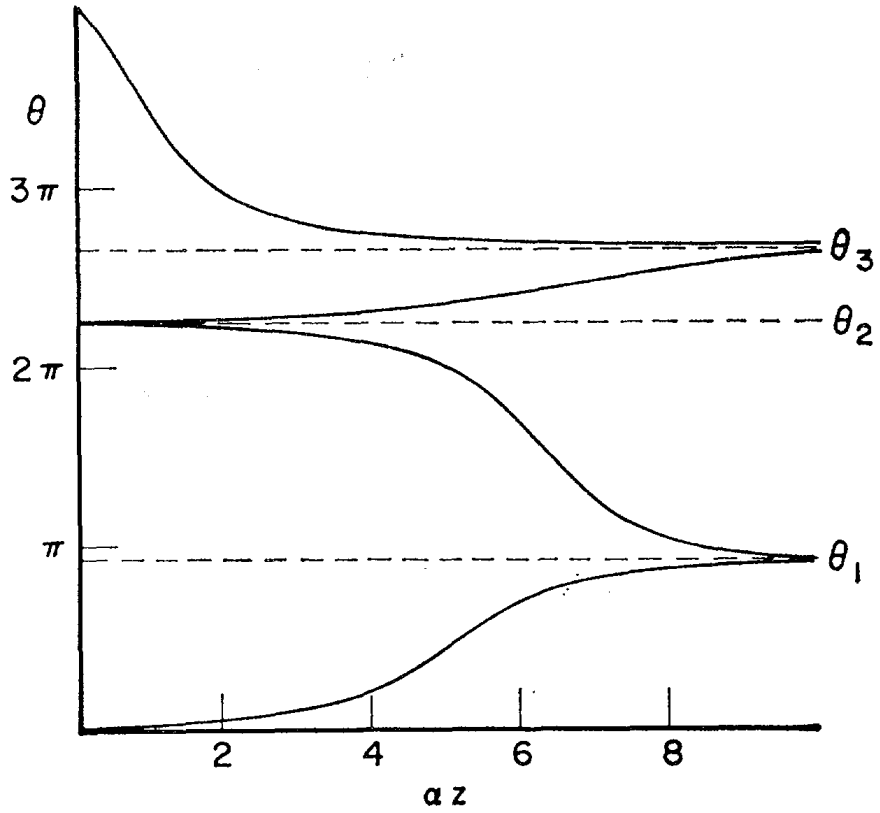


Figure 1.3: Branched solutions of the area theorem for an amplifier, $d\theta/dz = -\gamma\theta + \alpha\sin\theta$ [10, 11], with $\gamma/\alpha = 0.1$. $\gamma$ is the linear loss coefficient of a bulk medium, $\alpha$ is the Beer's gain/absorption length. The angle $\theta$ is plotted vs the dimensionless length $\alpha z$.

damping constant $\gamma$ in response to an applied electromagnetic field. If an electric field, $E(t)$, is applied to the atom, the displacement $x$ of each damped harmonic oscillator in one dimension obeys the differential equation

$$m\frac{d^2x}{dt^2} + 2\gamma m\frac{dx}{dt} + m\omega_0^2 x = -eE(t). \tag{1.13}$$

By using the ansatz $x(t) = x_\omega e^{-i\omega t}$, the driven solution to this equation is found, where $x_\omega = \frac{-eE_0}{m(-\omega^2+\omega_0^2-2i\gamma\omega)}$. Near resonance, the expression for $x_\omega$ is estimated and by using $P(t) = -Nex(t)$ for $N$ atoms, the polarization field is calculated. Therefore, the electric susceptibility is obtained by using $P(t) = \varepsilon_0\chi^{(1)}E(t)$. The result is

$$\chi^{(1)} = \chi' + i\chi'', \tag{1.14}$$

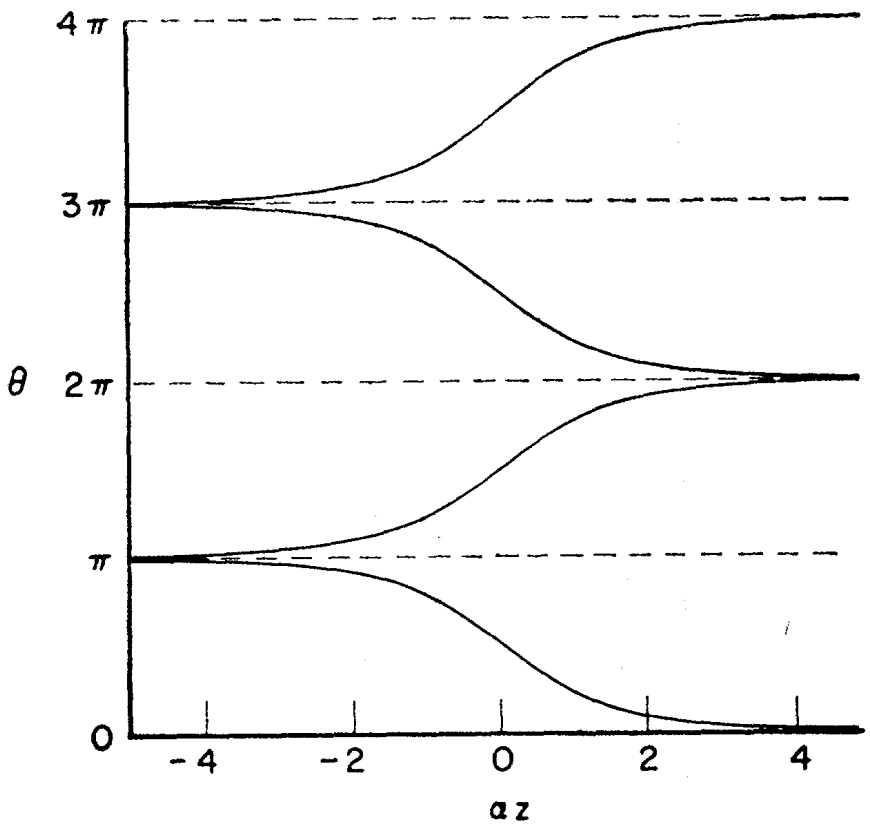


Figure 1.4: Branched solutions of the area theorem for an absorber with $\gamma = 0$.

where

$$\chi' = \frac{-Ne^2}{2\varepsilon_0 m\omega_0}\left[\frac{\omega-\omega_0}{(\omega-\omega_0)^2+\gamma^2}\right], \tag{1.15}$$

and

$$\chi'' = \frac{Ne^2}{2\varepsilon_0 m\omega_0}\left[\frac{\gamma}{(\omega-\omega_0)^2+\gamma^2}\right]. \tag{1.16}$$

These equations are quite useful in approximating of the linear susceptibility near resonance with the applied field. Fig. 1.6 shows the frequency dependence of the real (dispersive) and imaginary (absorptive) parts of the susceptibility. The real part of the susceptibility contributes to the refractive index $n = 1 + \chi'/2$. The imaginary part leads to the damping of the wave if $\chi'' > 0$. The width of the absorption line or the bandwidth of the absorber is determined by the phase relaxation rate $1/T_\perp$ of the dipole moment. In off resonance regime, the imaginary part goes very quickly to zero, while the real part approaches a constant value below resonance, and goes to zero for off resonance, but slower than the

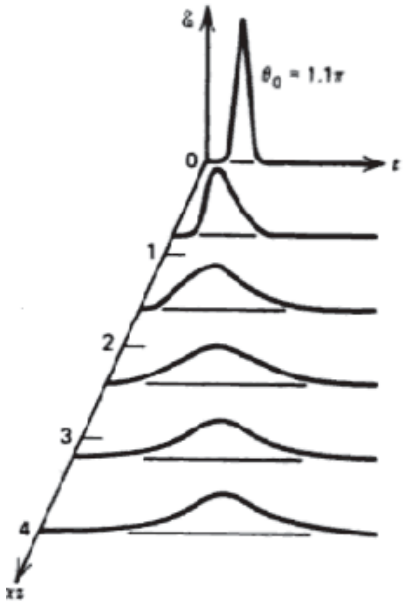


Figure 1.5: Self-induced transparency and soliton formation.

imaginary part. It means that in off resonance there is still a contribution to the index but the loss is practically zero.

These expressions for the electric susceptibility are applied for a CW field. As illustrated in the figure, the dispersion is changing drastically and the absorption is so high near the resonance. However far from the resonance, the absorption is near zero and the dispersion is changing slightly. As a result, the dispersion relation $k(\omega)$, when it is slowly varying over the pulse spectrum, can be represented by its Taylor expansion

$$k(\omega) = k'(\omega_c)(\omega-\omega_c) + \frac{k''(\omega_c)}{2}(\omega-\omega_c)^2 + \frac{k^{(3)}(\omega_c)}{6}(\omega-\omega_c)^3 + O((\omega-\omega_c)^4), \quad (1.17)$$

when $\omega_c$, the carrier frequency of the pulse, is far from the resonance frequency $\omega_0$. The derivative of the dispersion relation at the carrier frequency is the velocity of the wave packet or group velocity. Keeping only the first linear term, the pulse shape is invariant during propagation. If the intensity of an applied pulse is high or the spectrum of the pulse is broad, the second order term plays its role. Monochromatic componenets of the pulse with different frequencies propagate with different velocities and therefore the pulse spreads. The spreading of a wave due to the second term in the dispersion relation is called group velocity dispersion (GVD). In general the GVD broadens the pulse except when the

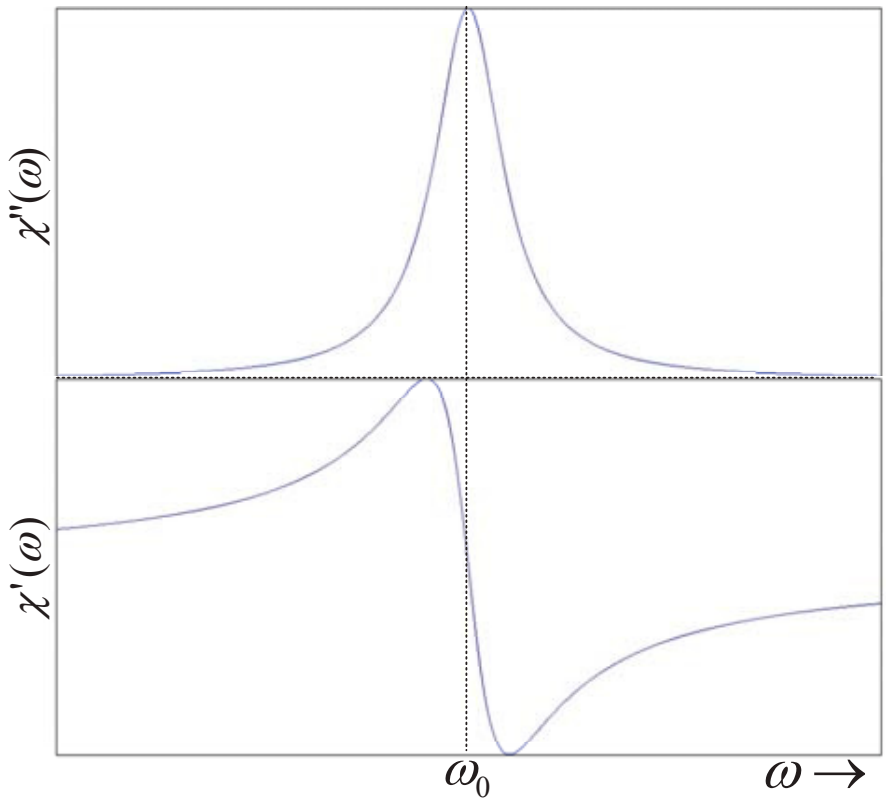


Figure 1.6: Imaginary (top) and real (bottom) parts of the complex susceptibility as functions of frequency.

pulse is initially chirped properly. In other word, a chirped pulse can be compressed during the early stage of propagation whenever the GVD parameter and the chirp parameter have opposite signs such that their multiplication is negative.

When a pulse propagates through a dispersive medium, it acquires a linear chirp, so its phase becomes parabolic. The derivative of the phase in respect to time is the instantaneous frequency. As shown in Fig. 1.7, for positive dispersion the low frequencies are in the front of the pulse, while the high frequencies are in the back of the pulse due to the positive dispersion $k'' > 0$; that is wave packets with lower frequencies travel faster than wave packets with higher frequencies.

The imaginary part of the refractive index is determined by using the complex susceptibility and relation between the refractive index and susceptibility. The loss can be incorporated into the imaginary part of complex refractive index in a lossy medium. The region where the refractive index is decreasing with wavelength is called normal dispersion regime, while the region when refractive index is increasing with wavelength is called

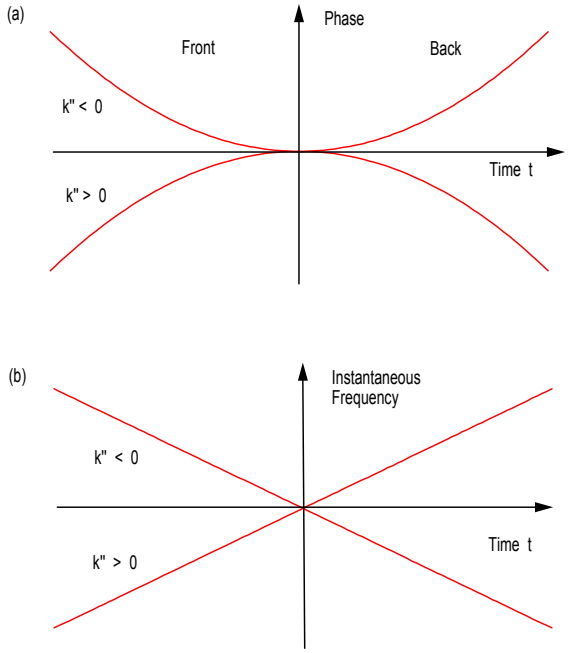


Figure 1.7: Phase (a) and instantaneous frequency (b) of a Gaussian pulse in a medium.

anomalous dispersion regime.

### 1.3.5 Inhomogeneous Broadening

In the absence of a driving field, the dipole oscillations must decay and finally dye away. Because of this finite natural radiative lifetime, each absorption or emission line of the atom has a finite width, which is called homogeneous width. In reality the effective lifetime of dipoles is usually shorter than its purely lifetime, since there are some incoherent interactions such as collisions which affect all atoms homogeneously. In addition, the total relaxation/decay rate is increased due to the inhomogeneous broadening as well. The most common origin of the inhomogeneous lifetime is the Doppler effect in gases or atomic vapors. In the reference frame moving with the velocity of the atom $\vec{v}$, the frequency of the wave, $\omega$, is shifted to $\omega^{'} = \omega - \vec{k}.\vec{v}$. Since atoms in gases have different velocities, this frequency shift is different for each atom. Hence, in a moving reference frame each atom sees different frequencies of the wave according to its velocity. This causes random distribution

of resonant frequencies which leads to changes in total transverse decay time, $T_\perp$ as [8]

$$\frac{1}{T_\perp} = \frac{1}{T'_\perp} + \frac{1}{T^*_\perp}, \tag{1.18}$$

where $T'_\perp$ is the homogeneous lifetime, $T^*_\perp$ is the inhomogeneous lifetime and $T_\perp^{-1}$ is the total relaxation rate. In Fig. 1.8 the inhomogeneous broadening of an atom is shown.

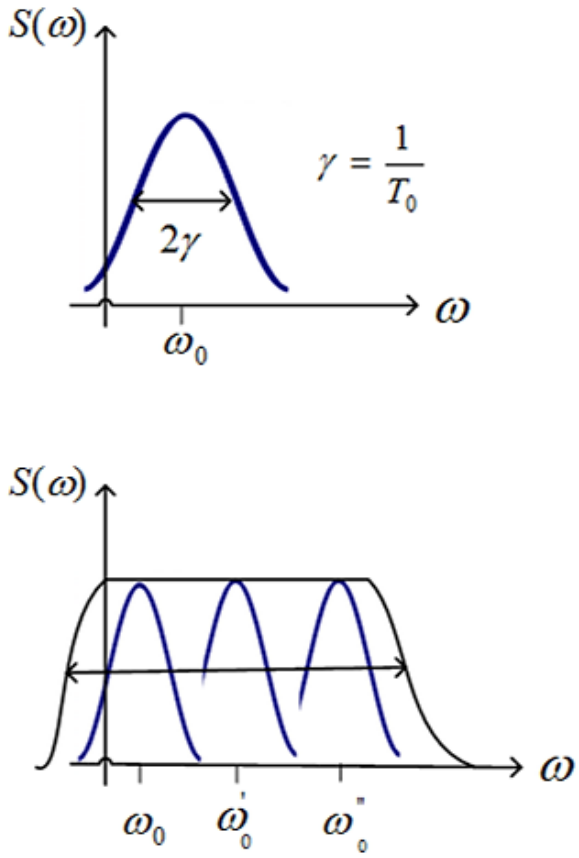


Figure 1.8: The homogeneous (top) and inhomogeneous (bottom) emissin lines spectrum. $\gamma$ is the homogeneous decay rate.

### 1.3.6 Optical Kerr Effect

In an isotropic and homogeneous medium with optical Kerr effect nonlinearity, the refractive index depends quadratically on the field, i.e. on the intensity

$$n = n(\omega, |A|^2) \approx n_0(\omega) + n_2|A|^2, \tag{1.19}$$

where, $A$ is the field envelope, $n_0$ is the linear refractive index, and $n_2$ is the nonlinear refractive index coefficient. For many transparent materials the intensity dependent refractive index is positive, i.e. the nonlinear refractive index of the medium increases with the intensity.

If the field is a light beam propagating inside a nonlinear medium with refractive index dependent on the beam intensity, the light rays near the center experience stronger refraction since the intensity in the beam center is the highest. Therefore, the rays bend toward the center and the intensity increases toward the beam center on propagation in the medium. This behavior is called self-focusing of light in a nonlinear medium with a positive refractive index. As a result of self-focusing, the beam narrows and its peak intensity is increased on propagation in the medium. On the contrary, diffraction causes every beam to spread which leads to decreasing light intensity at the center. If these two opposing trends balance each other, the spatial solitons can form, an optical structure when the beam width as well as its amplitude remain unchanged during propagation.

### 1.3.7 Self-Phase Modulation

The intensity-dependent refractive index imposes an additional self-phase shift on the pulse/beam envelope during propagation, which is proportional to the instantaneous intensity of the pulse/beam. In other words, the intensity-dependent nonlinear refractive index modulates the optical phase of the pulse/beam. This phenomenon is called self-phase modulation (SPM) leading only to a phase shift in the temporal/spatial domain. As a result, the intensity profile of the pulse remains unchanged while the spectrum of the pulse/beam changes. Moreover, as the intensity and phase dynamics of the field in nonlinear media depend on each other, the change in the phase of the optical field due to nonlinear refractive index induces modification of the field intensity profile. The effect of nonlinearity becomes important over distances where the phase accretion is of the order of one radian, i. e. nonlinear length. In the presence of SPM the pulse redistributes its energy, such that the low frequency contributions are in the front of the pulse and the high frequencies are in the back of the pulse, similar to the case of positive dispersion.

### 1.3.8 Absorbers and Amplifiers

Assuming a CW wave, when the wave envelope $\mathscr{E}$ is constant over lifetimes $T_{\parallel}$ and $T_{\perp}$ which are much shorter than the inhomogeneous relaxation time, the equation governing the attenuation or amplification of the propagating wave can be written as [8]

$$\frac{\partial}{\partial z}I = \alpha(\Delta)[\frac{w_{eq}}{1+\mathscr{L}I(z)}]I(z), \tag{1.20}$$

where $I$ is the field intensity, $\mathscr{L}$ is the Lorentzian factor, $\mathscr{L} = \frac{1}{[1+(\Delta T_{\perp}^{'})^2]}$, $\alpha(\Delta)$ is the small signal gain/absorption coefficient. $w_{eq} = -1$ in an absorber, and so the intensity of the pulse is attenuated with increasing the propagation distance $z$. However if the resonant atoms are prepared in their excited states, $w_{eq} > 0$, $I(z)$ grows with propagation distance; i.e. the light field is amplified.

In reality, the medium that acts as host for the resonant atoms interacts with the field, if the intensity is high enough. This interaction is usually weak and causes the linear absorption which leads to saturation of amplification. As $I(z)$ increases large enough to interact with the host medium, the growth rate gradually decreases to zero and the amplifier will be saturated. At large distances of the propagation, the pulse only transfers the energy of the inversion in the resonant medium to the host medium through the linear absorption [8].

## 1.4 Motivation

Near resonance regime can be considered as an intermediate between the regimes of classical theory and the quantum optical theory; Many semiclassical optical equations arising directly form a quantum mechanical treatment are central to the analysis of resonant phenomena. Many coherent resonant interactions do involve only two levels of an atom. In addition, some of the nonclassical effects e.g. self-induced transparency can only occur when the atoms and the field are close resonance, i.e. when the field frequency falls within the inhomogeneous atomic absorption line of the atoms.

In the classical oscillator model, an oscillator can oscillate with an arbitrary amplitude. On the contrary, the quantum mechanical two-level atoms can only have a finite dipole moment because of the upper level population saturation. These limits on the ranges of

energies and moments of the atom cause various coherent and incoherent physical effects. Such coherent phenomena as Bloch vector behavior, area theorem and self-induced transparency lead to many optical structures such as similaritons and solitons.

However there is a drawback in working very near to resonance. As discussed in the previous sections, the absorption is high near resonance. When the electric field on resonance with the transition frequency of the atom interacts with the atom, the dipole moments of the atom take most of the energy of the electric field to oscillate, so the electric field decays.

To overtake this obstacle it should be noticed that the pulse absorption depends on the width of the pulse $\tau_p$ relative to $T_\perp$. For pulses that satisfy the limit $\tau_p \lesssim T_\perp$, that is for pulses shorter than the relaxation time, the absorption of energy occurs much more slowly. In Fig. 1.9 this development in pulse energy is sketched for Gaussian pulse for different pulse widths $\tau_p$. The explanation for this improvement is that only pulses shorter than $T_\perp$ have spectral widths that exceed the total width of the absorption spectrum, $1/T_\perp$. As a result, the major portion of the pulse energy is located in regions of the spectrum where there is no absorption. On the contrary, long pulses interactions with atoms are much more; dipole moments have more time to take energy form pulse so the pulse looses more energy [8].

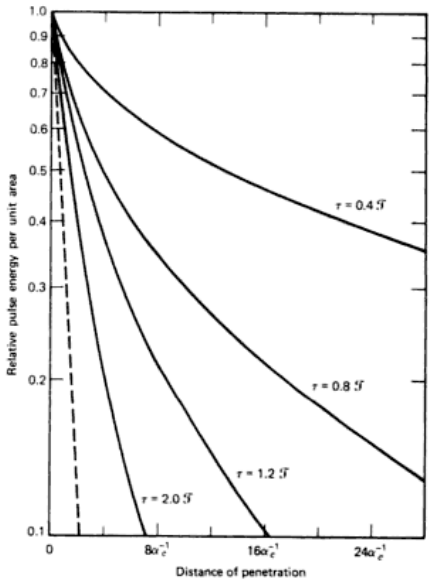


Figure 1.9: Variation of pulse energy per square centimeter with propagation distance into the absorber for different pulse lengths $\tau$. The input pulse is Gaussian.

Generation of short and ultrashort pulses opened a new area in the field of optical physics. To date, their applications have extended to high precision measurements, nonlinear optics, optical signal processing, optical communications, etc. Attaining high power which is essential in many nonlinear optics phenomena was always a problem. By using short pulses the high intensities at low average powers are possible. It leads to many applications in nonlinear physics including frequency conversion, laser material processing, surgery, and high intensity physics including x-ray generation. Short pulses also have large bandwidths which is useful in optical communications, as there are many channels available from one source and the bit-rate stream is high as well.

In addition to referred advantages of working in near resonance regime, another important benefit comes into mind when investigating optical absorbers and amplifiers. The single atom absorption coefficient $\alpha(\Delta)$ determines the rate of amplification in an amplifier. It is proportional to the transverse relaxation time $T_\perp$ and inversely proportional to the detuning $\Delta$. In fact $\alpha(\Delta) \to 0$ when $\Delta >> 1/T_\perp$, so the strong amplification is not feasible when the pulse is highly detuned from resonance.

All in all, near resonance limit in the study of the electric field and atom interaction reveals details buried in the near resonance effects which are inaccessible in off-resonance regimes. Such a wealth of knowledge about the on-resonance behavior of the atom can be utilized to extract structures that are very interesting in the field of optics. This indeed is a great encouragement for researchers to study the potential applications of on-resonance regime in many optical systems. This thesis is intended to address the above issues.

## 1.5 Objectives

This thesis explores the resonant interaction of short pulses with matter. To achieve such main objective of the present study, large variety of optical systems near resonance have been investigated and the innovative near resonance optical structures related to these systems have been discovered. Many near-resonance effects in the two-level systems are analyzed and finally optical structures such as similaritons, kinks and solitons associated with the resonant light-matter interactions are explored. During each case studies, universal asymptotic solutions of any near-resonant short pulses propagating in different regimes of various optical systems are investigated. Applying these systems under proper conditions

enables the user to construct practical systems and use these near resonance structures experimentally. The broad field of study includes different regimes such as quasi CW regime, coherent transient regime and coherent regime.

In this thesis, the validity of both near resonance similariton and soliton structures in a wide range of materials is analytically and numerically investigated and verified with the study of stability. Amplifiers, absorbers and conservative systems are utilized as the optical systems to explore the formation of similaritons and solitons initiated by propagating short input pulse/beam with the carrier frequency near the transition frequency of the medium atoms.

To bring about the primary goal, research on-resonance behavior of matter with applying an electric field, the short term goals, studying the optical systems and structures near resonance, includes various analytical and numerical case studies:

1. Analytical and numerical investigation of similariton structure in linear amplifiers in resonance regime;
2. Analytical and numerical investigation of similariton structure in linear absorbers in resonance regime;
3. Analytical and numerical investigation of similariton with kink structure in resonant nonlinear media;
4. Numerical investigation of kink structure in resonant nonlinear media with inhomogeneous broadening;
5. Numerical investigation of soliton structure in nonlinear media with quadratic nonlinearity;
6. Analytical and numerical investigation of similariton structure in nonlinear media having quintic nonlinearities.

## 1.6 Thesis Organization

The layout of this thesis is in the ”publication” format which incorporates the published or under-review papers generated as the outcome of the completed analytical and numerical studies. This thesis is divided into 8 chapters.

Chapter 2 presents an analytical and numerical study which is performed on the coherent linear amplifiers. In this study, the analytical description of novel self-similar pulses in homogeneous linear amplifier near resonance is presented. The distinct feature of these self-similar pulses, the universality, is demonstrated with numerical simulations. The salient features of new pulses such as energy gain factor and width of the pulse are presented to confirm the universality of this self-similar structure.

Chapter 3 outlines the analytical investigation on ultrashort self-similar pulses propagating in coherent linear absorbers near resonance. The required material parameters are discussed for experimental realization of the system. Finally the required input pulse profiles and energies are determined and it is described that the proposed self-similar pulses can be realized with picoseconds input pulses.

Chapter 4 presents the third analytical and numerical study completed for validation of similariton structure in resonant nonlinear media. In this study, the formation of a class of self-similar waves in resonant nonlinear media, optical kinks, is described in detail. Several classes of systems in which the kinks can be realized are mentioned. The aim of this study also is to investigate the regime based on the transverse and energy relaxation times and effects of these two on the creation of such self-similar kinks.

Chapter 5 presents the final numerical study completed for finding kink waves in resonant nonlinear media. In this study, the procedure is identical to the third study outlined in chapter 4. However, the effect of inhomogeneous broadening is considered in the formation of optical kinks in resonant nonlinear media.

Chapter 6 outlines the numerical study performed to explore temporal solitons in quadratic nonlinear media. A generic model to realize the system is proposed. The system contains a bulk nonlinear medium with quadratic nonlinearity doped with resonance impurities. The resonant impurities act in a two-level system and form the solitons while the substrate medium transfers the soliton structure to the second harmonic pulse. An extensive numerical simulation is performed to study the effects of different parameters such as group velocity mismatch and phase mismatch on the formation of solitons.

Chapter 7 outlines the analytical study performed for finding spatial similaritons in quintic nonlinear media. A description of the analytical calculations, proposed experimental conditions, numerical procedure, and simulation data are presented in detail. The system

contains two-level atoms ensemble in a nonlinear substrate with cubic-quintic nonlinearity. The main objective of this study is to explore the formation of spatial similaritons in nonlinear media with nonlinearities other than the Kerr nonlinearity.

Conclusions of the main findings from the research body as a whole as well as recommendations for future work are summarized in chapter 8. In this chapter, some practical applications of proposed systems are also discussed.

# Chapter 2

# Self-Similar Pulses in Coherent Linear Amplifiers

Soodeh Haghgoo and Sergey A. Ponomarenko
Published in: Optics Express, May 2011, Vol. 19, 9750.
URL: http://www.opticsinfobase.org/oe/abstract.cfm?uri=oe-19-10-9750


## 2.1 Abstract

We discover and analytically describe self-similar pulses existing in homogeneously broadened amplifying linear media in a vicinity of an optical resonance. We demonstrate numerically that the discovered pulses serve as universal self-similar asymptotics of any near-resonant short pulses with sharp leading edges, propagating in coherent linear amplifiers. We show that broadening of any low-intensity seed pulse in the amplifier has a diffusive nature: Asymptotically the pulse width growth is governed by the simple diffusion law. We also compare the energy gain factors of short and long self-similar pulses supported by such media.

## 2.2 Introduction

Only not too long ago did the optical community realize [12] that self-similarity is quite a ubiquitous feature of optical systems. The phenomena as diverse as optical pulse evolution in Hall gratings [13], stimulated Raman scattering [14], formation of self-written waveguides [15], and fractal formation in nonlinear media [16] exhibit self-similarity in one form or another. Recently, long-term self-similar evolution of pulses in nonlinear fiber amplifiers [17–19], in passive fibers of lasers [20] has received much attention due to its fundamental interest and potential applications. Lately, fiber lasers with self-similar evolution in the amplifier and soliton evolution in the anomalous dispersion segments [21] as well as all-normal-dispersion lasers working in a self-similar light propagation regime [22]

were proposed and experimentally realized. Self-similar dynamics of beams in nonlinear waveguide amplifiers and in conservative nonlinear media have also been explored [23–27].

Self-similar evolution of pulses and beams in resonant media has also been explored. In particular, universal quasi-self-similar asymptotics of ultrashort light propagation in coherent nondegenerate and degenerate nonlinear amplifiers was examined in Refs. [28] and [29], respectively. Also, self-similarity in superfluorescence in homogeneously broadened resonant media was explored as well [30]. In addition to the early pioneering work [28–30], however, some recent studies [26, 31] show that a wealth of self-similar regimes exists in such media. In particular, self-similar beams can be generated in cubic-quintic nonlinear media doped with resonant impurities in the limit of a large detuning from the impurity resonance [26]. By the same token, we have shown elsewhere [31] that in resonant nonlinear absorbers, self-similar optical kinks are formed as intermediate asymptotics of any incident pulse with a long tail in the trailing edge. In this context, it is instructive to explore the possibility of self-similar pulse formation in *resonant linear* media. At first glance, the very proximity to optical resonance(s), coupled with the system linearity, appears to preclude self-similarity of a sufficiently short pulse: Strong dispersion at resonance(s) would, in general, seem to cause severe pulse reshaping. One would then also wonder whether self-similar pulses in such media, if any, would be universal asymptotics of very weak seed pulses. The affirmative answer to the last question would augur well for the experimental realization of such similaritons.

In this paper, we demonstrate analytically that self-similar optical pulses, albeit of a highly asymmetric shape, can indeed propagate in resonant linear amplifiers. Such an asymmetric self-similar shape is a manifestation of dynamic balance between linear amplification and phase relaxation processes in resonant propagation of short pulses in the absence of inhomogeneous broadening and host medium dispersion. We further show that a low-intensity seed pulse of any profile with a sharp leading edge evolves into a self-similar one upon propagation inside the amplifier. The short pulse broadening has a universal diffusive character such that the rms width grows as a square root of the propagation distance. Thus, we demonstrate, both analytically and with numerical simulations that the discovered self-similar pulses are universal intermediate asymptotics in resonant coherent amplifiers. The intermediate character of the asymptotics is imposed by the system linearity: As long as the pulse area will have grown enough, our linear approximation surely breaks down;

sufficiently small initial pulse areas and/or short enough amplifier lengths are required for the linear approximation to hold over the entire amplifier length.

## 2.3 Physical Model and Mathematical Preliminaries

We model a resonant medium as a collection of two-level atoms with the resonance frequency $\omega_0$, thereby limiting our consideration to the case of one internal resonance. We assume hereafter that the pulse spectrum is mainly affected by homogeneous broadening, implying that $\gamma_\perp \gg \delta$, $\gamma_\perp$ and $\delta$ being transverse (dipole moment) relaxation rate and a characteristic spectral width of inhomogeneous broadening, respectively. Under these conditions, the evolution of a pulse with the carrier frequency $\omega$ in the medium is governed by a reduced wave equation,

$$\partial_\zeta \Omega = i\kappa\sigma; \tag{2.1}$$

subject to the slowly-varying envelope approximation (SVEA):

$$\partial_\zeta \Omega \ll k\Omega, \qquad \partial_\tau \Omega \ll \omega\Omega. \tag{2.2}$$

Here $\Omega = 2d_{eg}\mathscr{E}/\hbar$ is the Rabi frequency associated with the pulse amplitude $\mathscr{E}$, $d_{eg}$ is a dipole matrix element between the ground and excited states of any atom, labeled with the indices $g$ and $e$, respectively; $\kappa = \omega N|d_{eg}|^2/c\varepsilon_0\hbar$ is a coupling constant, $N$ is an atom density, $k = \omega/c$, and Eq. (2.1) is written in terms of the transformed coordinate and time, $\zeta = z$ and $\tau = t - z/c$. The dipole moment matrix element $\sigma$ and one-atom inversion $w$ obey the Bloch equations [8]

$$\partial_\tau \sigma = -(\gamma_\perp + i\Delta)\sigma - i\Omega w, \tag{2.3}$$

and

$$\partial_\tau w = -\gamma_\parallel (w - w_{eq}) - \tfrac{i}{2}(\Omega^*\sigma - \Omega\sigma^*). \tag{2.4}$$

In Eqs. (2.3) and (2.4) $\gamma_\parallel$ is a longitudinal relaxation rates associated with one-atom inversion damping, $\Delta = \omega - \omega_0$ is a detuning from the resonance and $w_{eq}$ is a value of the one-atom inversion in the absence of the pulse (equilibrium).

In the low-intensity limit, the atomic population is hardly affected by the pulse such

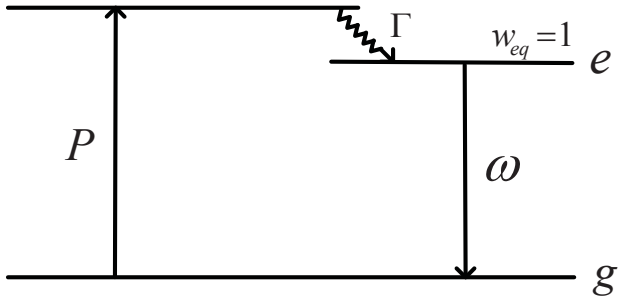


Figure 2.1: Schematics of a pump-probe three-level system modeling coherent linear amplifier. The resonant transition takes place between levels $e$ and $g$.

that the one-atom inversion is approximately given by its equilibrium value,

$$w \simeq w_{eq} = \pm 1, \tag{2.5}$$

where the upper/lower sign corresponds to amplifier/absorber case: All atoms remain in the upper/lower level. Physically, the linear amplification regime of a weak probe pulse can be realized using a strong pump in a three-level configuration, standard of laser systems, see e.g. [32]. The latter is illustrated schematically in Fig. 2.1 where the pump rate $P$ and the upper level relaxation rate must be large enough, $P \gg \gamma_\perp$ and $\Gamma \gg \gamma_\perp$, to achieve population inversion between levels "e" and "g".

Mathematically, the approximation (2.5) implies linearization of the dipole moment evolution equation viz.,

$$\partial_\tau \sigma = -(\gamma_\perp + i\Delta)\sigma \mp i\Omega. \tag{2.6}$$

In the following, we distinguish two limiting cases: "long" pulses, $t_p \gg T_\perp$ and "short" ones, $t_p \leq T_\perp$–in the case $t_p \ll T_\perp$, the pulses may be called "ultrashort"–where $T_\perp = \gamma_\perp^{-1}$ and $t_p$ is a characteristic pulse width.

*Long pulses.* In this case, the atomic variables can be adiabatically eliminated–using Eq. (2.6) and equating $\sigma$ to its quasi-steady-state value with respect to $\Omega$–which will result in the pulse evolution equation in the form

$$\partial_\zeta \Omega = \pm \left( \tfrac{\alpha + i\beta}{2} \right) \Omega. \tag{2.7}$$

Here we introduced an inverse Beer's gain/absorption length $\alpha$ and an overall phase accumulation rate $\beta$ by the expressions,

$$\alpha = \frac{2\kappa\gamma_\perp}{\gamma_\perp^2 + \Delta^2}, \qquad \beta = \frac{2\kappa\Delta}{\gamma_\perp^2 + \Delta^2}. \tag{2.8}$$

It follows at once from Eq. (2.7) that for sufficiently long pulses, *any* pulse grows/decays exponentially in such a medium, maintaining its overall shape,

$$\Omega(\tau, \zeta) = \Omega_0(\tau) e^{\pm(\alpha + i\beta)\zeta/2}, \tag{2.9}$$

where $\Omega_0(t)$ describes an initial pulse profile, and Eq. (2.9) is well-known Beer's amplification/absorption law.

*Short pulses.* For simplicity, we consider pulses exactly on resonance with the atomic transition, $\Delta = 0$; the pulse field and dipole moment evolution equations can then be written as

$$\partial_\zeta \Omega = \frac{i}{2}\gamma_\perp \alpha_0 \sigma, \tag{2.10}$$

and

$$\partial_\tau \sigma = -\gamma_\perp \sigma \mp i\Omega. \tag{2.11}$$

where $\alpha_0 = 2\kappa/\gamma_\perp$. Our treatment to this point is equally applicable to amplifying and absorbing media. Hereafter we focus on short pulse propagation in amplifiers.

## 2.4 Short Self-Similar Pulses

The inspection of Eqs. (2.10) and (2.11) reveals that the electric field of a self-similar pulse and atomic dipole moment profiles ought to be sought in the form

$$\Omega(\zeta, \tau) = \gamma_\perp \theta(\tau) \overline{\Omega}[\gamma_\perp \tau F(\zeta)] e^{-\gamma_\perp \tau}, \tag{2.12}$$

and

$$\sigma(\zeta, \tau) = \theta(\tau) G(\zeta) \overline{\sigma}[\gamma_\perp \tau F(\zeta)] e^{-\gamma_\perp \tau}. \tag{2.13}$$

Here $\theta(\tau)$ is a unit step function describing a sharp leading edge of the pulse, $F(\zeta)$ and $G(\zeta)$ are arbitrary at the moment and $\overline{\Omega}$ and $\overline{\sigma}$ are dimensionless functions. Substituting

the Ansatz (2.12) and (2.13) into Eqs. (2.10) and (2.11), we can show that self-similarity is sustained provided that

$$F(\zeta) = \alpha_0 \zeta + T_\perp / t_p; \qquad G(\zeta) = 1/F(\zeta). \tag{2.14}$$

Further, the dimensionless pulse envelope $\overline{\Omega}$ in the amplifying medium satisfies the equation,

$$\eta \overline{\Omega}'' + \overline{\Omega}' - \overline{\Omega}/2 = 0, \tag{2.15}$$

where we introduced a similarity variable $\eta$ by

$$\eta = \gamma_\perp \tau (\alpha_0 \zeta + T_\perp / t_p). \tag{2.16}$$

and the prime denotes a derivative with respect to $\eta$.

Analytically solving Eq. (2.15), we can obtain a self-similar pulse envelope in a linear amplifier. The overall pulse profile can then be represented as

$$\Omega(\eta, \tau) \propto \gamma_\perp \theta(\tau) {}_1F_1(1/2, 1, -2\sqrt{2\eta}) \exp(\sqrt{2\eta} - \gamma_\perp \tau), \tag{2.17}$$

where ${}_1F_1(a,c,x)$ is a confluent hypergeometric function, and we dropped an arbitrary (small) initial pulse amplitude. Eq. (2.17) can be expressed in a more compact form as

$$\Omega(\eta, \tau) \propto \gamma_\perp \theta(\tau) I_0(\sqrt{2\eta}) \exp(-\gamma_\perp \tau), \tag{2.18}$$

where $I_0(x)$ is a modified Bessel function of zero order. We note that for sufficiently long propagation distances, $\alpha_0 \zeta \gg T_\perp / t_p$, the self-similar pulse profile no longer depends on $t_p$, yielding a universal self-similar profile

$$\Omega(\tau, \zeta) \propto \gamma_\perp \theta(\tau) I_0(2\sqrt{\kappa \zeta \tau}) \exp(-\gamma_\perp \tau). \tag{2.19}$$

It can be inferred from the analysis of Eq. (2.18) that the pulse evolution is governed by a synergy of three factors: pulse shape asymmetry, coherent gain and dipole phase relaxation. In the absence of nonlinearity, the self-similarity arises as a consequence of dynamic balance between coherent gain and linear damping; the sharp leading edge of the pulse

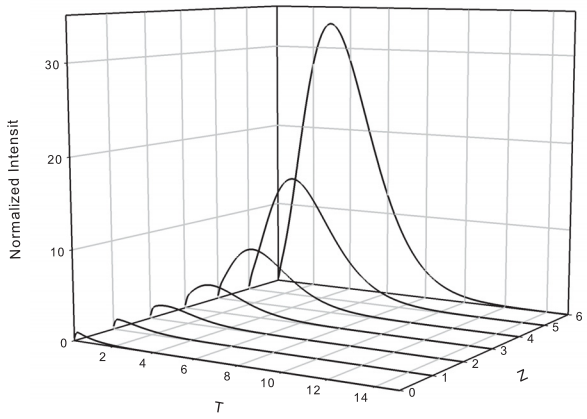


Figure 2.2: Normalized intensity of a short self-similar pulse as a function of dimensionless time $T = \tau/T_\perp$ and propagation distance $Z = \alpha_0\zeta$. The pulse intensity is normalized to its peak value at $Z = 0$. The initial pulse width is chosen to be $t_p = T_\perp$.

profile ensures the balance in the absence of bulk medium dispersion and inhomogeneous broadening. Thus, the asymmetry of a seed pulse shape appears to be the only requirement for self-similarity in the studied linear system to emerge.

We stress here that in the linear limit, damping of the trailing edge of the pulse by the linear relaxation processes allows for the finite energy self-similar pulse formation. The situation here is drastically different from quasi-self-similarity emerging in the nonlinear amplification of ultrashort pulses–the term should be understood in the sense defined in Sec. 2–studied in [28]. In the latter case, linear damping is negligible and the nonlinearity promotes the emergence of finite-energy pulses in the amplifying medium. We notice also that the discovered self-similar pulses have no chirp–since dispersion plays no role here–which sets them apart from more familiar parabolic pulses in nonlinear fiber amplifiers. The latter require a linear chirp to prevent wave breaking [17,19]. We also note that owning to a different physical nature, our similaritons are markedly different from recently discovered quasi-parabolic pulses in nonlinear amplifiers [33]. While the former are chirp-free self-similar pulses, the latter are phase-modulated steady-state pulses moving with the speed of light.

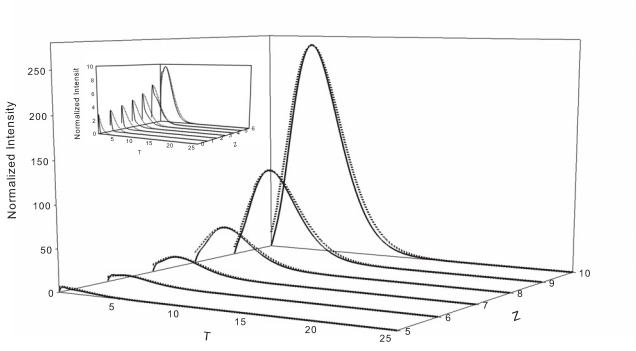


Figure 2.3: Normalized intensity of a short Gaussian (solid) and self-similar (dashed) pulses as functions of dimensionless time $T = \tau/T_\perp$ and propagation distance $Z = \alpha_0\zeta$. The pulse intensities are normalized to their peak values at $Z = 0$. The initial pulse width is chosen to be $t_p = T_\perp/2$ and $t_p = T_\perp$ for Gaussian and self-similar pulses, respectively. The inset shows pulse dynamics for short propagation distances.

## 2.5 Numerical Results and Discussion

We now proceed to describing the properties of new self-similar pulses. In Fig. 2.2, we display the self-similar pulse profile evolution as a function of the dimensionless time $T = \tau/T_\perp$ for several values of the dimensionless propagation distance $Z = \alpha_0\zeta$. The self-similar character of the pulse dynamics is clearly discernable in the figure. To demonstrate the universal nature of the discovered self-similar regime, we numerically simulate the evolution of a generic asymmetric Gaussian pulse, $\Omega_1(t,0) \propto \theta(t)\exp(-t^2/t_p^2)$, in the amplifier and compare its profile with the self-similar asymptotics. The results are presented in Figure 2.3 To ensure the two pulses are sufficiently different in the source plane, we take the Gaussian pulse to be half as long as the self-similar one at $Z = 0$: $t_p = T_\perp/2$. In the inset to the figure, we compare short-distance pulse dynamics of the two pulses. We see in the figure that although the Gaussian pulse profile deviates from the self-similar asymptotics over short distances–at least over first few Beer's amplification lengths as is seen in the inset–it quickly converges to the universal asymptotics over longer distances. It then is seen to coincide with the self-similar asymptotics profile to within numerical round-off errors [34]. We obtained qualitatively similar results for hyperbolic secant and exponential profiles with cut off leading edges: $\Omega_2(t,0) \propto \theta(t)\mathrm{sech}(t/t_p)$, and $\Omega_3(t,0) \propto \theta(t)\exp(-t/t_p)$.

To reenforce the message, we examine the rms width– defined as $\Delta T = \sqrt{\langle T^2\rangle - \langle T\rangle^2}$ and measured in the units of $T_\perp$–of the universal self-similar asymptotics on pulse propagation in the amplifier. The averaging is taken over the pulse intensity distribution, for

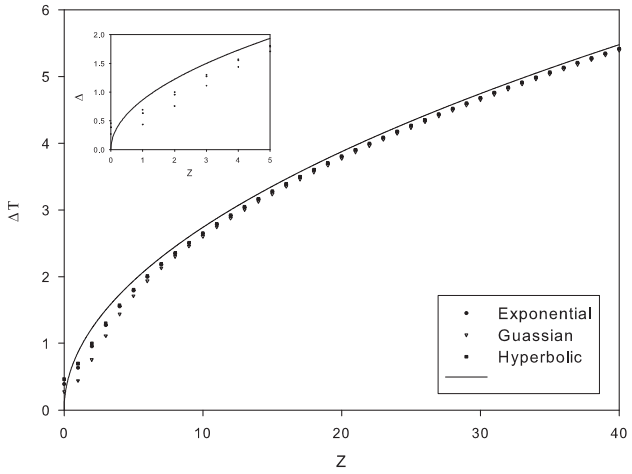


Figure 2.4: Average widths of Gaussian, secant hyperbolic and exponential pulses as functions of the dimensionless propagation distance $Z = \alpha_0 \zeta$. The self-similar asymptotic pulse width dependence on the propagation distance is shown as the solid curve.

instance,

$$\langle T^2(Z)\rangle \equiv \frac{\int_0^\infty dT T^2 |\mathscr{E}(T,Z)|^2}{\int_0^\infty dT |\mathscr{E}(T,Z)|^2}. \tag{2.20}$$

With the help of the asymptotic expansion of $I_0(x)$ [35], an analytical expression for the rms width can be derived and presented in an exceptionally simple form

$$\Delta T(Z) \simeq \sqrt{3Z}/2. \tag{2.21}$$

In other words, the pulse rms width grows with the distance in a diffusive manner with the effective diffusion coefficient equal to $3\alpha T_\perp^2/8$ (in original units). We then evaluate and display the behavior of asymmetric Gaussian, hyperbolic secant, and exponential pulse widths in Fig. 2.4 The self-similar asymptotic pulse width is drawn in a solid curve. In the inset to the figure, we exhibit the pulse width dynamics over a short range of propagation distances. We can conclude from the figure that although the width of an arbitrarily shaped seed pulse initially deviates from the self-similar pulse width, the former asymptotically tends to the latter over a long enough propagation distance, thereby underscoring the universal character of the discovered self-similar asymptotics.

Next, we observe that the applicability of SVEA is not, in general, guaranteed for pulses with sharp fronts. Hence, the presence of a step function has to be physically justified as follows. A practical realization of an ideal sawtooth-like pulse involves a finite switching

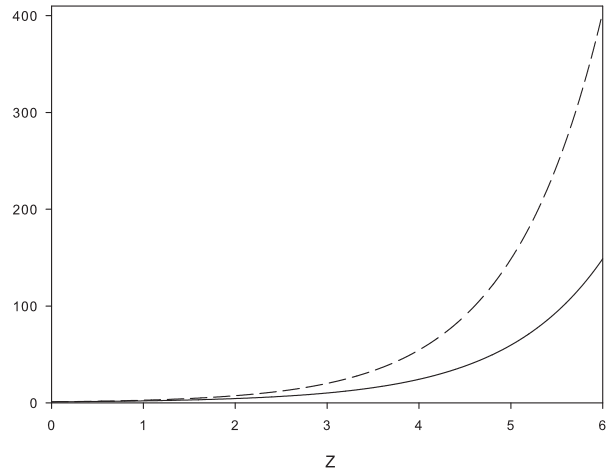


Figure 2.5: Energy gain factor $G(Z)$ for a short (solid) and long (dashed) self-similar pulse as a function of the dimensionless propagation distance $Z = \alpha_0 \zeta$.

time $t_{sw}$ describing the fast rise of its leading edge. Thus for a short pulse, $t_p \sim T_\perp$, the pulse duration (rise time of the pulse front edge) has to be much shorter than the pulse width, yet much longer than an optical cycle for the SVEA–see Eq. (2.2)–to hold:

$$\omega^{-1} \ll t_{sw} \ll t_p \sim T_\perp. \tag{2.22}$$

The complimentary conditions (2.22) can be realized in a laboratory for picosecond pulses in dilute atomic vapors, say, for which, typically $T_\perp \sim 1 \div 10$ ps [8] by choosing, for example, $t_{sw} \sim 10 \div 100$ fs. Mathematically, the leading front step function can then be approximated, for instance, as

$$\theta(\tau) \simeq [1 + \tanh(\tau/t_{sw})]/2, \tag{2.23}$$

with the excellent approximation attainable for $t_{sw} = 0.01 T_\perp$.

Finally, we exhibit in Fig. 2.5 a short-pulse energy gain factor,

$$G(\zeta) = \int d\tau |\mathscr{E}(\zeta,\tau)|^2 / \int d\tau |\mathscr{E}(0,\tau)|^2, \tag{2.24}$$

for the novel self-similar pulses as a function of the propagation distance. The exponential

gain factor for long pulses,

$$G_0(\zeta) = \exp(\alpha_0 \zeta), \tag{2.25}$$

is presented for comparison as well. On comparing the two, we conclude that for sufficiently long distances, long pulses are amplified much more efficiently than are short ones. This is because short pulses have very broad energy spectra with large fractions of their energies stored in the pulse tails. The latter lie well outside of the medium gain spectrum and are then not efficiently amplified. Narrow spectra of long pulses, on the other hand, fall entirely within the medium gain spectrum, which results in strong amplification. These qualitative conclusions are bourn out by the asymptotic analysis yielding the following universal long-term gain behavior for asymmetric short pulses

$$G_\infty(\zeta) \propto \frac{e^{\alpha_0 \zeta}}{\sqrt{\alpha_0 \zeta}}. \tag{2.26}$$

Hence, comparing Eqs. (2.26) and (2.25), we see that the long-pulse gain dwarfs the short-pulse one in the long-term limit.

## 2.6 Conclusion

In summary, we have discovered a self-similar regime of short pulse propagation in linear amplifiers in the vicinity of an optical resonance. The novel self-similar pulses have sharp leading front, resulting in a highly asymmetric sawtooth-like pulse profile. We have shown that the new pulses serve as intermediate universal asymptotics for any asymmetrically shaped pulse propagation in resonant amplifiers in the linear regime. We note that our results hold true in the absence of inhomogeneous broadening. It will be instructive to determine the influence of the latter on the emergence of universal self-similar asymptotics in the system.

# Chapter 3

# Shape Invariant Pulses in Resonant Linear Absorbers

Soodeh Haghgoo and Sergey A. Ponomarenko
Published in: Optics Letters, April 2012, Vol. 37, 1328.
URL: http://www.opticsinfobase.org/ol/abstract.cfm?uri=ol-37-8-1328


## 3.1 Abstract

We theoretically describe ultrashort self-similar pulses propagating in coherent linear absorbers near optical resonance and propose a method for their experimental realization.

## 3.2 Introduction

Shape-invariant light beams enjoy a special place in optics due to their self-similar structure on paraxial propagation in free space. Several classes of shape-invariant fully and partially coherent beams, including notably Hermite-Gaussian ones, are known to date [32, 36]. Owning to the space-time duality between evolution of beams in free space and pulses in optical fibers [37], similar shape-invariant pulses exist in weakly dispersive media far away from internal resonances.

Close to an optical resonance, however, one may expect to see, in general, pronounced pulse reshaping due to enhanced dispersion there [38]. Yet, we have shown elsewhere [39] that shape-invariant pulses emerge as universal intermediate asymptotics on near-resonant pulse propagation in coherent *linear amplifiers* as a result of dynamical balance between amplification and dissipation processes. Since no such balance is feasible in *linear absorbers*, the prospects for self-similarity there are open to debate.

In this Letter, we show that a broad class of shape-invariant ultrashort pulses is nevertheless supported by resonant linear absorbers. We stress that self-similarity arises here thanks to a particular class of initial spectral profiles with long wings where much of the

incident pulse energy is stored. We also discuss the potential for experimental realization of the new pulses in homogeneously broadened coherent absorbers and estimate the necessary pulse and optical media parameters.

We start by examining small-area pulse propagation in a homogeneously broadened resonant absorber under exact resonance condition: the pulse carrier frequency coincides with a resonant transition frequency of the medium atoms. An atomic vapor in the homogeneously broadening regime [32], filling the core of a hollow-core photonic crystal fiber (HCPCF) [40] can serve as a physical realization of the medium. Using the HCPCF, we can arrest spatial diffraction. Engineering the fiber to tune its zero group-velocity dispersion frequency to the gas resonance frequency enables us to eliminate bulk medium dispersion effects and focus on purely resonant properties of the system.

## 3.3 Analytical Study

In the slowly-varying envelope approximation (SVEA), the pulse field $\mathscr{E}(z,t)$ and atomic dipole moment $\sigma(z,t)$ can be shown to obey the classical Maxwell-Lorentz equations [8, 39]

$$\partial_\zeta \Omega = i\kappa\sigma, \tag{3.1}$$

and

$$\partial_\tau \sigma = -\gamma_\perp \sigma + i\Omega, \tag{3.2}$$

which are written in the transformed variables: $\zeta = z$ and $\tau = t - z/c$. Here we also introduced the field envelope in frequency units, $\Omega = -e\mathscr{E}/2m\omega x_0$, where $x_0$ is an amplitude of the electron displacement from equilibrium, the inverse dipole relaxation rate $\gamma_\perp = 1/T_\perp$, where $T_\perp$ is a characteristic dipole moment relaxation time, and a coupling constant, $\kappa = Ne^2/4\varepsilon_0 mc$. The coupled Maxwell-Lorentz equations, (3.1) - (3.2) can be solved using a Fourier transform technique, yielding the field envelope at any propagation distance in the form

$$\mathscr{E}(\tau,\zeta) = \int_{-\infty}^{\infty} d\nu\, \tilde{\mathscr{E}}_0(\nu) e^{-i\nu\tau} \exp\left[-\frac{\alpha\zeta}{2(1-i\nu T_\perp)}\right]. \tag{3.3}$$

Here $\alpha = 2\kappa/\gamma_\perp$ is a small-signal absorption coefficient and we introduced the spectral amplitude of the incident pulse by the expression

$$\tilde{\mathscr{E}}_0(\nu) = \int_{-\infty}^{\infty} \frac{dt}{2\pi} \mathscr{E}(t,0) e^{i\nu t}. \tag{3.4}$$

With an eye on shape-invariant pulse evolution, we consider the following family of incident pulses:

$$\mathscr{E}_s(t,0) = \mathscr{E}_{0s}\theta(t)(\kappa\zeta_0 t)^{s/2} J_s(2\sqrt{\kappa\zeta_0 t}) e^{-\gamma_\perp t}, \tag{3.5}$$

where $s$ is a nonnegative real mode index and $\theta(t)$ is a unit step function, mathematically describing a physical zero-index pulse with a very short rise time $t_r$. As was discussed in detail in the amplifier context in Ref. [39], the inequality $\omega^{-1} \ll t_r \ll T_\perp$ must be respected for the SVEA to work.

Using the integral representation [35]

$$\int_0^\infty dx x^{s+1} e^{-a^2x^2} J_s(bx) = \tfrac{b^s}{(2a^2)^{s+1}} e^{-b^2/4a^2}, \tag{3.6}$$

and changing the variable of integration, we can obtain the pulse spectral amplitude in the source plane as

$$\tilde{\mathscr{E}}_{0s}(\nu) = \frac{\tilde{\mathscr{E}}_{ms}}{(1-i\nu T_\perp)^{s+1}} \exp\left[-\frac{\alpha\zeta_0}{2}\left(\frac{i\nu T_\perp}{1-i\nu T_\perp}\right)\right]. \tag{3.7}$$

Here we introduced the peak spectral amplitude $\tilde{\mathscr{E}}_{ms}$ as

$$\tilde{\mathscr{E}}_{ms} = \frac{\mathscr{E}_{0s} T_\perp}{2\pi} \left(\frac{\alpha\zeta_0}{2}\right)^s e^{-\alpha\zeta_0/2}, \tag{3.8}$$

which is linking $\zeta_0$ to the other pulse parameters. Next, on comparing the Fourier decomposition of the incident pulse,

$$\mathscr{E}_s(t,0) = \int_{-\infty}^{\infty} d\nu\, \tilde{\mathscr{E}}_{s0}(\nu) e^{-i\nu t}, \tag{3.9}$$

with that at any $\zeta \geq 0$–see Eq. (3.3)–and using Eq. (3.7), we infer by inspection that the examined pulse (3.5) indeed remains self-similar on propagation in the resonant medium

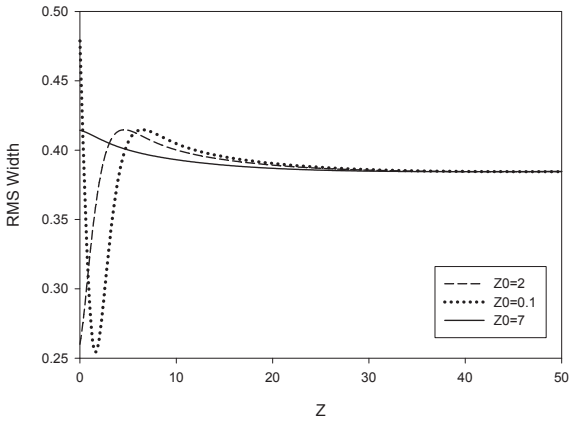


Figure 3.1: Rms width of the zero-index pulse as a function of $Z$ for three values of $Z_0$.

with the pulse profile given by

$$\mathscr{E}_s(\tau,\zeta) = \frac{\mathscr{E}_{0s}\theta(\tau)}{(1+\zeta/\zeta_0)^s}\,\eta^{s/2}J_s(2\sqrt{\eta})\,e^{-\gamma_\perp\tau}. \tag{3.10}$$

Here the similarity variable $\eta$ is defined as $\eta = \kappa(\zeta+\zeta_0)\tau$. Hereafter, we will refer to $\{\mathscr{E}_s\}$ as a set of resonant linear absorber modes. Notice that the new mode index $s$ need not be an integer which sets the discovered modes apart from, for instance, familiar Hermite-Gaussian (HG) ones encountered in the laser resonator theory [32].

Next, over sufficiently long propagation distances, $\zeta \gg \zeta_0$, the pulse shape is independent of its initial rms width, $\mathscr{E}_s(\tau,\zeta) \propto \theta(\tau)(\kappa\tau/\zeta)^{s/2}J_s(2\sqrt{\kappa\zeta\tau})e^{-\gamma_\perp\tau}$. Hence, the rms width of the pulse must be independent of $\zeta_0$ in the long-term limit as well, a feature that further distinguishes novel modes from the HG ones. The rms pulse width of the zero-index mode is exhibited in Fig. 3.1 as a function of the propagation distance for different initial conditions in the dimensionless variables: $T = \tau/T_\perp$, $Z = \alpha\zeta$ and $Z_0 = \alpha\zeta_0$.

It follows at once from Eqs. (3.3) and (3.7) that the spectrum of the shape-invariant pulse of index $s$ can be represented as

$$S_s(\omega,Z) = \frac{S_0}{(1+\omega^2)^{s+1}}\exp\left(-\frac{Z+Z_0}{1+\omega^2}\right). \tag{3.11}$$

The spectral profile of the zero-index mode is shown in Fig. 3.2–the other mode spectra look qualitatively similar–as a function of dimensionless frequency $\omega = \nu T_\perp$ for $Z_0 = 0.5$ and $Z_0 = 7$. As is seen in the figure, the spectrum evolution scenario is determined by the

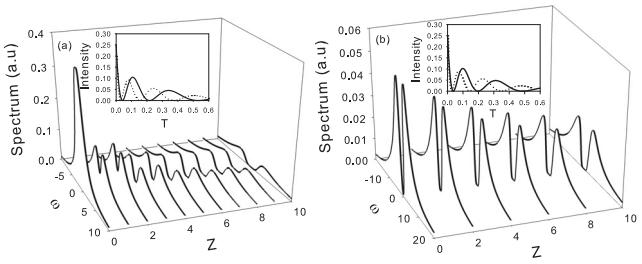


Figure 3.2: Pulse spectrum of the zero-index mode (in arbitrary units) as a function of dimensionless frequency $\omega$ and propagation distance $Z$ for $(a)$ $Z_0 = 0.5$ and (b) $Z_0 = 7$. Insets: Zero-index pulse intensity profile as a function of dimensionless time $T$; $Z = 70$, (dotted line) and $Z = 100$ (solid line).

interplay of resonant dispersion and absorption and it strongly depends on the magnitude of $Z_0$. For sufficiently small $Z_0$–see Fig 3.2a–the initial spectrum has a central peak. A hole is then burnt at the center of the pulse spectrum on propagation over a fraction of a characteristic absorption length. This is followed by spectral hole broadening as the energy is being steadily transferred toward the pulse wings and the pulse evolution becomes self-similar. A source with a greater $Z_0$ may already have a spectral hole–as is illustrated in Fig. 3.2b–resulting in shape-invariant pulse propagation from the outset. To exhibit self-similarity in the time domain we also display the zero-mode pulse evolution in the insets to Fig. 3.2.

The required pulse profile to generate self-similarity can be synthesized by exploring Eq. (3.7). It follows from Eq. (3.7) that the desired spectral shape consists of an atomic absorption profile–the Lorentzian prefactor–and a complex modulation factor, $H(\nu) = (1+\nu^2 T_\perp^2)^{-s} \exp[-\alpha\zeta_0/(1-i\nu T_\perp)]$. The amplitude and phase of the latter are sketched in Fig. 3.3 as functions of $\omega$.

Next, to generate the overall spectrum, one may first invert an atomic ensemble in a source gas cell with an ultrashort $\pi$-pulse, say. The excited atoms will then emit a homogeneously broadened pulse of Lorentzian spectral shape, which may in turn be spectrally filtered with the filter function $H(\nu)$ using, for example, one of the techniques reviewed in Ref. [41].

Further, we briefly discuss the required material parameters to realize the discussed pulses. First, the collision-induced spectral width $\delta\nu_c$–assuming dipole relaxation is mainly

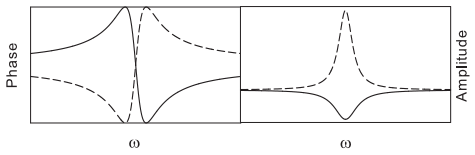


Figure 3.3: Left: the filter phase (solid) and the real part of the refractive index (dashed). Right: the filter amplitude (solid) and the imaginary part of the refractive index (dashed).

due to collisions, $T_\perp \sim \delta\nu_c^{-1}$ –must be much greater than the Doppler-induced inhomogeneous broadening width $\delta\nu_D$. To attain the homogeneous broadening regime, $\delta\nu_c \gg \delta\nu_D$, one can either collimate the gas beam or increase the gas pressure [32]. Taking the gas density to be $N \sim 10^{15}$ cm$^{-3}$–which is, at least, three orders of magnitude beyond the usual dilute vapor range [8]–and assuming $T_\perp \sim 10^{-12}$ sec for such a dense vapor, we estimate the linear absorption length $L_A = \alpha^{-1} \simeq 0.2$ mm. Thus, the self-similar pulse propagation regime can be observable in a few meter-long HCPCF.

Finally, let us estimate the required input pulse energy density, $W = (\varepsilon_0 c/2)\int_{-\infty}^{\infty} dt\,|\mathscr{E}|^2 = \pi\varepsilon_0 c\int_{-\infty}^{\infty} d\nu\,|\tilde{\mathscr{E}}|^2$. Using the peak spectral amplitude of the input pulse, the energy density can be roughly estimated as $\tilde{\mathscr{E}}_{ms}^2\Delta\nu$, where the spectral width (FWHM) is $\Delta\nu \sim T_\perp^{-1}$. The peak spectral amplitude can in turn be estimated using the pulse area, $\mathscr{A} = (2d/\hbar)\int_{-\infty}^{\infty} dt\mathscr{E} = 2\pi\tilde{\mathscr{E}}_m$. In the small-area regime, say, $\mathscr{A} \sim 0.1$, we arrive at $W \simeq 10$ nJ/cm$^2$, where we used $d \sim ea_0 \sim 10^{-29}$ Cm as a reasonably good estimate for the dipole moment magnitude in optical transitions [8]. Thus the proposed self-similar pulses can be realized with picosecond pulse sources of just 10 nJ/cm$^2$ energy.

# Chapter 4

## Self-Similarity and Optical Kinks in Resonant Nonlinear Media

Sergey A. Ponomarenko and Soodeh Haghgoo
Published in: Physical Review A, November 2010, Vol. 82, 051801.
URL: http://pra.aps.org/abstract/PRA/v82/i5/e051801


### 4.1 Abstract

We show that self-similar optical waves with a kink structure exist in a wide class of resonant nonlinear media, adequately treated in the two-level approximation. The self-similar structure of the present kinks is reflected in the time evolution of the field profile, atomic dipole moment and one-atom inversion. We develop an analytical theory of such kinks. We show that the discovered kinks are accelerating nonlinear waves, asymptotically attaining their shape and the speed of light. We also numerically explore the formation and eventual disintegration of our kinks due to energy relaxation processes. Thus, the present kinks can be viewed as intermediate asymptotics of the system.

### 4.2 Introduction

The quest for structurally stable nonlinear waves, which maintain their intensity – and sometimes even phase – profiles in open physical, chemical, and biological systems, has been in the forefront of contemporary nonlinear science. Self-similar waves or similaritons – whose intensity profiles remain scaled replicas of themselves on propagation – can serve as a prominent example of structurally stable waves in open systems. Although self-similarity has long become textbook material in fluid and gas [42, 43] and solid mechanics [43] as well as in plasma physics [44], the concept has only relatively recently percolated into nonlinear optics [12]. To date, self-similarity in Bragg gratings [13], stimulated Raman scattering [14], self-written waveguides [15], and fractal formation in nonlinear media [16]

have been studied among other topics. More recently, however, the focus has shifted to two major classes of similaritons: asymptotic and soliton-like ones. The asymptotic temporal [17, 19] or spatio-temporal [45] similaritons, forming in fiber amplifiers in the normal dispersion regime over long propagation distances, were theoretically predicted [17, 19] and experimentally realized [19, 20]. At the same time, bright and dark soliton-like similaritons have been theoretically investigated in fiber [46–50] and graded-index waveguide amplifiers [23–25], and in trapped Bose-Einstein condensates [51, 52]. The vast majority of research on optical similaritons has however been aimed at understanding their behavior sufficiently far away from any internal resonance of the medium.

In this Rapid Communication, we show that an altogether different kind of optical similaritons, kink-like similaritons, can be supported by resonant nonlinear media. The novel self-similar kinks accelerate, asymptotically acquiring the speed of light. An initial stage of their fast self-steepening is followed by asymptotically slow formation of quasi-steady-state kinks. All these features make the new kinks markedly different from the previously examined steady-state ones, Raman induced in optical fibers away from any resonance [53, 54]. Interestingly, there is a direct analogy between the new optical kinks and the corresponding shocks in gas dynamics. The transverse relaxation processes, which determine the temporal width of the kink, are counterparts of gas viscosity. At the same time, the longitudinal relaxation processes, which lead to kink decay and eventual disintegration, are direct analogs of thermal processes in gases which cause shock disappearance. There are, however, two fundamental differences between optical kinks and shocks in gases or fluids. First, while the former do not require any background intensity, the latter form against a finite velocity background, determining the sound velocity in a gas or fluid. Second, whereas the gas shocks propagate with a constant supersonic speed, the present kinks are accelerating self-similar waves.

In this work, we treat resonant media in the two-level approximation. The model is sufficiently general to describe a broad range of resonant nonlinear media from atomic vapors and solids, doped with resonant atoms [8], to bulk semiconductors, doped with quantum dots [55]. Thus our analytical and numerical results may find applications to a multitude of physical systems as diverse as dilute gases and solids.

## 4.3 Theoretical Background

We begin by considering a light pulse with a carrier frequency $\omega$ near optical resonance frequency $\omega_0$ of a two-level atom medium. To focus on the main aspects of the problem, we make two assumptions. First, we assume that the pulse is not chirped, implying that $\Omega^* = \Omega$. Second, we assume that the transverse relaxation rate $\gamma_\perp$–defined as the corresponding inverse relaxation time–dwarfs the longitudinal one, $\gamma_\parallel$, as well as the characteristic width of inhomogeneous broadening $\delta$,

$$\gamma_\perp \gg \delta, \qquad \gamma_\perp \gg \gamma_\parallel. \tag{4.1}$$

The first inequality implies that all impurity atoms are assumed to be effectively on resonance with the field such that inhomogeneous broadening can be ignored. The second inequality means that the atomic dipole moments evolve much faster than the atomic population dynamics unfolds. The existence of a hierarchy of widely separated in time relaxation processes results in the emergence of two widely separated in space characteristic propagation distances: a typical distance $\zeta_*$ over which the new kinks are formed and a characteristic energy relaxation distance $\zeta_{**}$ beyond which the kinks gradually decay. The novel kinks maintain their self-similar structure in the intermediate range, $\zeta_* \ll \zeta \ll \zeta_{**}$.

Within the framework of our model and subject to the slowly varying envelope approximation (SVEA), the pulse evolution is governed by the reduced wave equation in the form

$$\partial_\zeta \Omega = \frac{\omega N |d_{eg}|^2}{c\varepsilon_0 \hbar} v, \tag{4.2}$$

Here $\Omega = 2d_{eg}\mathscr{E}/\hbar$ is the Rabi frequency associated with the pulse amplitude $\mathscr{E}$, $N$ is a density of impurity atoms, and $d_{eg}$ is a dipole matrix element between the ground and excited states of any atom; the two relevant atomic states are appropriately labeled with the indices $g$ and $e$. Further, Eq. (4.2) is written in terms of the transformed coordinate and time, $\zeta = z$ and $\tau = t - z/c$. The relevant atomic dipole moment $v$ and one-atom inversion $w$ obey the Bloch equations [8] which, in our case, are simplified as

$$\partial_\tau v = -\gamma_\perp v + \Omega w, \tag{4.3}$$

and

$$\partial_\tau w = -\Omega v. \tag{4.4}$$

In deriving Eqs. (4.3) and (4.4), we neglected longitudinal relaxation processes, an assumption to be examined later with the help of numerical simulations.

The inspection of Eqs. (4.2) – (4.4) reveals the existence of self-similar solutions for the Rabi frequency

$$\Omega(\tau,\zeta) = \gamma_\perp \overline{\Omega}(\eta), \tag{4.5}$$

and for the atomic variables

$$v(\tau,\zeta) = e^{-\gamma_\perp \tau}\overline{v}(\eta), \qquad w(\tau,\zeta) = e^{-\gamma_\perp \tau}\overline{w}(\eta). \tag{4.6}$$

Here the similarity variable is defined by the expression

$$\eta = \alpha\zeta e^{-\gamma_\perp \tau}; \qquad \alpha = \frac{2kN|d_{eg}|^2}{\gamma_\perp \varepsilon_0 \hbar}, \tag{4.7}$$

where we introduced a linear absorption coefficient $\alpha$ and $k = \omega/c$.

The dimensionless Rabi frequency $\overline{\Omega}$ and scaled atomic variables, $\overline{v}$ and $\overline{w}$, obey the set of ordinary differential equations (ODE)

$$2\overline{\Omega}' = \overline{v}, \tag{4.8}$$

$$\eta\overline{v}' = -\overline{\Omega}\overline{w}, \tag{4.9}$$

and

$$(\eta\overline{w})' = \overline{\Omega}\overline{v}, \tag{4.10}$$

where the prime denotes a derivative with respect to the similarity variable. Combining Eqs. (4.8) – (4.10) and integrating once with the aid of the asymptotic condition $\overline{\Omega}(0) = \overline{\Omega}_\infty$, we arrive at the ODE for a kink profile,

$$\eta^2\overline{\Omega}'' = -\tfrac{1}{2}\overline{\Omega}(\overline{\Omega}^2 - \overline{\Omega}_\infty^2). \tag{4.11}$$

The analysis of Eq. (4.11) indicates that at the trailing edge of the pulse, $\tau \to +\infty$, the

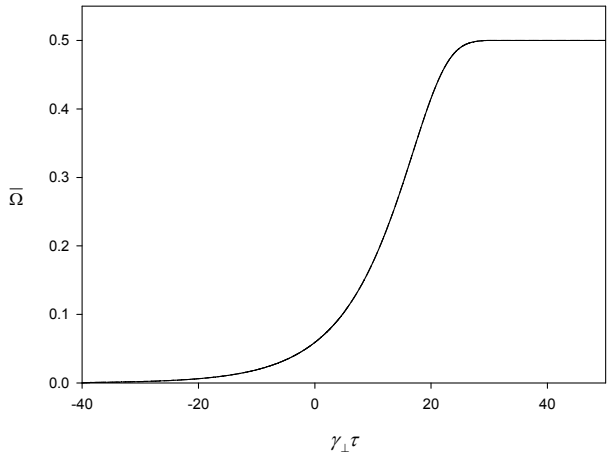


Figure 4.1: Kink profile as a function of time, measured in the units of the transverse relaxation time, $T_\perp = 1/\gamma_\perp$. The dimensionless Rabi frequency jump is taken to be $\overline{\Omega}_\infty = 1/2$.

kink profile at any propagation distance asymptotically behaves as

$$\overline{\Omega} = \overline{\Omega}_\infty - |C|\eta^s; \qquad s = \frac{1+\sqrt{1-4\overline{\Omega}_\infty^2}}{2}, \tag{4.12}$$

where $C$ is a constant. By the same token, at the leading edge, $\tau \to -\infty$, the kink field strength falls off as

$$\overline{\Omega} \sim \eta^{-q}, \qquad q = \frac{-1+\sqrt{1+2\overline{\Omega}_\infty^2}}{2}. \tag{4.13}$$

The kink profile is exhibited in Fig. 4.1 as a function of time. It follows from (4.12) and (4.13) that (i) the kink structure is determined entirely by the magnitude of the Rabi frequency jump, $\Omega_\infty$, and (ii) the kink has no chirp if the latter satisfies the inequality

$$\Omega_\infty \leq \gamma_\perp/2, \tag{4.14}$$

otherwise our solution is not consistent. The condition (4.14) specifies the range of parameters for which kinks with monotonous profiles are realized in resonant media. It can be physically interpreted as follows. The Rabi frequency jump must be smaller than a certain critical value determined by the transverse damping constant such that the system is in an overdamped regime with no Rabi oscillations. The latter would lead to pulse chirping which, in turn, would cause modulations of the kink profile.

Further, we can infer from Eqs. (4.8) - (4.10) that the one-atom inversion can be expressed as

$$w(\zeta,\tau)=\frac{1}{\alpha\zeta}\left[\overline{\Omega}^2(\eta)-\overline{\Omega}_\infty^2\right]. \tag{4.15}$$

It follows at once from Eq. (4.15) and the definition of the inversion that at the leading edge of the kink: $w_\infty=-\overline{\Omega}_\infty^2/\zeta\geq -1$, implying that our self-similar solution is valid over the distances such that

$$\zeta\geq\zeta_*=\frac{\Omega_\infty^2}{\alpha\gamma_\perp^2}. \tag{4.16}$$

Here $\zeta_*$ is the lower bound of a characteristic distance over which the kink is formed. Thus the present kink-like similaritons are intermediate asymptotics of the system in the spirit of Ref. [43]. On the one hand, they form over distances of the order of $\zeta_*$, after the transient dynamics, induced by specific initial conditions, have died away. On the other hand, the new kinks remain intact only over spatial scales much shorter than the characteristic energy relaxation distance determined by the longitudinal relaxation constant $\gamma_\parallel$.

We also note that at any (finite) propagation distance over which our kinks have already formed, the atomic dipole moment $v$ asymptotically tends to zero, albeit asymmetrically, at both ends of the kink: $v\sim -e^{q\gamma_\perp\tau}$ at the leading edge, and $v\sim -e^{-s\gamma_\perp\tau}$ at the trailing edge of the pulse, respectively. The time evolution of $w$ and $v$ is displayed in Fig. 4.2 for several propagation distances; a self-similar structure of the atomic state evolution is unambiguously reflected in the figure. Physically the behavior of the inversion can be explained by observing that at the leading edge of the kink, where the light intensity is very small, there are much more atoms in their ground states than are excited atoms, resulting in a negative value of $w$. At the trailing edge, however, a large pulse amplitude saturates the medium, implying zero inversion.

Further, we reveal unusual dynamic properties of the discovered kinks. It follows from Eq. (4.7) that the speed $U$ of a kink wavefront depends on the propagation distance according to

$$U(\zeta)=\frac{\gamma_\perp\zeta c}{c+\gamma_\perp\zeta}. \tag{4.17}$$

Thus the novel kinks accelerate on propagation, asymptotically attaining the speed of light. In reality, however, a characteristic distance over which their speed becomes sufficiently close to $c$, can be quite short, of the order of $\zeta_\infty\simeq c/\gamma_\perp$. For example, for solids or semiconductors doped with resonant atomic impurities or quantum dots, $10^{11}\leq\gamma_\perp\leq 10^{13}$, $\mathrm{s}^{-1}$,

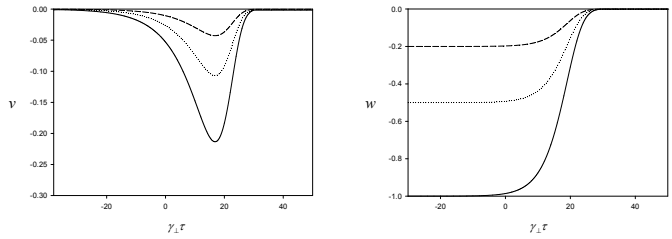


Figure 4.2: Atomic dipole moment (left) and one-atom inversion (right) as functions of dimensionless time, $\gamma_\perp\tau$, displayed at several propagation distances: Solid, $\alpha\zeta = 25$; dotted, $\alpha\zeta = 40$, and dashed, $\alpha\zeta = 50$. The propagation distances are measured in the units of inverse Beer's absorption length, $\alpha^{-1}$.

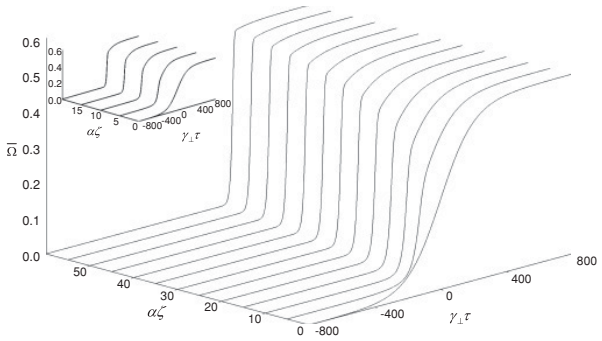


Figure 4.3: Dimensionless Rabi frequency $\overline{\Omega}$ of a forming kink as a function of dimensionless time, $\gamma_\perp\tau$, and propagation distance $\alpha\zeta$. The ratio of transverse to longitudinal relaxation times is $T_\perp/T_\parallel = 10^{-4}$. The initial parameters are $\Omega_0 = 0.5\gamma_\perp$ and $\tau_p = 100T_\perp$. The inset shows the initial stage of fast self-steepening.

leading to the estimate, $0.03 \leq \zeta_\infty \leq 3$ cm.

## 4.4 Numerical Considerations

We now discuss kink formation. A constant background intensity at the trailing edge of the input wave is required to produce a kink. In laboratory, such pulses can be generated by switching on cw lasers, for example. In our numerical simulations, we then consider an adiabatically switched cw wave of the form

$$\Omega(0,t) = \frac{\Omega_0}{1+e^{-t/\tau_p}}, \tag{4.18}$$

where $\Omega_0$ is the amplitude – measured in frequency units – of the cw laser field and $\tau_p$ is a characteristic time constant of the switching process. We emphasize that a particular functional form (4.18) is not important: we obtained qualitatively similar results for wave self-steepening and kink formation with different input wave profiles having a finite background intensity at the trailing edge.

The atoms are assumed to be initially in their ground states and the one-atom inversion obeys the Bloch equation

$$\partial_\tau w = -\gamma_\parallel (w+1) - \Omega v, \tag{4.19}$$

where the energy (longitudinal) relaxation processes are taken into account. Our numerical simulations indicate that monotonous kinks form provided that

$$\Omega_c \leq \Omega_0 \leq \gamma_\perp/2, \tag{4.20}$$

where the magnitude of a critical amplitude $\Omega_c$ depends on the value of $\gamma_\parallel$. The presence of a critical power threshold for kink formation is explained as follows. The incident wave should have enough power to start self-steepening despite energy losses caused by longitudinal relaxation processes. Clearly, the shorter the longitudinal relaxation time, the greater the initial amplitude is required to generate a kink.

The results of numerical simulations of Eqs. (4.2), (4.3) and (4.19), with the initial condition (4.18), are displayed in Figs. 4.3 and 4.4. In Fig. 4.3, we show self-similar kink formation for sufficiently long energy relaxation times, $T_\parallel/T_\perp = 10^4$. After a brief stage of fast self-steepening, exhibited in the inset to the figure, the wave self-steepening slows down at distances of the order of $\zeta_\infty$, corresponding to the kink having attained the speed close to the speed of light. The subsequent asymptotic self-steepening leads to quasi-steady-state kink formation. The critical amplitude in this case is found to be $\Omega_c = 0.2\gamma_\perp$. The numerically obtained kink profile coincides, to a good accuracy, with the analytically determined one, which justifies neglecting the longitudinal relaxation processes in Eq. (4.4) [56]. In Fig. 4.4, we exhibit the influence of the latter on kink formation. One can see in the figure that for relatively short energy relaxation times–in our instance for $T_\parallel/T_\perp = 10^2$–the emerging kinks survive only briefly: the energy dissipation eventually takes its toll over longer distances.

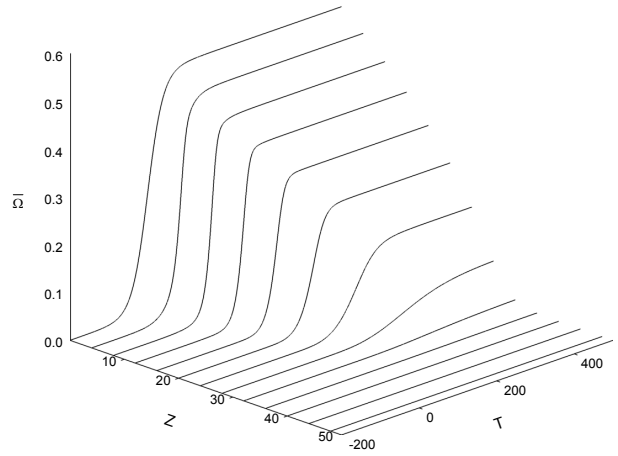


Figure 4.4: Dimensionless Rabi frequency $\overline{\Omega}$ of a forming kink as a function of dimensionless time, $\gamma_\perp \tau$, and propagation distance $\alpha\zeta$. The ratio of transverse to longitudinal relaxation times is $T_\perp/T_\parallel = 10^{-2}$. The initial parameters are $\Omega_0 = 0.5\gamma_\perp$ and $\tau_p = 20T_\perp$.

## 4.5 Physical Model

Finally, we briefly mention the systems in which present kinks can be realized. The characteristic transverse and longitudinal relaxation times for solids, doped with resonant atom impurities, fall into the ranges $10^{-6} \leq T_\parallel \leq 10^{-3}$ and $10^{-13} \leq T_\perp \leq 10^{-11}$ s [57, 58], respectively. Thus, $10^5 \leq \gamma_\perp/\gamma_\parallel \leq 10^{10}$, which makes solids ideal for realization of the novel kinks, provided inhomogeneous broadening can be reduced by preparing clean enough samples. At the same time, relaxation times for bulk semiconductors, doped with quantum dots, range as follows, $10^{-12} \leq T_\parallel \leq 10^{-4}$ and $10^{-13} \leq T_\perp \leq 10^{-12}$ s [57]. Consequently, $1 \leq \gamma_\perp/\gamma_\parallel \leq 10^9$, and hence our kinks can be realized in some semiconductor systems as well.

## 4.6 Conclusion

In conclusion, we have discovered and analytically described a novel class of self-similar waves in resonant nonlinear media, optical kinks. The present kinks can form in two-level media under the assumption that the longitudinal relaxation time is much longer than the transverse one. Thus a wide range of intermediate propagation distances exists over which the kinks are formed as a result of the interplay of optical nonlinearity and the phase (transverse) relaxation processes; yet the influence of the energy (longitudinal) relaxation

processes is still negligible. We stress, however, that our results pertain to the case of negligible inhomogeneous broadening, which requires rather clean samples, and for chirp-free waves. We conjecture that the presence of a chirp may lead to oscillatory kink profiles.

# Chapter 5

# Optical Shocks in Resonant Media: The Role of Inhomogeneous Broadening

Soodeh Haghgoo and Sergey A. Ponomarenko

Publication Status: Accepted in Optics Communications, September 2012

## 5.1 Abstract

We discover and numerically describe optical shock wave formation in inhomogeneously broadened resonant nonlinear media. Our results extend our previous work to the case of inhomogeneously broadened two-level media. We also describe in detail the atomic variable behavior as the optical shocks form in the medium.

## 5.2 Introduction

Shock waves have been discovered in a variety of physical systems, including fluids and gases [42, 43]. In general, shock waves are generated by sudden and violent changes in pressure, density, and/or temperature. In most fluid systems, the energy of shocks dissipates due to the viscous damping in the medium through which it travels. However, systems such as cold plasmas [59–62], superfluids and Bose-Einstein condensates [63–66], where the viscosity and damping effects are negligible, support dispersive shock waves.

Shock waves in optics have also been examined by invoking the analogy between superfluid and nonlinear optical wave behaviors [67–69]. The analogy has been explored in Ref. [70] to explain the observed behavior of dispersive optical shocks–which are the optical equivalent of condensate shock waves–in the spatial domain. Dispersive optical shocks have also been observed in the temporal domain using ultrashort pulses in optical fibers [54, 71–78].

At the same time, much less attention has been devoted to optical shocks in resonant nonlinear media. Nevertheless, we have shown elsewhere [31] that in homogeneously

broadened resonant nonlinear absorbers, optical shocks are formed as intermediate self-similar asymptotics of any incident pulse with a long tail in the trailing edge. In particular, such shocks can be generated in solids, doped with resonant impurities, and bulk semiconductors, doped with quantum dots. However, in the systems we discussed in Ref. [31], the inhomogeneous broadening plays an important role in shaping the input pulse and hence it cannot be really ignored.

In this paper, we explore the possibility of shock-like pulse formation in resonant nonlinear media in the presence of inhomogeneous broadening. We show that similar to our previous work [31], the interplay between the optical nonlinearity and the transverse relaxation processes–which are responsible for the temporal width of the shocks–cause self-steepening of the input pulse and shock formation. On the other hand, the longitudinal relaxation processes lead to decay and eventual disappearance of the shocks. We stress that the discovered optical shocks form in the pulse envelope, with their charectristic width being determined by the dipole relaxation time. The latter is much longer than an optical cycle, thereby justifying the use of the slowly varing envelope approximation.

## 5.3 Mathematical Preliminaries and Physical Model

We model the resonant medium as a two-level system with the resonance frequency $\omega_0$. We assume that the transverse (dipole) relaxation time $T_\perp$ is much shorter than the longitudinal (energy) one, $T_\parallel$, yet much longer than an optical cycle,

$$\omega_0^{-1} \ll T_\perp \ll T_\parallel. \tag{5.1}$$

The inequality (5.1) implies that the atomic dipole moments evolve much faster than the atomic population dynamics unfolds. By this assumption, the shocks are formed by atomic dipole evolution over a much shorter distance than that over which energy dissipation takes its toll. We consider solids, doped with resonant atoms [8], or bulk semiconductors, doped with quantum dots [55] as particular realizations of the system. The characteristic transverse and longitudinal relaxation times for solids doped with resonant atom impurities, fall into the ranges $10^{-6} \leq T_\parallel \leq 10^{-3}$ and $10^{-13} \leq T_\perp \leq 10^{-11}$ s [57], respectively, implying $10^5 \leq T_\parallel/T_\perp \leq 10^{10}$. Also, relaxation times for bulk semiconductors doped with quantum dots range as follows, $10^{-12} \leq T_\parallel \leq 10^{-4}$ and $10^{-13} \leq T_\perp \leq 10^{-12}$ s [57] such that

$1 \leq T_{\|}/T_{\perp} \leq 10^9$. Therefore our results are applicable to many physical systems, including all solids and some semiconductor systems.

We consider a light pulse with a carrier frequency $\omega$ near the optical resonance frequency $\omega_0$ of a two-level atom medium. We also assume that the pulse spectrum is mainly affected by inhomogeneous broadening. Under these conditions, the slowly varying field envelope of the pulse in terms of the transformed coordinate and time, $\zeta = z$ and $\tau = t - z/c$, obeys the reduced wave equation

$$\frac{\partial \Omega}{\partial \zeta} = \frac{\omega N |d_{eg}|^2}{c\varepsilon_0 \hbar} < \sigma > . \tag{5.2}$$

Here $\Omega = 2d_{eg}\mathscr{E}/\hbar$ is the Rabi frequency associated with the pulse amplitude $\mathscr{E}$, $N$ is a density of impurity atoms, $d_{eg}$ is a dipole matrix element between the ground and excited states of any atom; the two relevant atomic states are appropriately labeled with the indices $g$ and $e$, and $\sigma$ is a dipole envelope function of atomic dipole moment. The average over a distribution of frequency detunings from atomic resonances, $\Delta = \omega - \omega_0$, is defined as

$$< \sigma > \equiv \int d\Delta g(\Delta)\sigma(\Delta). \tag{5.3}$$

In this work, we assume the inhomogeneous broadening distribution to be a generic Gaussian function in the form

$$g(\Delta) = \frac{1}{\sqrt{2\pi}\delta} \exp\left(-\frac{\Delta^2}{2\delta^2}\right), \tag{5.4}$$

where $\delta$ is a spectral width of inhomogeneous broadening. The quantum dipole moment $\sigma = u - iv$ and inversion $w$ envelope functions obey the Bloch equations which can be written as [8]

$$\partial_\tau \sigma = -(\gamma_\perp + i\Delta)\sigma - i\Omega w, \tag{5.5}$$

$$\partial_\tau w = -\gamma_{\|}(w - w_{eq}) - \tfrac{i}{2}(\Omega^* \sigma - \Omega \sigma^*). \tag{5.6}$$

Here $\gamma_\perp$ and $\gamma_{\|}$ are defined as the corresponding inverse transverse relaxation time and energy relaxation time, $T_\perp$ and $T_{\|}$, respectively. Since a constant background intensity at the trailing edge of the input wave is required to produce a shock, we then consider as an initial condition, a Q-switched laser input of the form

$$\Omega(0,t) = \frac{\Omega_0}{1 + e^{-t/\tau_p}}, \tag{5.7}$$

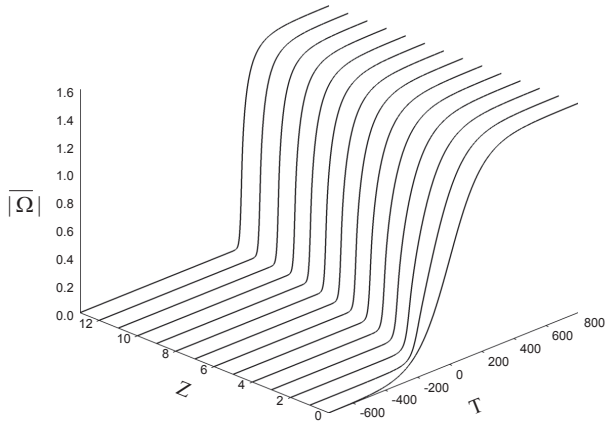


Figure 5.1: Dimensionless Rabi frequency $\overline{\Omega}$ of a forming shock as a function of dimensionless time, $T$, and propagation distance $Z$. The ratio of transverse to longitudinal relaxation times is $T_\perp/T_\parallel = 10^{-7}$. The initial parameters are $\Omega_0 = 1.5\gamma_\perp$, and $\tau_p = 100T_\perp$.

where $\Omega_0$ is the amplitude – measured in frequency units – of the cw laser field and $\tau_p$ is a characteristic time constant of the switching process. Hereafter, it will prove convenient to introduce dimensionless variables as $T = \gamma_\perp \tau$, $Z = \alpha\zeta$; $\alpha = kN|d_{eg}|^2/\sqrt{2\pi}\varepsilon_0\delta\hbar$, being a linear absorption coefficient, $\overline{\Omega} = \Omega/\gamma_\perp$, $\overline{\Delta} = \Delta/\gamma_\perp$, and recast Eqs. (5.2) – (5.7).

### 5.4 Numerical Simulations

We then numerically solve Eq. (5.2), together with the Bloch equations (5.5) and (5.6), subject to the initial condition (5.7). The simulations reveal the existence of a shock-like solution for the Rabi frequency. In Fig. 5.1, we show shock formation for sufficiently long energy relaxation times, $T_\parallel/T_\perp = 10^7$, and the other parameters such that $\delta = 10^{12}s^{-1}$, and $T_\perp = 10^{-13}s$. A fast self-steepening stage results in the steady-state shock formation. It can be inferred from the figure that the shock structure, which is determined by the magnitude of the Rabi frequency jump $\Omega_0$, becomes steep as it propagates in the medium.

Our numerical simulations show that to form a shock, $\Omega_0$ may not be less than a certain critical value $\Omega_c$, which depends on the magnitude of $\gamma_\parallel$. The presence of a critical power threshold for shock formation is necessary because the incident wave should have enough power to overcome energy losses due to longitudinal relaxation processes. In our case, $T_\parallel/T_\perp = 10^7$, the critical amplitude is found to be $\Omega_c = 7\times10^6\gamma_\parallel \simeq 7\times10^{12}$ s$^{-1}$. Translating this to real life units, we can estimate the critical intensity required to form a shock, $I_c = \varepsilon_0 nc\hbar^2\Omega_c^2/8d_{eg}^2$. Estimating the dipole moment of a typical impurity atom in a solid

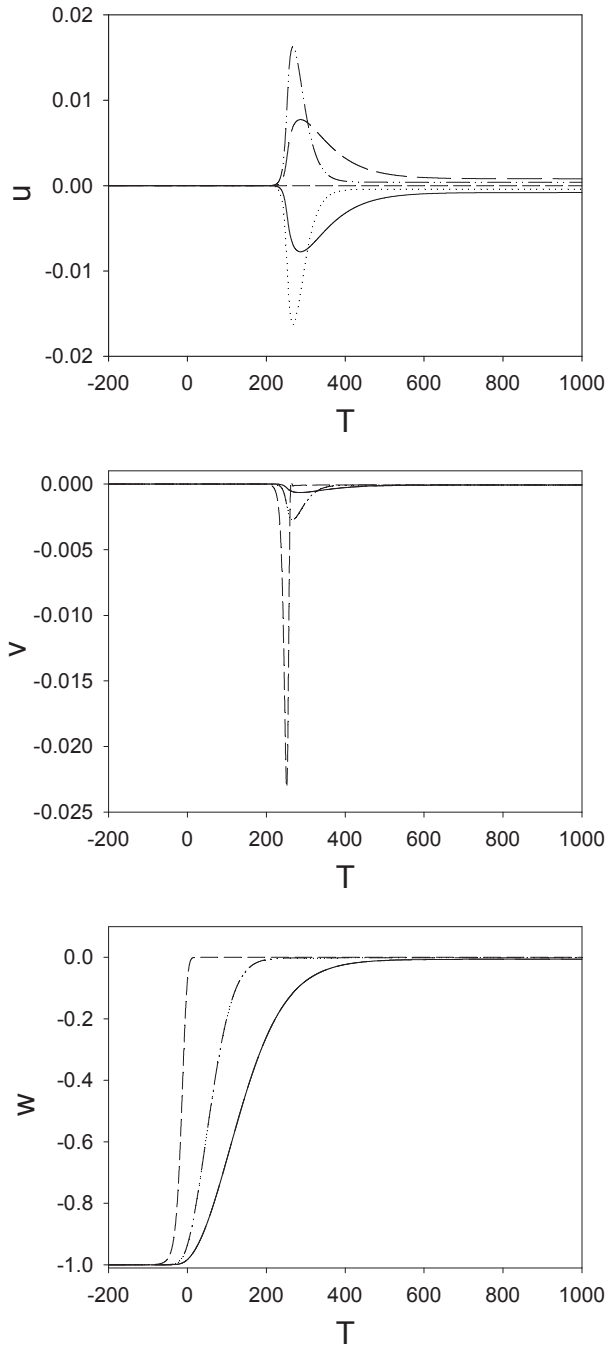


Figure 5.2: Atomic dipole moment components ($u$, $v$) and one-atom inversion $w$ as functions of dimensionless time, $T$, displayed at several dimensionless frequency detuning, $\overline{\Delta}$, and at the propagation distance, $Z = 13$: Solid, $\overline{\Delta} = -12$; dotted, $\overline{\Delta} = -6$; dashed, $\overline{\Delta} = 0$; dash-dotted, $\overline{\Delta} = 6$; and long-dashed, $\overline{\Delta} = 12$.

to be $d_{eg} \simeq 2 \times 10^{-29}$ C m [8] and the refractive index of a bulk solid material as $n \simeq 2$, we arrive at a rough estimate $I_c \simeq 10$ MW/cm$^2$, which is an order-of-magnitude below the

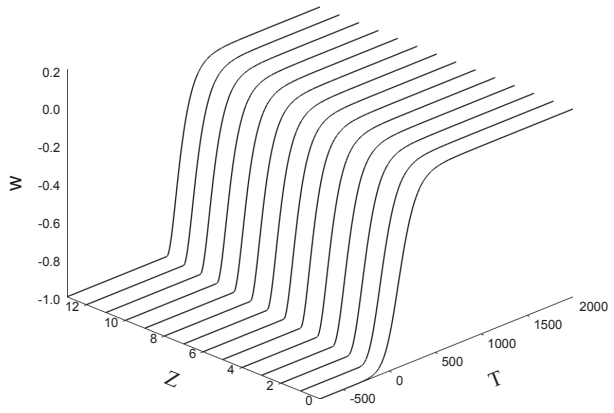


Figure 5.3: One-atom inversion $w$ as a function of dimensionless time, $T$, displayed at several propagation distances, and $\overline{\Delta} = 15$. The ratio of transverse to longitudinal relaxation times is $T_\perp/T_\parallel = 10^{-7}$. The initial parameters are $\Omega_0 = 1.5\gamma_\perp$, and $\tau_p = 100T_\perp$.

optical breakdown intensity of a typical solid [79]. One would then have to use high power Q-switched lasers to generate the proposed optical shocks.

To better understand shock formation and to elucidate the role of inhomogeneous broadening, the time evolution of the atomic variables, $u$, $v$, and $w$ is displayed in Fig. 5.2 for several values of $\Delta$ . First, we observe that at a fixed $Z$, $w$ evolution mimics that of the shock amplitude. The reason being that at the leading edge of the shock–where its amplitude is low–no atom inversion takes place and $w$ remains close to its initial value, $w_0 = -1$. On the other hand, a large shock amplitude at the trailing edge saturates the medium implying that $w_\infty = 0$. By the same token, the absorptive component $v$ of the atomic dipole moment peaks only at the trailing edge of the $w$ profile where there is a substantial probability–roughly a half–to find an impurity atom in its excited state. Although the behavior of $v$ is independent of the sign of $\Delta$, its peak amplitude strongly depends on the detuning: the magnitude of the peak is reduced precipitously as the detuning from resonance increases. The dispersive component $u$ does depend on the sign of $\Delta$. And, unlike $v$, it is more pronounced for the atoms that are farther detuned from resonance. The presence of finite $u$ causes pulse chirping which, in turn, results in smoothing out the transition between the shock edges.

Finally, to explain the behavior of the inversion, we display in Fig. 5.3, the time evolution of inversion for different propagation distances at a fixed frequency detuning. As we can see in the figure, at the leading edge of the shock, where the light intensity is very small, the atomic population is hardly affected by the pulse such that the one-atom inversion is approximately given by its equilibrium value, $w_{eq} = -1$. At the trailing edge, however, a

large pulse amplitude saturates the medium, implying zero inversion.

## 5.5 Conclusion

In summary, we have numerically shown that the results of our previous work [31] on the novel class of optical shocks in resonant nonlinear media, can be qualitatively extended to the case of inhomogeneously broadened media. The shocks are formed as a result of the interaction between optical nonlinearity and the transverse relaxation processes in the limit of negligible energy relaxation processes.

# Chapter 6

# Self-Induced Transparency Quadratic Solitons

Soodeh Haghgoo and Sergey A. Ponomarenko
Published in: Optics Express, June 2012, Vol. 20, 13988.
URL: http://www.opticsinfobase.org/oe/abstract.cfm?uri=oe-20-13-13988


## 6.1 Abstract

We discover and theoretically explore self-induced transparency quadratic solitons (SIT-QS) supported by the media with quadratic optical nonlinearities, doped with resonant impurities. The fundamental frequency of input pulses is assumed to be close to the impurity resonance. We envision an ensemble of inhomogeneously broadened semiconductor quantum dots (QD) in the strong confinement regime grown on a substrate with a quadratic nonlinearity to be a promising candidate for the laboratory realization of SIT-QS. We also examine the influence of inhomogeneous broadening as well as wave number and group-velocity mismatches on the salient properties of the introduced solitons.

## 6.2 Introduction

The solitons have been at the heart of nonlinear physics for more than three decades. The reason being they emerge as ultimate survivors of virtually any wave evolution scenario in conservative nonlinear systems of unprecedented physical diversity, from hydrodynamic [42, 80] and plasma waves [80] to pulses in optical fibers [81] and matter waves in Bose-Einstein condensates [81, 82]. In the optical context in particular, the interest in the quadratic solitons (QS), which are coupled self-trapped entities in the media with quadratic nonlinearities, has been recently reinvigorated thanks to the advances in fabrication of phase matching structures, see Ref. [83] for a review.

Although the history behind QS can be traced back to 1967 when Ostrovskii discovered self-induced phase changes in nonlinearly coupled fundamental wave (FW) and second harmonic (SH) in a noncentrosymmetric crystal [84, 85], the QS were not experimentally observed for a while. As soon as high-damage optical materials with long enough interaction lengths became available, however, spatial QS were observed in the bulk $\chi^{(2)}$ media [86] and in planar $\chi^{(2)}$ waveguides [87].

On the other hand, most common quadratic materials have very low group-velocity dispersion (GVD) and fairly large group-velocity mismatch (GVM). Thus, extremely long samples and/or short pulses are required to explore the quadratic soliton regime [83]. These obstacles hampered temporal QS generation until the application of an ingenious technique for tailoring GVD and GVM culminated in the experimental observation of their key signatures [88]. Yet, in the pioneering experiment [88] the nonlinear crystal was too short and pulses too long to unequivocally observe a dispersion-free propagation regime over several dispersion lengths. Thus, the existence of alternative routes to temporal QS formation–not relying on balancing $\chi^{(2)}$ nonlinearities with the GVD–is a highly relevant question, which, to our knowledge, has not yet been adequately addressed. We note, however, that in the three-wave interaction situation in $\chi^{(2)}$-media, neutrally stable QS were discovered [89] which do not rely on the GVD for their existence, but require three waves with different carrier frequencies to mix.

In this paper, we present a new type of QS, self-induced transparency quadratic solitons (SIT-QS), formed in resonant $\chi^{(2)}$ media. The SIT-QS generation does not at all require any bulk medium GVD, thereby circumventing the major obstacle for temporal $\chi^{(2)}$ soliton generation. The proposed SIT-QS have a hybrid nature: the mutual self-trapping of FW and SH is achieved by the joint action of both resonant nonlinearity, induced by exciting one-exciton transitions in QDs, and the quadratic nonlinearity of the bulk medium. Specifically, we assume that an input FW pulse is nearly resonant with one-exciton transitions in QDs, grown and randomly spread over a substrate exhibiting a quadratic nonlinear optical response. As the FW pulse enters the medium, it coherently excites the QD ensemble and– provided the pulse has a right area– it can open a "transparency window" in the medium leading to the fundamental soliton formation via the SIT phenomenon [8]. At the same time, the SH is generated via the $\chi^{(2)}$ nonlinearity, provided a characteristic resonant

absorption length is of the same order as a typical length associated with the bulk $\chi^{(2)}$ nonlinearity. The SH pulse is "dragged" by the FW into the transparency window forming a mutually self-trapped SIT-QS pair. We stress that our results reveal a hitherto unbeknown extension of quantum optical SIT solitons to the realm of quadratic solitons in $\chi^{(2)}$ media.

Next, we emphasize that the SIT-QS formation demands neither large GVD nor extremely high input pulse intensity–and hence ultrashort duration–which sets them apart from the conventional temporal QS in quadratic media. Further, the discovered SIT-QS are fundamentally different from the previously reported small-amplitude quasisolitons supported by resonant media with quadratic nonlinearities [90]. First, while the latter exist for large wave number mismatch, the SIT-QS require rather accurate phase matching which can be realized in quasi-phase-matched structures. More importantly, though, the QS of Ref. [90] are supported by media with collective plasmonic resonances which, being far from saturation, can be modeled by the classical anharmonic oscillator model. In contrast in the SIT-QS case, the FW interaction with an ensemble of individual QD resonances involves a swift time evolution of the QD level populations which can only be adequately described quantum mechanically.

### 6.3 Quantitative Analysis and Physical Model

We now present our quantitative model. We begin by examining short pulse propagation in a $\chi^{(2)}$ medium, randomly doped with QDs. The dopants can be modeled as two-level systems. The fundamental pulse carrier frequency $\omega$ is assumed to be very close to the resonance frequency $\omega_0$ of a one-exciton transition in a QD; bi-exciton transitions in the QD ensemble are forbidden by restricting ourselves to the case of circularly polarized FW and SH pulses [91]. Thus, only is the FW resonantly coupled with the exciton transition, while the SH is only coupled with the FW via the $\chi^{(2)}$ nonlinearity. Provided the cubic nonlinear effects are negligible [92], the slowly varying field envelopes $\mathscr{E}_1$ and $\mathscr{E}_2$ of the fundamental and second harmonic pulses, respectively, obey the coupled wave equations

$$\left(\frac{\partial}{\partial z}+\frac{1}{v_{g1}}\frac{\partial}{\partial t}\right)\mathscr{E}_1=\frac{iNd_{eg}\omega^2}{2k_1\varepsilon_0c^2}<\sigma>-\frac{i\omega^2\chi_{eff}^{(2)*}}{2k_1c^2}\mathscr{E}_1^*\mathscr{E}_2e^{i\Delta kz}, \tag{6.1}$$

$$\left(\frac{\partial}{\partial z}+\frac{1}{v_{g2}}\frac{\partial}{\partial t}\right)\mathscr{E}_2=-\frac{i\omega^2\chi_{eff}^{(2)}}{k_2c^2}\mathscr{E}_1^2e^{-i\Delta kz}. \tag{6.2}$$

Here $v_{g1}(v_{g2})$ is a group velocity of the fundamental (second harmonic) pulse, $\chi^{(2)}_{eff}$ is an effective second-order susceptibility of the bulk medium, $\Delta k = 2k_1 - k_2$ is a wave number mismatch factor, $N$ is a density of dopants, $d_{eg}$ is a dipole matrix element of the ground-to-excited state QD transition – the states are appropriately labeled by the indices $g$ and $e$ – and $\sigma$ is a quantum dipole envelope function describing the temporal evolution of the QD dipole moment. Further, the quantum dipole moment $\sigma$ and inversion $w$ envelope functions obey the Bloch equations which can be written in the circular polarization basis as [8, 93]

$$\partial_\tau \sigma = -(\gamma_\perp + i\Delta)\sigma - i\Omega_1 w, \tag{6.3}$$

$$\partial_\tau w = -\gamma_\parallel (w - w_{eq}) - \tfrac{i}{2}(\Omega_1^* \sigma - \Omega_1 \sigma^*). \tag{6.4}$$

Here we introduced the Rabi frequencies, $\Omega_{1,2} = 2d_{eg}\mathscr{E}_{1,2}/\hbar$ of the FW and SH as well as the transverse (dipole) and longitudinal (energy) relaxation rates as $\gamma_\perp$ and $\gamma_\parallel$, respectively.

Hereafter, it will prove convenient to transform to the reference frame moving with the fundamental pulse by changing variables viz., $\tau = t - z/v_{g1}$ and $\zeta = z$. In the dimensionless variables, $Z = \zeta/L_A$, $T = \tau/\tau_p$ and $\overline{\Omega}_{1,2} = \Omega_{1,2}\tau_p$, the coupled wave equations take the form

$$\frac{\partial \overline{\Omega}_1}{\partial Z} = i < \sigma > -\frac{iL_A}{4L_{NL}} \overline{\Omega}_1^* \overline{\Omega}_2 e^{i(\delta Z + \phi_0)}, \tag{6.5}$$

and

$$\left( \frac{\partial}{\partial Z} + \frac{s_\pm L_A}{L_W} \frac{\partial}{\partial T} \right) \overline{\Omega}_2 = -\frac{ik_1 L_A}{2k_2 L_{NL}} \overline{\Omega}_1^2 e^{-i(\delta Z + \phi_0)}. \tag{6.6}$$

Here $\tau_p$ is a characteristic duration of the input FW pulse, $\delta = \Delta k L_A$ is the dimensionless wave number mismatch, $\phi_0$ is a constant relative phase of the effective susceptibility and the dipole matrix element, and $s_\pm = +1(-1)$ for $\nu > 0 (< 0)$ specifies the sign of the group-velocity mismatch (GVM), $\nu = v_{g2}^{-1} - v_{g1}^{-1}$. Further, we introduced three key physical length scales to this problem: the linear absorption length $L_A$, the walk-off length $L_W$ associated with the group velocity mismatch (GVM) of the fundamental and second-harmonic pulses, and the characteristic nonlinear length $L_{NL}$ in the $\chi^{(2)}$ medium defined as

$$L_A = \frac{1}{\alpha}; \qquad L_W = \frac{\tau_p}{|\nu|}; \qquad L_{NL} = \frac{k_1 c^2 |d_{eg}| \tau_p}{\hbar \omega^2 |\chi_{eff}|}, \tag{6.7}$$

where $\alpha = N|d_{eg}|^2 \omega^2 / \sqrt{2\pi}\hbar b k_1 \varepsilon_0 c^2$ is a linear absorption coefficient, and $b$ is a spectral

width of inhomogeneous broadening.

Next, the average over a distribution of dimensionless frequency detunings from one-exciton resonances in QDs, $\overline{\Delta} = (\omega - \omega_0)\tau_{\rm p}$, is defined as

$$<\sigma>\equiv \int d\overline{\Delta} g(\overline{\Delta})\sigma(\overline{\Delta}). \tag{6.8}$$

In this work, we assume the inhomogeneous broadening distribution to be a generic Gaussian function in the form

$$g(\overline{\Delta}) = \frac{1}{\sqrt{2\pi}b\tau_{\rm p}} \exp\left(-\frac{\overline{\Delta}^2}{2b^2\tau_{\rm p}^2}\right). \tag{6.9}$$

In the coherent transient regime we explore, the pulses must be short enough: $\tau_{\rm p} \ll \min(T_\perp, T_\parallel)$, where $T_\perp = \gamma_\perp^{-1}$ and $T_\parallel = \gamma_\parallel^{-1}$ are the transverse and longitudinal relaxation times. Thus, the Bloch Eqs. (6.3) and (6.4) reduce to

$$\partial_T \sigma = -i\overline{\Delta}\sigma - i\overline{\Omega}_1 w, \tag{6.10}$$

$$\partial_T w = -\tfrac{i}{2}(\overline{\Omega}_1^*\sigma - \overline{\Omega}_1\sigma^*). \tag{6.11}$$

In our numerical simulations, we consider In(Ga)As QDs grown on a GaAs substrate as a prototype for our system. GaAs is known to have a sizable second-order nonlinearity, $\chi^{(2)}_{{\rm e}ff} \simeq 2\times 10^{-10}$ m/V [94]. Moreover, high efficiency SHG was experimentally demonstrated in the medium thanks to efficient quasi-phase matching in orientation-patterned GaAs samples [95, 96]. We take $N \simeq 10^{21}\ m^{-3}$, the dipole moment matrix element to be $d_{eg} \simeq 5\times 10^{-29}$ Cm, all magnitudes consistent with recent simulations [55, 97] and experimental work [97, 98].

Further, we work with the input $2\pi$-pulses in the picosecond range, say, $\tau_{\rm p} \simeq 1$ ps which is also consistent with the previous experimental and numerical work on SIT on bound [97] and free [99] exciton resonances. As the characteristic relaxation times for typical QDs are $T_\perp \simeq 2T_\parallel \sim 100$ps at room temperature– and are several times longer if the sample is cooled down to cryogenic temperatures [100]– the pulses are well within the coherent transient regime. The inhomogeneous broadening width depends on the ensemble preparation; a typical estimate runs as $b \simeq 10^7$ MHz [55]. Using the above numerical values, we estimate

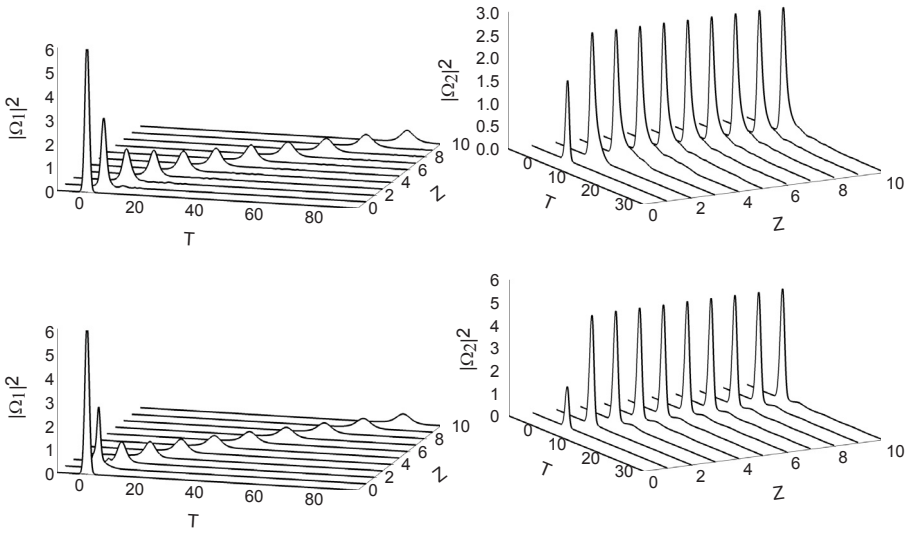


Figure 6.1: Top row: intensity profiles of the FW and SH soliton pair. The parameters are $b = 10^7$MHz, $\delta = 0$, and $L_W = \infty$. Bottom row: same as the top row except there is no inhomogeneous broadening.

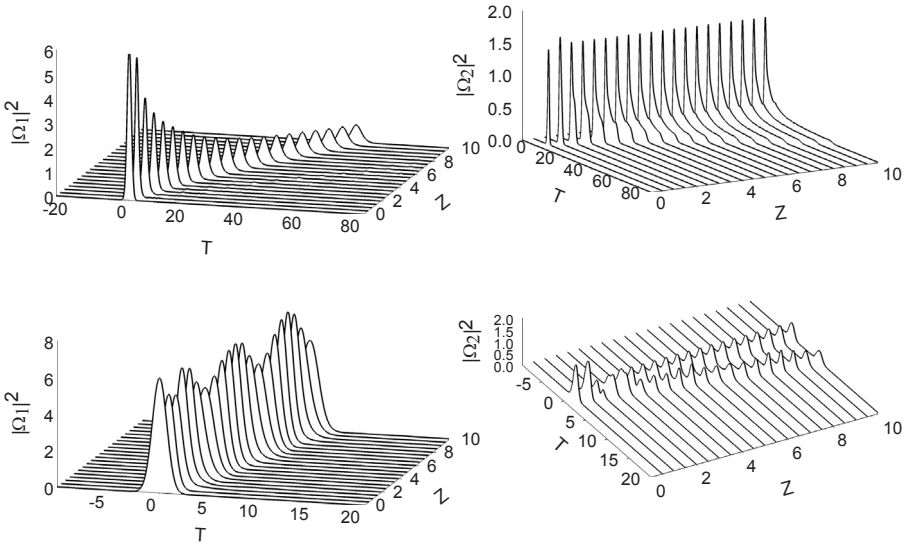


Figure 6.2: Top row: intensity profiles of the FW and SH soliton pair. The parameters are $b = 10^7$MHz, $\delta = 3$, and $L_W = \infty$. Bottom row: same as above except $b = 0$.

$L_{\mathrm{A}} \simeq 1.5$ mm and $L_{\mathrm{NL}} \simeq 0.8$ mm, implying that $L_{\mathrm{A}} \sim L_{NL}$ which is favorable for the SIT-QS pair formation. Taking into account that $\nu$ is typically in the range 0.1-1 ps/mm for most $\chi^{(2)}$ crystals [101], we estimate $L_{\mathrm{W}}$ to fall in the range from 1 mm to 1 cm.

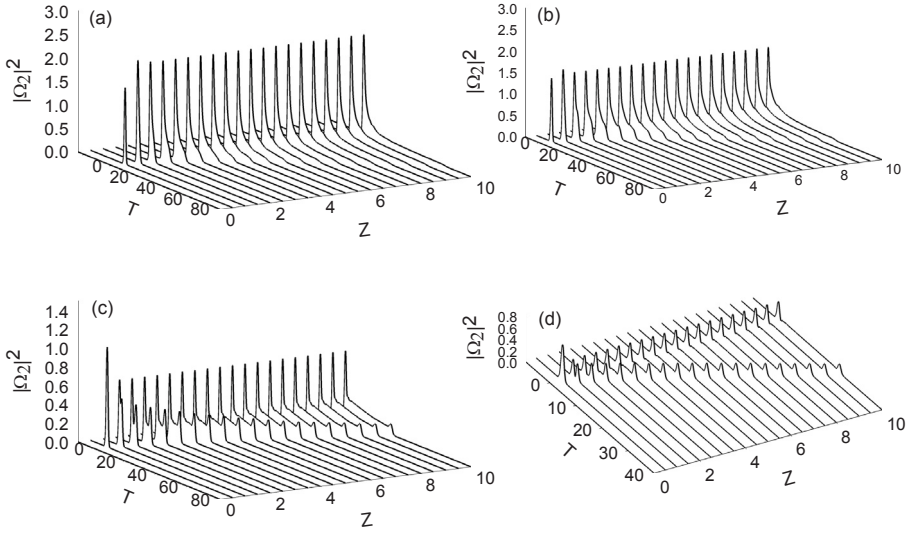


Figure 6.3: Intensity profile of the SH wave for (a) $\delta = 2$, (b) $\delta = 3$, (c) $\delta = 5$ and (d) $\delta = 7$. The other parameters are $b = 10^7$MHz and $L_W = \infty$.

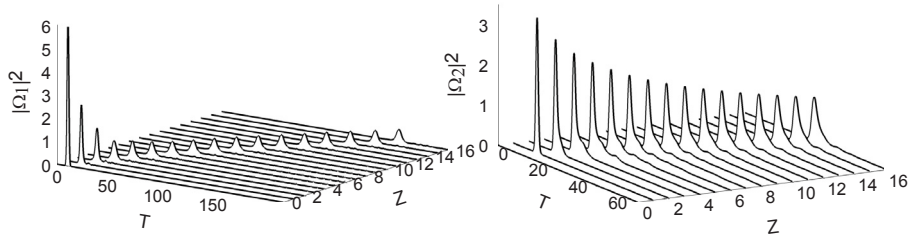


Figure 6.4: Intensity profiles of the FW and SH soliton components. The parameters are $b = 10^7$MHz, $\delta = 1$, and $L_W = 1$mm.

## 6.4 Numerical Simulations

A qualitative analysis–borne out by subsequent numerical simulations–reveals that the SIT-QS formation and stability crucially depend on the magnitudes of the four factors: inhomogeneous broadening width, wave number mismatch, temporal walk-off length, and the area of the incident fundamental pulse. In our numerical simulations using Eqs. (6.5) and (6.6) as well as Eqs. (6.8) – (6.11), we consider a $2\pi$-Gaussian input FW pulse entering the medium; we assume there is no power in the SH at $Z = 0$. To illustrate the SIT-QS formation in the presence of inhomogeneous broadening, we exhibit in Fig. 6.1 the evolution of the FW and SH pulse intensities as functions of the propagation distance $Z$. For simplicity, we assume perfect phase matching and no temporal walk-off. It is seen in the figure that

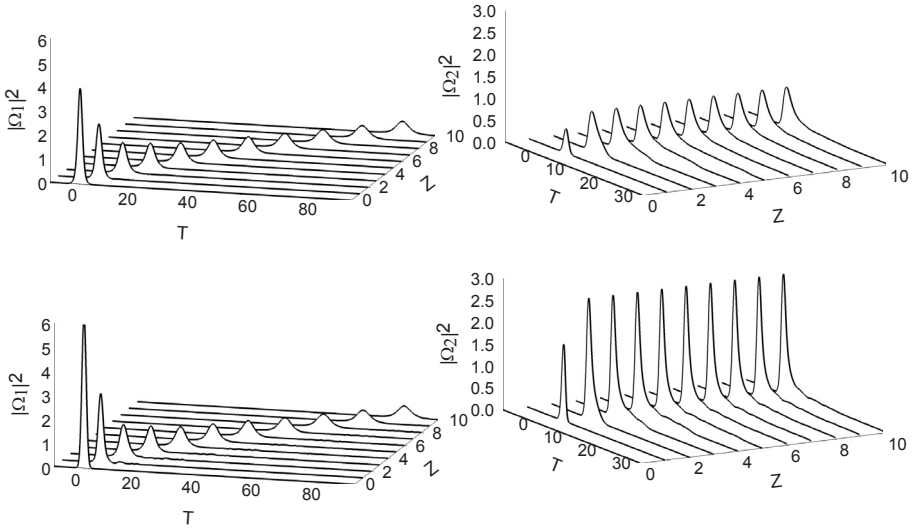


Figure 6.5: Intensity profiles of the FW and SH soliton pair for secant hyperbolic (top row) and Gaussian (bottom row) input $2\pi$ fundamental pulses. The other parameters are $b = 10^7$MHz, $\delta = 0$ and $L_W = \infty$.

a stable SIT-QS pair emerges over two characteristic propagation distances for an inhomogeneously broadened sample with $b = 10^7$MHz (top row of Fig. 6.1). We stress that we have numerically propagated the solitons over several dozens of characteristic absorption lengths and found no trace of instability. For comparison, the SIT-QS pair formation is also displayed for an ideal homogeneously broadened sample in the bottom row of Fig. 6.1. We observe that as the resonant light-QD interaction efficiency decreases due to the inhomogeneous broadening–which is always present for realistic QD samples–the second-harmonic soliton pulse develops a tail at the trailing edge.

Next, we examine the role of inhomogeneous broadening in the SIT-QS formation with a finite phase mismatch. In Fig. 6.2 we compare the SIT-QS pair formation in the presence of the wave number mismatch, $\delta = 3$ in homogeneously and inhomogeneously broadened samples. It is seen in the figure that in a perfectly clean sample even a moderate phase mismatch causes breathing of the FW and splitting of the SH pulses, respectively. In contrast, the inhomogeneous broadening inhibits the instability and promotes stable SIT-QS pair generation albeit with the SH component developing a tail at the trailing edge.

The tail, however, grows rather slowly (adiabatically) on propagation, implying that the SH component can be interpreted as a quasi-stable soliton even in the moderate phase

mismatch situation. As the phase mismatch increases, though, the inhomogeneous broadening can no longer prevent the SH component break-up into two small-amplitude pulses. This situation is clearly illustrated in Fig. 6.3 where the SH component intensity profile is displayed for four values of the dimensionless wave number mismatch. Thus, we conclude that while the inhomogeneous broadening plays a stabilizing role, the lack of the perfect phase matching can result in the internal dynamics of the SIT-QS leading to their eventual disintegration.

Further, we study the temporal walk-off influence on the SIT-QS dynamics. In Fig. 6.4 we plot the SIT-QS pair formation for the case of an inhomogeneously broadened sample with a modest wave number mismatch, $\delta = 1$ and with the walk-off length of 1 mm. As is seen in the figure, a stable SIT-QS pair is generated, although the peak amplitude of the SH component decreases on the soliton propagation as the overlap between the FW and SH is reduced due to walk-off. Thus the SIT-QS formation is possible even in the presence of a rather substantial temporal walk-off.

Next, we performed a number of numerical simulations with the input FWs of various temporal profiles, including Gaussian and secant hyperbolic. The latter corresponds to a fundamental SIT soliton in the FW component. Our simulations indicate that salient features of the SIT-QS formation are largely insensitive to the initial temporal profile of the fundamental pulse. To illustrate this point, we present in Fig. 6.5 a comparison of the SIT-QS evolution for the $2\pi$-secant hyperbolic (top row) and Gaussian (bottom row) input pulses for the perfectly phase-matched situation with zero GVM, for simplicity. One can see in the figure that although the efficiency of SHG with secant hyperbolic pulses is reduced, the key qualitative features of the SIT-QS pair persist. In physical terms, the different SHG efficiency is explained by the fact that powers of the input $2\pi$ Gaussian and secant hyperbolic pulses are quite different, of course.

On the other hand, the SIT-QS evolution scenario strongly depends on the input FW area, $\mathscr{A} \equiv \int_{-\infty}^{\infty} \Omega_1 d\tau$. In fact, we discovered that no SIT-QS formation is possible whenever the magnitude of $\mathscr{A}$ is below $\pi$. For any input FW pulse with the area, $\pi \leq \mathscr{A} \leq 2\pi$, though, the area magnitude goes through several oscillatory cycles, asymptotically attaining the value of $2\pi$; the same holds true for pulses with the area greater than $2\pi$. The oscillatory transient dynamics of the area distinguishes the SIT-QS case from the pure SIT case in which the area monotonously approaches $2\pi$ [8].

## 6.5 Conclusion

In conclusion, we have discovered and numerically explored a new type of solitons, self-induced transparency quadratic solitons supported by noncentrosymmetric nonlinear media, doped with resonant impurities. We have shown that the SIT-QS evolution and stability does not depend on the shape of the input FW, but are strongly influenced by the interplay of inhomogeneous broadening and phase mismatch in the system. Whereas the former is a stabilizing factor, the latter causes the instability that can result in the QS disintegration. To experimentally realize the envisioned SIT-QS, we recommend that relatively long–a few centimeter long, say–quasi-phase-matched samples be used. We have also demonstrated that the GVM does not substantially affect the SIT-QS formation as long as the samples are sufficiently short. To mitigate–to the point of eliminating–the GVM effects in long samples, one can use tilted input pulses, following the technique of Ref. [88]. Finally, we note that although we considered only quadratic bulk nonlinearities in the manuscript [92], the third-order nonlinearities can become important for femtosecond input pulses and/or sufficiently large phase mismatch. The resulting competition between $\chi^{(2)}$- and $\chi^{(3)}$-effects, similar to those discussed in Ref. [102], can lead to new interesting soliton regimes in the system. We plan to address this issue in the new context of SIT-QSs in a forthcoming publication.

# Chapter 7

# Spatial Optical Similaritons in Conservative Nonintegrable Systems

Sergey A. Ponomarenko and Soodeh Haghgoo

Published in: Physical Review A, May 2010, Vol. 81, 051801.
URL: http://pra.aps.org/abstract/PRA/v81/i5/e051801



## 7.1 Abstract

We demonstrate analytically and numerically that stable spatial similaritons can be supported by homogeneous conservative optical media with quintic nonlinearities. Unlike previously discussed spatial similaritons, the novel waves may exist in a broad parameter regime. We also present a generic model for a quintic nonlinearity by considering a centrosymmetric nonlinear medium doped with resonant impurities in the limit of a large light carrier frequency detuning from impurity resonance.

## 7.2 Introduction

Similarity and self-similarity have been recurring themes in various branches of nonlinear physics, including nuclear physics, gas dynamics, fracture and fluid mechanics, and hydrodynamical turbulence, to mention but a few areas [43]. Lately, self-similarity has gained prominence in nonlinear optics, triggered by recent theoretical discovery [17] and experimental realization [19, 20] of stable self-similar pulses, optical similaritons, in nonlinear fiber amplifiers in the normal dispersion regime. These advances generated a flurry of activity which is reviewed in Ref. [12]. Unlike solitons which are static (equilibrium) structures, formed as a result of balance between diffraction/dispersion and nonlinearity, the similaritons are quintessentially non-equilibrium waves – existing in either conservative or dissipative/gain media – that maintain their structural stability (intensity profiles).

To date, research on self-similarity in optics has primarily focused on asymptotic temporal similaritons that form over long propagation distances in optical fiber amplifiers [12], although asymptotic spatial and spatio-temporal similaritons have also been studied [45, 103]. At the same time, soliton-like temporal [46–50,104] as well as spatial (1+1)D [23,25] similaritons have been shown to exist in the media with Kerr-type nonlinearities – in the fiber or planar waveguide geometries – with gain/loss and, in general, in presence of spatial inhomogeneities. The similaritons of soliton-like nature can form at any propagation distances. Moreover, provided a certain compatibility condition among the parameters of the media is satisfied, they are directly related to the well-known $(1+1)$D solitons of homogeneous cubic nonlinear media; in particular, such similaritons have the same spatial/temporal profiles as the corresponding solitons. The integrability of the $(1+1)$D Kerr case guarantees stability of soliton-like similaritons. To stress a connection between the soliton-like similaritons of open inhomogeneous systems and the solitons of homogeneous integrable systems with the same nonlinearity, the term non-autonomous solitons was coined [51].

The concept of soliton-like similaritons appears, however, to extend to non-integrable nonlinear systems. Indeed, the important role self-similarity plays in Kerr-like systems of higher dimensionality has been recently elucidated in Refs. [27, 105]. In particular, self-focusing of $(2+2)$D beams in homogeneous Kerr media was numerically studied and a self-similar character of the beam collapse established. It was shown that regardless of the initial beam intensity profile, the central part of the beam collapses to a universal soliton-like profile – termed the Townesian – which essentially corresponds to an unstable $(2+2)$D soliton in a self-focusing Kerr medium [81, 106]. All this prompts a fundamental question: Can soliton-like similaritons be supported by other than Kerr (non-integrable) nonlinear media? And if so, under what conditions, if any, such similaritons are structurally stable?

In this Rapid Communication, we show analytically and numerically that stable $(1+1)$D spatial similaritons can propagate in media with self-focusing quintic nonlinearities. Depending on the sign of a phase chirp, novel similaritons are either self-focusing or spreading for the same – assumed to be positive hereafter – sign of the quintic medium nonlinearity. We demonstrate that soliton-like similaritons can be realized in a wide range of parameters of quintic nonlinear media. We estimate an input power required for the experimental realization of such similaritons. Similariton stability is established with the aid of numerical simulations. We also present a generic model for the quintic nonlinearity by

considering a centrosymmetric medium, doped with resonant impurities whose resonant frequencies lie sufficiently far away from the beam carrier frequency. We show how the detuning from impurity resonance can serve as a useful control parameter to engineer the desired nonlinearity of the medium.

### 7.3 Generic Model of the Quintic Nonlinearity

We begin by considering a planar waveguide, filled with a centrosymmetric nonlinear medium, which is, in turn, doped with resonant impurities. The latter could be rare-earth element atoms or quantum dots (QD); eurbium- or QD-doped glasses, or semiconductors doped with quantum dots, for instance, can serve as possible realizations of the system. We treat the impurities in the two-level approximation. Within this framework, the slowly varying envelope $\mathscr{E}$ of a quasi-monochromatic light beam obeys the Maxwell equation in the form

$$\frac{\partial \mathscr{E}}{\partial z} - \frac{i}{2k}\frac{\partial^2 \mathscr{E}}{\partial x^2} = \frac{iNd_{eg}\omega^2}{2\varepsilon_0 kc^2}\sigma_\infty + \frac{i\omega}{c}(n_2|\mathscr{E}|^2 + n_4|\mathscr{E}|^4)\mathscr{E}. \tag{7.1}$$

Here the first term on the r. h. s. of Eq. (7.1) describes the nonlinear polarization due to the resonant impurities while the remaining terms characterize the nonlinear interaction of light with the bulk medium. In Eq. (7.1), $N$ is the dopant density, $d_{eg}$ is a dipole matrix element between the excited and ground states – appropriately labeled – of an individual impurity atom; $\sigma_\infty$ is a steady-state value of the atomic dipole moment, and $n_2$ as well as $n_4$ are cubic and quintic nonlinear coefficients of the bulk medium response.

The impurity dipole moment and inversion obey the standard Bloch equations [8]

$$\partial_t \sigma = -\gamma_\perp \sigma - i\Delta\sigma - \tfrac{i}{2}\Omega w, \tag{7.2}$$

and

$$\partial_t w = -\gamma_\parallel (w+1) + i(\Omega\sigma^* - \sigma\Omega^*), \tag{7.3}$$

where $\gamma_\perp$ ($\gamma_\parallel$) is a transverse (longitudinal) decay rate of the atomic dipole moment (inversion); $\Omega = 2d_{ge}\mathscr{E}/\hbar$ is the Rabi frequency, $\Delta$ is a detuning of the incident light from atomic impurity resonance, and it is assumed that in equilibrium all atoms are in a (nondegenerate) ground state. It can be shown that in the cw limit and assuming the light carrier frequency lies sufficiently far off resonance with the impurities – the detuning is much larger than the

transverse relaxation rate, $\Delta \gg \gamma_\perp$ – we can use Eqs. (7.2) and (7.3) to adiabatically eliminate the atomic variables. The resulting steady-state dipole moment may then be developed into a series in inverse $\Delta$ as

$$\sigma_\infty \simeq \frac{2d_{ge}\mathscr{E}}{\hbar\Delta}\left(1-\frac{4|d_{ge}|^2|\mathscr{E}|^2\gamma_\perp}{\hbar^2\Delta^2\gamma_\parallel}+\frac{16|d_{ge}|^4|\mathscr{E}|^4\gamma_\perp^2}{\hbar^4\Delta^4\gamma_\parallel^2}\right). \tag{7.4}$$

We can easily infer from Eqs. (7.1) and (7.4) that sufficiently far away from impurity resonances, the dopant response is approximately purely dispersive, leading to the renormalization of the nonlinearity coefficients of the bulk medium. In particular, while the first term in (7.4), rescaling the global phase of the field envelope, may well be omitted, the second and third ones govern the off-resonance impurity contributions to the third- and fifth-order nonlinearities, respectively. Accordingly, the analysis indicates that for a judicious choice of the frequency detuning,

$$\Delta_* = \left(\frac{4\gamma_\perp|d_{ge}|^4N}{\gamma_\parallel n_0\varepsilon_0\hbar^3 n_2}\right)^{1/3}, \tag{7.5}$$

the impurity-generated and the bulk third-order nonlinearities cancel each other, resulting in an effective renormalized quintic nonlinearity with the coefficient

$$n_{4eff} = n_4 + n_2\left(\frac{4\gamma_\perp n_2^2 n_0^2\varepsilon_0^2}{\gamma_\parallel N^2|d_{ge}|^2}\right)^{1/3}, \tag{7.6}$$

where $n_0$ is a linear refractive index of the bulk medium, and we have used Eqs. (7.1), (7.4), and (7.5) to obtain Eq. (7.6).

Prior to introducing scaled dimensionless variables, let us estimate the order-of-magnitude of the necessary detuning and the effective quintic nonlinearity coefficient. To this end, we consider a realistic example of a silica-glass matrix doped with CdS QDs. In general, the transverse (phase) relaxation rate is a few times greater than the longitudinal (population) one, so we assume, for simplicity, $\gamma_\perp = 2.5\gamma_\parallel$; we also consider a typical value of the dipole matrix element to be $|d_{ge}| \simeq 10^{-28}$ Cm at a transition wavelength in the middle of the visible spectrum $\lambda \simeq 500$ nm [107]. Further, we have for silica glass, $n_0 \simeq 1.45$ and $n_2 \simeq 10^{-22}$ m$^2$/V$^2$. With these numerical values, we can show that $\Delta_*$ and $n_{4eff}$ scale with the dopant

density $N$ as

$$\Delta_* \simeq 10^8 \times N^{1/3}, \mathrm{s}^{-1}; \;\; n_{4eff} \simeq 10^{-25} \times N^{-2/3}, \mathrm{m}^4/\mathrm{V}^4. \tag{7.7}$$

We note in passing that in deriving Eq. (7.7), we have neglected the bulk quintic nonlinearity which is "the worst case scenario" as far the the critical power for similariton formation is concerned. Indeed, if the bulk contribution is comparable with, or greater than the impurity contribution, the critical power for similariton formation in such a material will be lower than that evaluated toward the end of this work.

It follows from Eqs. (7.7) that the effective nonlinearity can be boosted by reducing $N$ at the expense of decreasing the detuning. The acceptable trade-off can in fact be accomplished for sufficiently dilute QD samples: For instance for $N \simeq 10^{12}$ m$^{-3}$, $n_{4eff} \simeq 10^{-33}$ m$^4$/V$^4$, while $\Delta_* \simeq 10^{12}$ s$^{-1}$. Note that a typical exciton lifetime of roughly 100 ps [55,107] translates into $\gamma_\perp \simeq 10^{10}$ s$^{-1}$ such that the system is well within the confines of a purely dispersive large-detuning regime, $\Delta_* \gg \gamma_\perp$.

The nonlinear wave equation for the field envelope in the medium with the renormalized nonlinearity then simplifies as

$$i\frac{\partial \mathscr{E}}{\partial z} + \frac{1}{2k}\frac{\partial^2 \mathscr{E}}{\partial x^2} + \frac{k n_{4eff}}{n_0}|\mathscr{E}|^4 \mathscr{E} = 0. \tag{7.8}$$

In the following, it will prove convenient to introduce dimensionless variables as $X = x/w_0$, $Z = z/L_D$; $L_D = kw_0^2$, being a characteristic diffraction length, $U = (k n_{4eff} L_D/n_0)^{1/4}\mathscr{E}$ and recast Eq. (7.8) as

$$i\frac{\partial U}{\partial Z} + \frac{1}{2}\frac{\partial^2 U}{\partial X^2} + |U|^4 U = 0. \tag{7.9}$$

### 7.4 Similariton Solutions and Their Properties

We surmise by inspection of Eq. (7.9) that a family of spatial similaritons is supported by the media with quintic nonlinearity; the similariton field is sought in the form

$$U(X,Z) = \frac{1}{\sqrt{W(Z)}} R\left[\frac{X - X_g(Z)}{W(Z)}\right] e^{i\Phi(X,Z)}, \tag{7.10}$$

where $W$ is a similariton width and $X_g$ is a guiding center coordinate. The self-similar profile (7.10) conserves the beam power $\mathscr{P}$ (per unit length in the other transverse dimension),

$$\mathscr{P} = \int dX|U|^2 = \int d\eta|U(\eta)|^2 = const, \tag{7.11}$$

where we have introduced the similarity variable $\eta$ viz.,

$$\eta = \frac{X - X_g(Z)}{W(Z)}. \tag{7.12}$$

Substituting the profile (7.10) back into Eq. (7.9), we obtain an ordinary differential equation for the similariton envelope whose bound solution is

$$R(\eta) = \sqrt{\sqrt{\frac{3}{8}}\mathrm{sech}\eta}. \tag{7.13}$$

We note in passing that a fundamental $(1+1)$D bright soliton, supported by the quintic nonlinearity, has the same intensity profile, but it is known to be unstable [108]. The explicit dynamics of the field profile depends on the particulars of the phase evolution which is found to be given by

$$\Phi(X,Z) = -\tfrac{1}{2}C(Z)(X - X_{c0})^2 + \Theta(Z). \tag{7.14}$$

Here the phase chirp $C$ obeys the equation

$$C(Z) = \frac{C_0}{1 - C_0 Z}, \tag{7.15}$$

where $X_{c0}$ is the coordinate of the center of curvature, and the offset phase is given by

$$\Theta(Z) = \frac{1}{8C_0(1 - C_0 Z)}. \tag{7.16}$$

As a result of amplitude-phase coupling, the similariton width and guiding center dynamics are governed by the equations

$$W(Z) = 1 - C_0 Z, \tag{7.17}$$

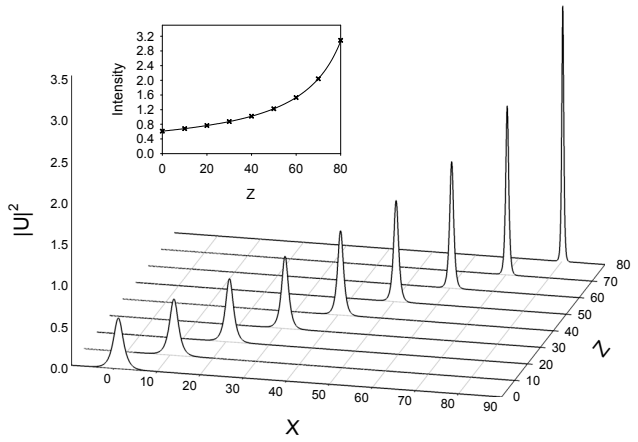


Figure 7.1: Intensity profile of a self-focusing similariton with as a function of the propagation distance in dimensionless variables. $X_{g0} = 1$, $X_{c0} = 100$, and $C_0 = 0.01$. Inset: straight line represents the theoretical peak intensity as a function of the propagation distance; crosses show numerical values of the peak intensity at chosen propagation distances.

and

$$X_g(Z) = X_{g0} - C_0(X_{g0} - X_{c0})Z. \tag{7.18}$$

It follows from Eq. (7.17) that depending on the chirp sign, the similaritons in quintic media can be either self-focusing – with rapidly increasing amplitude and shrinking width – or spreading at a faster rate than do freely propagating beams. As can be inferred from Eq. (7.18), the guiding center moves with a constant velocity $V = C_0(X_{g0} - X_{c0})$. The direction of motion depends on the sign of the chirp and relative initial positions of the guiding center and the center of curvature. Further, observe that as follows from Eqs. (7.10) and (7.17), the peak intensity of each similariton scales as

$$I_{max}(Z) \propto \frac{1}{1 - C_0 Z}. \tag{7.19}$$

### 7.5 Simulations and Results

First, consider the self-focusing case, $C_0 > 0$. In Fig. 7.1 we display numerical evolution of a self-focusing similariton profile on propagation in the medium. We observe that the similariton maintains its structural integrity over, at least, 80 diffraction lengths. In the inset to Fig. 7.1, we exhibit the evolution of the peak similariton intensity. The solid curve represents our analytical result, Eq. (7.19), and the crosses indicate numerically evaluated

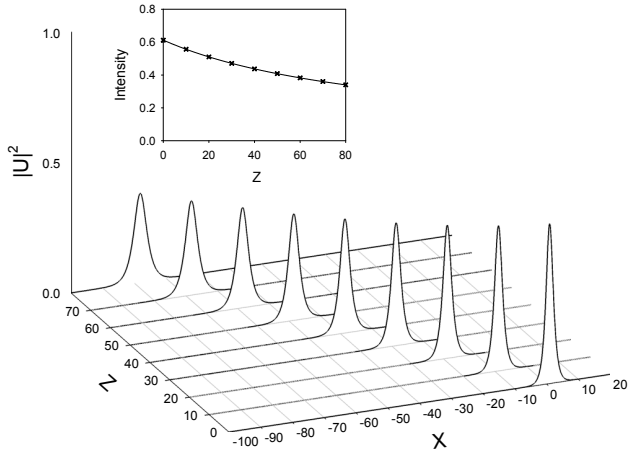


Figure 7.2: Intensity profile of a self-defocusing similariton with as a function of the propagation distance in dimensionless variables. $X_{g0} = 1$, $X_{c0} = 100$, and $C_0 = -0.01$. Inset: straight line represents the theoretical peak intensity as a function of the propagation distance; crosses show numerical values of the peak intensity at chosen propagation distances.

peak intensities at chosen propagation distances. After having initially increased almost linearly over small propagation distances, the peak intensity is seen to start increasing faster with the distance in accord with our theory. The crosses all lie on the theoretical curve, within tiny round off numerical errors.

We can infer from Eqs. (7.17) and (7.19) that the width decreases and peak intensity increases without limit over a finite propagation distance, $Z_\infty = 1/C_0$, although the total power still remains finite. Our solution becomes invalid long before the collapse takes place, though, as the paraxial approximation breaks down for small enough beam widths. We then stress that present self-focusing similaritons, just as the Townes profile for $(2+1)$ D Kerr case [105], describe a self-similar stage of beam self-focusing, leading eventually to the collapse. Thus, our similaritons can be viewed as intermediate asymptotics in the spirit of Ref. [43].

Next, we consider the self-defocusing case, $C_0 < 0$. The corresponding numerical evolution of the similariton profile is shown in Fig. 7.2. The similariton width is seen to increase with the propagation distance. Unlike the self-focusing case, there is no constraint on the range of propagation distances over which the self-defocusing solution is theoretically valid. In the inset, we again compare the theoretical behavior of the similariton peak intensity (solid line) with the numerically evaluated one (crosses). We note excellent agreement between the analytical and numerical results.

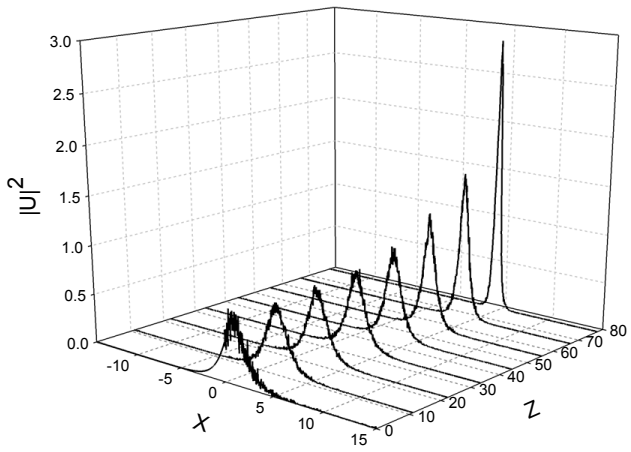


Figure 7.3: Numerical evolution of the similariton with added 5% asymmetric noise. The initial parameters are $X_{g0} = 1$, $X_{c0} = 10$ and $C_0 = 0.01$.

To further ascertain structural stability of the novel self-similar solutions, we add 5% asymmetric noise to the initial similariton profile and numerically propagate the combined beam. The result is displayed in Fig. 7.3, and it clearly attests to the similariton stability.

Finally, we estimate the critical power needed to generate the novel similaritons. As they all have the same power by the scaling properties of Eq. (7.10), the latter can serve as the critical power which can be expressed as

$$P_{cr} = \sqrt{\frac{3n_0}{8n_{4eff}}}\left(\frac{n_0\varepsilon_0 c\lambda l_\perp}{4}\right), \tag{7.20}$$

where $l_\perp$ is a waveguide width in the trapped direction. Using the above estimated effective nonlinearity coefficient, we obtain

$$P_{cr} \simeq 10^3 \times l_\perp N^{1/3},\ \text{W}. \tag{7.21}$$

It is seen from Eq. (7.21) that for $N \simeq 10^{12}$ m$^{-3}$ and $l_\perp \simeq 5\,\mu$m, we can arrive at the estimate, $P_{cr} \simeq 50$ W. Such input powers are easily achievable with quasi-cw – millisecond long, say – laser pulses for which our cw theory is perfectly appropriate.

## 7.6 Conclusion

In summary, we have demonstrated that stable spatial similaritons can be supported by quintic nonlinear media. Depending on the sign of the chirp, the similaritons can be self-focusing and self-defocusing. We also show how quintic nonlinearities can be engineered in centrosymmetric media doped with low-density impurities of resonant atoms or quantum dots. In the limit of large detuning of light from the impurity resonance frequency, the detuning serves as a convenient control parameter to design the right kind of nonlinearity, much like the phase mismatch parameter does in the case of cascaded second harmonic generation process studied elsewhere [109].

# Chapter 8

# Conclusion Remarks and Recommendations

## 8.1 Conclusion Remarks

This thesis explored the asymptotic response of atoms to an applied electric field when the frequency of field $\omega$ is close to the resonance frequency of atoms. The exploration was carried out through a project comprised of a set of analytical and numerical studies aimed at investigating near resonance behavior in optical systems and novel optical structures. Physical realizations of these systems were proposed and different media parameters were considered to have a practical view of systems under consideration. The procedure is based on many calculations to find the near resonance behavior of light and matter, exploring different regimes, studying the stability and finally suggestions for the experimental realization. Consequently, an asymptotic universal response of optical systems near resonance and the conditions for different parameters have been studied.

In summary, to accomplish the main objective of the project, three objectives considered to fulfill. The first goal was to analytically find a asymptotic solution of electromagnetic field coupled to atoms when the carrier frequency detuning is near zero. The second goal was to verify the universality, stability and other characteristics of this response by various numerical simulations. Identifying a practical system and system conditions like initial condition was the last objective.

To accomplish these three objectives, a set of analytical and numerical studies was performed on various optical systems, hosting different types of on-resonance media. A summary of each study and its main findings is given in following.

**1$^{st}$ study:** Exploring self-similar pulses in coherent resonant linear amplifiers.

In this study, self-similar pulses in homogeneously broadened linear amplifying media in a vicinity of an optical resonance were investigated. Physical model and mathematical analyses were presented in detail. The analytical results are presented for both short and long pulses. For long pulses, any pulse grows exponentially in the medium while maintaining its shape. Evolution of short pulses exactly on resonance with the atomic transition

was comprehensively described and self-similar asymptotic solutions were found.

To demonstrate the universal nature of the self-similar solution, the evolution of Gaussian, hyperbolic secant, and exponential profiles were simulated numerically and compared with the self-similar asymptotic. The results showed the universal character of the self-similar asymptotic. To reinforce this, the rms widths of the self-similar asymptotic and different initial profiles were compared. The widths of arbitrary shaped initial pulses asymptotically tend to the asymptotic self-similar pulse width over a long enough propagation distance.

Finally, a physical model for pulses with the fast rise of their leading edge, which is essential to form the self-similar asymptotic, was presented for picosecond pulses in dilute atomic vapors. The energy gain factors of short and long self-similar pulses supported by such media was compared and found that the short pulse gain dwarfs the long pulse one over long propagation distances.

**2nd study:** Investigating shape-invariant pulses in resonant linear absorbers.

In this study, ultrashort self-similar pulse propagating in linear absorber near optical resonance was described. It was observed that self-similar pulses arise when the initial spectral profile has long wings where much of the incident pulse energy is stored. The coupled Maxwell-Bloch equations were solved using a Fourier transform technique and it was inferred that the found solution remains self-similar on propagation in the resonant medium. It was shown that over long propagation distances, the pulse shape is independent of its initial rms width. The spectra of the shape-invariant pulses were presented and sketched. The spectrum evolution scenario is determined by the interplay of resonant dispersion and absorption and it depends on the initial profile parameters. The required pulse profile to generate self-similarity was presented and the method to generate the novel pulses was discussed.

The experimental realization of the novel pulses was also described. A dilute atomic vapor which is cooled down in order to neglect the inhomogeneous broadening, filling the core of a hollow-core photonic crystal fiber (HCPCF) can serve as a physical realization of the medium. Bulk medium dispersion effects can be eliminated and spatial diffraction can be arrested by using HCPCF.

**3rd study:** Analytical and numerical investigations of self-similar optical kinks in resonant nonlinear media.

In this study, it was shown that self-similar optical waves with a kink structure form in a resonant nonlinear media. It was also found that this self-similar structure is reflected in the time evolution of atomic dipole moment and inversion as well. Two assumptions were considered for the analytical analysis. First, the pulse is not chirped. Second, the inhomogeneous broadening can be ignored, and the atomic dipole moments evolve much faster than the atomic population dynamics unfolds. The new kinks form between two typical distances.The energy relaxation process was ignored in all calculations and its effect was evaluated by the aid of numerical simulations.

A constant background intensity at the trailing edge of the input wave is required to form a kink. Therefore, an experimental model of such pulses was proposed. Considering a switched CW wave as an initial condition, the numerical simulations were presented. The formation and eventual decay of the kinks due to energy relaxation processes were explored numerically. It was shown that for short energy relaxation times, the emerging kinks decay and they survive only for short propagation distances. The critical amplitude to form the kinks was also found. Finally the systems in which the kinks can be realized were briefly discussed.

**4$^{th}$ study:** Exploring self-similarity and optical kinks in inhomogeneous resonant media.

In this study, self-similar optical waves with a kink structure in resonant nonlinear media in the presence of inhomogeneous broadening were described. Similar to previous study on kink formation in homogeneously broadened resonant nonlinear media, it was also observed that to form kinks, the energy relaxation time should be much longer than the transverse one. It was concluded that these kinks are formed due to an interplay of optical nonlinearity and transverse relaxation processes.

To consider the inhomogeneous broadening, a generic Gaussian function was assumed as the inhomogeneous broadening distribution. A numerical study conducted to examine the effect of inhomogeneous broadening on kink formation. It revealed the existence of self-similar solutions for the pulse amplitude and for the atomic dipole moment components and inversion. The importance of critical power in kink formation and its dependence on the dipole and energy relaxation times, $T_{\perp}$ and $T_{\parallel}$, was discussed. The presence of the critical power is necessary to start self-steepening and kink formation. Systems where the proposed self-similar kinks can be realized were also discussed.

**5th study:** Studying self-induced transparency quadratic solitons near resonance.

In this study, self-induced transparency quadratic solitons (QS) were explored. The frequency of the fundamental input pulse was assumed to be close to resonance frequency of impurities which are embedded into a medium with quadratic optical nonlinearities. What makes this new type of quadratic solitons special is that they do not require any bulk medium GVD at all.It was shown that the proposed QS form due to the mutual self-trapping of FW and SH by the joint action of both resonant nonlinearity and the quadratic nonlinearity of the bulk medium. It was assumed that an input FW pulse is nearly resonant with resonance frequency of impurities. The quantitative model was presented with demonstrating different parameters such as group velocity mismatch, inhomogeneous broadening effect and phase mismatch in coupled Maxwell-Bloch equations.

For numerical simulations, In(Ga)As QDs grown on a GaAs substrate were considered as a prototype of the system. Taking into account all parameters the linear absorption length, the nonlinear length and the walk-off length were calculated. The linear absorption length and the nonlinear length was of the same order of magnitude which is essential for the QS formation.

Results form both qualitative analysis and numerical simulations showed that the QS formation and stability depend on the magnitude of inhomogeneous broadening width, wave number mismatch, temporal walk-off length, and the area of the incident fundamental pulse. The influence of these four factors was elucidated with the aid of numerical simulations. Comparison of the results form the ideal case with zero phase mismatch and inhomogeneous broadening revealed that although phase mismatch causes splitting of the SH soliton pulses, the inhomogeneous broadening inhibits the instability. The effect of temporal walk-off was also studied and it was observed that a stable QS pair is generated. However the peak amplitude of the SH component decreases due to walk-off during propagation.

Finally, a number of numerical simulations were performed to show that the QS formation is insensitive to the initial profile of the fundamental pulse. The QS evolution strongly depends on the input FW area; no QS formation is possible for area below $\pi$, while for any input FW pulse with the area between $\pi$ and $2\pi$, the solitons form and the area asymptotically attains the value of $2\pi$.

**$6^{th}$ Study:** An analytical and numerical investigation of spatial similaritons in conservative systems.

In this study, analytical analysis indicated that for a choice of the frequency detuning, stable spatial similaritons can propagate in homogeneous conservative optical media with quintic nonlinearities. The sign of the phase chirp determines whether the new similaritons are self-focusing or self-defocusing.

In addition, a generic model for a quintic nonlinearity was presented. These spatial similaritons can be realized in a broad parameter regime of quintic nonlinear media. A centrosymmetric nonlinear medium, doped with resonant impurities, considered as a generic model of quintic nonlinearity.

The result of the analytical study indicated that depending on the chirp sign, the similaritons in quintic media can be self-focusing when the amplitude is increasing and the width is decreasing during propagation, or spreading when the amplitude keeps decreasing while the width is increasing. The direction of the motion also depends on the chirp sign and relative initial positions of the guiding center and the center of curvature.

Similariton stability was studied with the help of numerical simulations. To further verify the structural stability of the self-similar solutions, 5% asymmetric noise was added to the initial similariton profile and it was found that the similaritons remain stable on propagation.

An important estimation was also made regarding the critical power needed to generated the novel similaritons. It was shown that an input power required for the formation of such similariotns depends on both linear and quintic nonlinearities along with the waveguide width.

Overall, the response of atoms to an applied electric field near resonance investigated in this thesis can be regarded as a relatively broad study which includes various optical systems and regimes. The studies accomplished in this study are interpreted as an encouraging step towards establishing a practical study for investigating the optical on-resonance structures including kinks, self-similarities, and solitons. Having in mind the advantages of working near resonance, the next section is devoted to some applications of studied systems and structures.

## 8.2 Applications of Similaritons

One of the most significant features of the interest in self-similarity is that it has reminded of an extensive array of mathematical tools that can be used to find analytic solutions to complex problems. In many areas of nonlinear optics sophisticated numerical simulation and modeling are required. The underlying physics is then difficult to readily visualize. The existance of representing self-similar solutions makes everything understandable. For example, in mode-locked lasers the search for universal patterns will remain a very profitable direction of research [12].

Self-similar pulses lead to interesting practical applications in the field of pulse shaping, pulse compression [47, 48, 110–113], pulse amplification and generally in the generation of high-power pulses. Particularly, they can be used in the design of high-power amplifiers [114, 115], efficient temporal compressors [19, 114, 115] and similariton lasers [20]. New experimental studies have also used similaritons in optical pulse synthesis [116, 117], 10-GHz telecom multi-wavelength sources [118] and optical regeneration of telecom signals [119]. Nonlinear fiber amplifiers with self-similar evolution dynamics are also mature alternatives to other pulse generation and shaping techniques [12].

Another practical motivation behind the interest in self-similar pulse propagation is that the energy of ultrashort optical pulses is generally limited by wave breaking, which is a consequence of excessive nonlinearity. For example, short-pulse fiber devices produce high intensities and then large nonlinear phase shifts. Similaritons can tolerate strong nonlinearity without wave breaking [17].

One of the areas where parabolic shape wave-breaking-free pulses were used is fiber-grating compression. The grating is a linear dispersive delay line having anomalous dispersion. Calculation shows enhancement in the compression factor. The latter is enhanced because the degrading effect of wave breaking is eliminated. In conventional compressors, the wave breaking is so severe that the compression starts to deteriorate [17].

## 8.3 Applications of Optical Shocks

It seems probable that the kinks could be used as an alternative to the usual solitons in optical logic units when the stable soliton pulses cannot form due to an energy input and system losses [54].

The study of shock waves in optics has also been found interesting and practical in understanding the behavior of the shocks in superfluid systems. Since dispersive shock waves are difficult to study experimentally, and analytical solutions to the equations that govern them have only been found in one dimension, by examining the correspondence between the behavior of superfluids and nonlinear optical materials, the dynamics of dispersive shock waves can be studied. From an experimental viewpoint, the mapping to nonlinear optics allows the isolation of a coherent wave in order to study the basic properties of shocks in a dispersive fluid in detail. Observations, control of the input conditions and direct imaging of the output are significantly easier in the optical case [70].

## 8.4 Applications of Solitons

Soliton refers to any optical pulse of a specific shape and energy propagating through a nonlinear medium while remaining unchanged in spite of large absorption losses. This property makes the solitons a smart choice for using in designing optic communication systems. Among various kinds of solitons, quadratic solitons might be used not only for all-optical signal processes but also for using as a stable and coherent light source. An important issue for practical applications of solitons is to reduce the power level at which solitons are formed. To minimize the formation threshold, media with large $\chi^{(2)}$ nonlinear coefficient should be chosen. Nowadays the highest element of $\chi^{(2)}$ nonlinear tensor can be employed thanks to the quasi-phase-matching (QPM) technique [83].

## 8.5 Recommendations for Future Work

Despite the successful exploring of on-resonance systems in both analytical and numerical framework, the practical issues involved when considering the applications field have not yet been sufficiently investigated. It is believed that following recommendations will further establish the effectiveness of the proposed systems.

The first recommendation is to validate the proposed systems in applications. In the present research, all of the investigations were carried out by analytical calculations and numerical simulations and under controlled conditions and assumptions. However, validity of the proposed on-resonance systems should be examined in applications. From practical viewpoint, preparing clean enough samples in order to eliminate the inhomogeneous

broadening is not simple. The environmental conditions can produce inhomogeneities in system, and may also induce significant changes on the structures. Moreover, the effect of inhomogeneous broadening should be further investigated to assure the validity of systems in both ideal and real conditions. Inhomogeneous broadening can be caused by random local strain fields in solids caused by environmental conditions, or for example, by Doppler effect in gases and dilute vapors.

Inspecting universality of the spatial similaritons in quintic media is another recommendation for future work on the proposed system.

The last recommendation is to investigate the influence of Kerr nonlinearity in the self-induced transparency quadratic solitons. The Kerr nonlinearity effect is significant for short and high intensity pulses and it should be taken into account in the study of the system. In the proposed system in this thesis

$$\frac{P^{(3)}}{P^{(2)}} \sim \frac{\chi^{(3)}\mathscr{E}_m}{\chi^{(2)}}, \tag{8.1}$$

when $P^{(3)}$ and $P^{(2)}$ are the contributions of cubic and quadratic nonlinearities to the polarization, respectively. $\mathscr{E}_m$ is the peak field amplitude of the fundamental input pulse. The peak field amplitude $\mathscr{E}_m$ of a picosecond $2\pi$ input pulse is estimated using the area concept as

$$\mathscr{E}_m \tau_p \times \frac{2d_{ge}}{\hbar} = 2\pi, \tag{8.2}$$

$$\mathscr{E}_m \simeq \frac{\pi\hbar}{d_{ge}\tau_p}, \tag{8.3}$$

$$\mathscr{E}_m \simeq \frac{h}{2d_{ge}\tau_p}, \tag{8.4}$$

$$\frac{P^{(3)}}{P^{(2)}} \simeq \frac{h\chi^{(3)}}{2d_{ge}\tau_p\chi^{(2)}}. \tag{8.5}$$

Using $\chi^{(3)} \simeq 10^{-18} m^2/V^2$ for GaAs and substituting the order-of-magnitude values for relevant parameters of the system under consideration, $\frac{P^{(3)}}{P^{(2)}} \simeq 3.5 \times 10^{-2} << 1$, i.e. the maximum of $P^{(3)}$ is 3.5% of the maximum of $P^{(2)}$, so quadratic nonlinearities dominate when $\tau_p \simeq 1ps$. However, for a few-hundred femtosecond or shorter pulses, the cubic

nonlinearities are large enough to consider in the analysis of the system.

## Bibliography


[1] H. A. Lorentz, *The theory of electrons* (Dover Publications, New York, 1952).

[2] M. Born and E. Wolf, *Principles of optics,* 7th (expanded) ed. (Cambridge University Press, New York, 1999).

[3] T. H. Maimann, "Stimulated optical radiation in ruby," Nature **187**, 493-494, 1960.

[4] F. P. Schfer, F. P. W. Schmidt, and J. Volze, "Organic dye solution laser," Appl. Phys. Lett. **9**, 306-309, 1966.

[5] C. V. Shank and E. P. Ippen, "Subpicosecond kilowatt pulses from a mode-locked cw dye laser," Appl. Phys. Lett. **24**, 373-375, 1974.

[6] R. Ell, U. Morgner, F. X. Kärtner, J. G. Fujimoto, E. P. Ippen, V. Scheuer, G. Angelow, and T. Tschudi, "Generation of 5-fs pulses and octave-spanning spectra directly from a Ti:sapphire laser,", Opt. Lett. **26**, 373-375, 2001.

[7] H. Hentschel, R. Kienberger, Ch. Spielmann, G. A. Reider, N. Milosevic, T. Brabec, P. Corkum, U. Heinzmann, M. Drescher, and F. Krausz, "Attosecond metrology," Nature **414**, 509-513, 2001.

[8] L. Allen and J. H. Eberly, *Optical resonance and two-level atoms* (Dover Publications Inc., New York, 1975).

[9] A. Icsevgi and W. E. Lamb, "Propagation of Light Pulses in a Laser Amplifier," Phys. Rev. **185**, 517-545, 1969.

[10] S. L. McCall and E. L. Hahn, "Self-induced transparency," Phys. Rev. **183**, 457-485, 1969.

[11] S. L. McCall and E. L. Hahn, "Self-induced transparency by pulsed coherent light," Phys. Rev. Lett. . **18**, 908-911, 1967.

[12] J. M. Dudley, C. Finot, D. J. Richardson, and G. Millot, "Self-similarity in ultrafast nonlinear optics," Nat. Phys. **3** 597-603, 2007.

[13] S. An, and J. E. Sipe, "Universality in the dynamics of phase grating formation in optical fibers," Opt. Lett. **16**, 1478-1480, 1991.

[14] C. R. Menyuk, D. Levi, and P. Winternitz, "Self-similarity in transient stimulated Raman scattering," Phys. Rev. Lett. **69**, 3048-3051, 1992.

[15] T. M. Monroe, P. D. Millar, P. L. Poladian, and C. M. de Sterke, "Self-similar evolution of self-written waveguides," Opt. Lett. **23**, 268-270, 1998.

[16] M. Soljacic, M. Segev, and C. R. Menyuk, "Self-similarity and fractals in soliton-supporting systems," Phys. Rev. E **61**, R1048-R1051, 2000.

[17] D. Anderson, M. Desaix, and M. Karlsson, M. Lisak, and M. L. Quiroga-Teixeiro, "Wave-breaking-free pulses in nonlinear optical fibers," J. Opt. Soc. Am. B **10**, 1185-1190, 1993.

[18] K. Tamura and M. Nakazawa, "Pulse compression by nonlinear pulse evolution with reduced optical wave breaking in erbium-doped fiber amplifiers," Opt. Lett. **21**, 68-70, 1996.

[19] M. E. Fermann, V. I. Kruglov, B. C. Thomsen, J. D. Dudley, and J. D. Harvey, "Self-similar propagation and amplification of parabolic pulses in optical fibers," Phys. Rev. Lett. **84**, 6010-6013, 2000.

[20] F. O. Ilday, J. R. Buckley, W. G. Clark, and F. W. Wise, "Self-similar evolution of parabolic pulses in a laser," Phys. Rev. Lett. **92**, 213902, 2004.

[21] B. Oktem, F. O. Ulgudur, and F. O. Ilday, "Soliton-similariton fibre laser," Nat. Photon., **4**, 307-311, 2010.

[22] W. H. Renninger, A. Chong, and F. W. Wise, "Self-similar pulse evolution in an all-normal-dispersion laser," Phys. Rev. A **82**, 021805(R), 2010.

[23] S. A. Ponomarenko and G. P. Agrawal, "Do soliton-like self-similar waves exist in nonlinear optical media?" Phys. Rev. Lett. **97**, 013901, 2006.

[24] S. A. Ponomarenko and G. P. Agrawal, "Optical similaritons in nonlinear waveguides," Opt. Lett. **32**, 1659-1661, 2007.

[25] L. Wu, J-F Zhang, L. Li, and Q. Tian, "Similaritons in nonlinear optical systems," Opt. Express, **16**, 6352-6360, 2008.

[26] S. A. Ponomarenko and S. Haghgoo, "Spatial optical similaritons in conservative nonintegrable systems," Phys. Rev. A **81**, 051801(R), 2010.

[27] K. D. Moll, A. Gaeta and G. Fibich, "Self-similar optical wave collapse: observation of the townes profile," Phys. Rev. Lett. **90**, 203902, 2003.

[28] S. V. Manakov, "Propagation of an ultrashort optical pulse in a two-level laser amplifier," Sov. Phys. JETP, **56**, 37, 1982.

[29] I. R. Gabitov and S. V. Manakov, "Propagation of ultrashort pulses in degenerate laser amplifiers," Phys. Rev. Lett. **50**, 495-498, 1983.

[30] I. R. Gabitov, V. E. Zakharov, and A. V. Mikhailov, "Nonlinear theory of superfluorescence," Sov. Phys. JETP, **59**, 703, 1984.

[31] S. A. Ponomarenko and S. Haghgoo, "Self-similarity and optical kinks in resonant nonlinear media," Phys. Rev. A **82**, 051801(R), 2010.

[32] P. W. Milonni and J. H. Eberly, *Lasers,* (Wiley, New York, 1985).

[33] V. V. Kozlov and S. Wabnitz, "Quasi-parabolic pulses in a coherent nonlinear optical amplifier," Opt. Lett. **35**, 2058-2060, 2010.

[34] A small deviation from the universal asymptotics in the pulse tails can be explained by limited accuracy of our sharp leading edge approximation.

[35] M. Abramowitz and I. A. Stegan, *Handbook of mathematical functions* (Dover, New York, 1972).

[36] F. Gori, "Collett-Wolf sources and multimode lasers," Opt. Commun. **34**, 301-305, 1980.

[37] J. Lancis, V. Torres-Company, E. Silvestre, and P. Andrés, "Space-time analogy for partially coherent plane-wave-type pulses," Opt. Lett. **30**, 2973-2975, 2005.

[38] M. D. Crisp, "Optical free induction decay," Phys. Rev. A **6**, 2001-2007, 1972.

[39] S. Haghgoo and S. A. Ponomarenko, Opt. Express, "Self-similar pulses in coherent linear amplifiers," **19**, 9750-9758, 2011.

[40] P. St. J. Russell, "Photonic-crystal fibers," J. Lightwave Tech., **24**, 4729-4749, 2006.

[41] C. Froehly, B. Colombeau, and M Vampouille, *Progress in optics,* Vol. **20**, 115, 1981, E. Wolf, Ed.

[42] G. B. Whitham, *Linear and nonlinear waves* (Wiley, New York 1974).

[43] G. I. Barenblatt, *Scaling, self-similarity and intermediate asymptotics* (Cambridge University Press, Cambridge, UK 1996).

[44] V. I. Karpman, *Nonlinear waves in dispersive media* (Pergamon, Elmsford, New York 1975).

[45] S. H. Chen and J. M. Dudley, "Spatiotemporal nonlinear optical self-Similarity in three dimensions," Phys. Rev. Lett. **102**, 233903, 2009.

[46] V. I. Kruglov and J. D. Harvey, "Asymptotically exact parabolic solutions of the generalized nonlinear Schrödinger equation with varying parameters," J. Opt. Soc. Am. B **23**, 2541-2550, 2006.

[47] S. H. Chen, L. Yi, D-S Guo, and P. Lu, "Self-similar evolutions of parabolic, Hermite-Gaussian, and hybrid optical pulses: Universality and diversity," Phys. Rev. E **72**, 016622, 2005.

[48] V. I. Kruglov, A. C. Peacock, and J. D. Harvey, "Exact self-Similar solutions of the generalized nonlinear Schrödinger equation with distributed coefficients," Phys. Rev. Lett. **90**, 113902, 2003.

[49] S. A. Ponomarenko and G. P. Agrawal, " Interactions of chirped and chirp-free similaritons in optical fiber amplifiers," Opt. Express **15**, 2963-2973, 2007.

[50] S. A. Ponomarenko and G. P. Agrawal, " Nonlinear interaction of two or more similaritons in loss- and dispersion-managed fibers," J. Opt. Soc. Am. B **25**, 983-989, 2008.

[51] V. Serkin, A. Hasegawa, and T. S. Belyaeva, "Nonautonomous solitons in external potentials," Phys. Rev. Lett. **98**, 074102, 2007.

[52] J. Belmonte-Beita, V. M. Pèrez-Garciía, V. Vekslerchik, and V. V. Konotop, "Localized nonlinear waves in systems with time- and space-modulated nonlinearities," Phys. Rev. Lett. **100**, 164102, 2008.

[53] G. P. Agrawal and C. Headley III, "Kink solitons and optical shocks in dispersive nonlinear media," Phys. Rev. A **46**, 1573-1577, 1992.

[54] Y. S. Kivshar and B. A. Malomed, "Raman-induced optical shocks in nonlinear fibers," Opt. Lett. **18**, 485-487, 1993.

[55] G. Panzarini, U. Hohenester, and E. Molinari, "Self-induced transparency in semiconductor quantum dots," Phys. Rev. B **65**, 165322, 2002.

[56] In Fig. 4.3, we chose a wide time window to better accommodate initially shallow wave input.

[57] J. C. Diels and W. Rudolph, *Ultrashort laser pulse phenomena,* (Academic Press, Amsterdam 2006), 2nd ed., p. 148.

[58] We consider only long enough relaxation times such that SVEA is satisfied.

[59] R. Z. Sagdeev, "The fine structure of a shock-wave front propagated across a magnetic field in a rarefied plasma," Sov. Phys. –Tech. Phys **6**, 867-871, 1962.

[60] V. I. Karpman, "Structure of shock front propagating at an angle to a magnetic field in a low-density plasma," Sov. Phys. –Tech. Phys **8**, 715-719, 1964.

[61] H. Washimi and T. Taniuti, "Propagation of ion-acoustic solitary waves of small amplitude," Phys. Rev. Lett. **17**, 996-998, 1966.

[62] R. J. Taylor, D. R. Baker, and H. Ikezi, "Observation of collisionless electrostatic shocks," Phys. Rev. Lett. **24**, 206-209, 1970.

[63] B. Damski, "Formation of shock waves in a Bose-Einstein condensate," Phys. Rev. A **69**, 043610, 2004.

[64] A. M. Kamchatnov, A. Gammal, and R. A. Kraenkel, "Dissipationless shock waves in Bose-Einstein condensates with repulsive interaction between atoms," Phys. Rev. A **69**, 063605, 2004.

[65] Z. Dutton, M. Budde, C. Slowe, and L. V. Hau, "Observation of quantum shock waves created with ultra-compressed slow light pulses in a BoseEinstein condensate," Sience **293**, 663-668, 2001.

[66] N. S. Ginsberg, J. Brand, and L. V. Hau, "Observation of hybrid soliton vortex-ring structures in BoseEinstein condensates," Phys. Rev. Lett. **94**, 040403, 2005.

[67] G. Lenz, P. Meystre, and E. M. Wright, "Nonlinear atom optics," Phys. Rev. Lett. **71**, 3271-3274, 1993.

[68] S. L. Rolston and W. D. Phillips, "Nonlinear and quantum atom optics," Nature **416**, 214-219, 2002.

[69] B. Anderson and P. Meystre, "Nonlinear atom optics," Contemp. Phys. **44**, 473-483 (2003).

[70] W. Wan, S. Jia, and J. W. Fleischer, "Dispersive superfluid-like shock waves in nonlinear optics," Nature Physics **3**, 46-51, 2007.

[71] F. DeMartini, C. H. Townes, Tk Gustafso, and P. L. Kelley, "Self-steepening of light pulses," Phys. Rev. **1**, 312, 1967.

[72] D. Anderson and M. Lisak, "Non-linear asymmetric self-phase modulation and self-steepening of pulses in long optical-waveguides," Phys. Rev. A **27**, 1393-1398, 1983.

[73] J. E. Rothenberg and D. Grischkowsky, "Observation of the formation of an optical intensity shock and wave breaking in the nonlinear propagation of pulses in optical fibers," Phys. Rev. Lett. **62**, 531, 1988.

[74] Y. S. Kivshar, "Dark-soliton dynamics and shock-waves induced by the stimulated Raman effect in optical fibers," Phys. Rev. A **42**, 1757-1761, 1990.

[75] D. N. Christodoulides, "Fast and slow Raman shock-wave domains in nonlinear media," Opt. Commun **86**, 431-436, 1991.

[76] Y. Kodama and S. Wabnitz, "Analytical theory of guiding-center nonreturn-to-zero and return-to-zero signal transmission in normally dispersive nonlinear optical fibers," Opt. Lett. **20**, 2291-2293, 1995.

[77] M. G. Forest and K. T. R. McLaughlin, "Onset of oscillations in nonsoliton pulses in nonlinear dispersive fibers," J. Nonlinear Sci. **8**, 43-62, 1998.

[78] M. G. Forest, J. N. Kutz, and K. T. R. McLaughlin, "Nonsoliton pulse evolution in normally dispersive fibers," J. Opt. Soc. Am. B **16**, 1856-1862, 1999.

[79] E. G. Sauter, *Nonlinear Optics,* (Wiley, New York 1996) p. 117.

[80] G. B. Lamb, *Elements of soliton theory* (Wiley, New York, 1980).

[81] Y. S. Kivshar and G. P. Agrawal, *Optical solitons: from fibers to photonic crystals* (Academic Press, Boston, 2003).

[82] L. Pitaevskii and S. Stringari, *Bose-Einstein condensation* (Clarendon, Oxford, 2003).

[83] A. V. Buryak, P. D. Trapani, D. V. Skryabin, and S. Trillo, "Optical solitons due to quadratic nonlinearities: from basic physics to futuristic applications," Phys. Rep. **370**, 63-235, 2002.

[84] L. A. Ostrovskii, "Propagation of wave packets and space-time self-focusing in a nonlinear medium," Sov. Phys. JETP **24**, 797-800, 1967.

[85] G. I. Stegeman, D. J. Hagan, and L. Torner, "$\chi^{(2)}$ cascading phenomenaand their applications to all-optical signal processing, mode-locking, pulse, compression and solitions," Opt. Quantm Electron. **28**, 1691-1740, 1996.

[86] W. E. Torruellas, Z. Wang, D. J. Hagan, E. W. VanStryland, and G. I. Stegeman, "Observation of two-dimensional spatial solitary waves in a quadratic medium," Phys. Rev. Lett. **74**, 5036-5039, 1995.

[87] R. Schiek, Y. Baek, and G. I. Stegeman, "One-dimensional spatial solitary waves due to cascaded second-order nonlinearities in planar waveguides," Phys. Rev. E **53**, 1138-1141, 1996.

[88] P. Di Trapani, D. Caironi, G. Valiulis, A. Dubietis, R. Danielius, and A. Piskarskas, "Observation of temporal solitons in second-harmonic generation with tilted pulses," Phys. Rev. Lett. **81**, 570-573, 1998.

[89] A. Degasperis, M. Conforti, F. Baronio, and S. Wabnitz, "Stable Control of Pulse Speed in Parametric Three-Wave Solitons," Phys. Rev. Lett. **97**, 093901, 2006.

[90] D. V. Skryabin, A. V. Yulin, and A. I. Maimistov, "Localized polaritons and second-harmonic generation in a resonant medium with quadratic nonlinearity," Phys. Rev. Lett. **96**, 163904-163907, 2006.

[91] We assume that a photon of a given circular polarization promotes an electron-hole pair (exciton) creation with a well-defined spin orientation such that only linearly polarized light can generate biexcitons, cf., L. Jacak, P. Hawrylak, and A. Wojs, *Optical properties of semiconductor quantum dots* (Springer, Berlin, 1997).

[92] The contributions of cubic and quadratic nonlinearities to the polarization can be roughly estimated as $\mathscr{P}^{(3)}/\mathscr{P}^{(2)} \sim \chi^{(3)}_{\mathrm{e}ff}\mathscr{E}_m/\chi^{(2)}_{\mathrm{e}ff} \sim 5\times 10^{-2}$, using $\chi^{(3)}_{\mathrm{e}ff} \simeq 10^{-18}$ $\mathrm{m}^2/\mathrm{V}^2$ for GaAs. Here the peak field amplitude $\mathscr{E}_m$ of a picosecond $2\pi$ input pulse

was estimated using the known pulse area as $\mathscr{E}_m \sim \pi\hbar/d_{eg}\tau_p$. Thus quadratic nonlinearities indeed dominate in our case.

[93] In the circular polarization basis, the Bloch equations are exact such that no rotating wave approximation is needed, see for details Ref. [8].

[94] T. Brunhes, P. Boucaud, and S. Sauvage, "Infrared second-order optical susceptibility in InAs/GaAs self-assembled quantum dots," Phys. Rev. B **61**, 5562-5570, 2000.

[95] S. J. B. Yoo, C. Caneau, R. Bhat, M. A. Koza, A. Rajhel, and N. Antoniades, "Wavelength conversion by difference frequency generation in AlGaAs waveguides with periodic domain inversion achieved by wafer bonding," Appl. Phys. Lett. **68**, 2609-2611, 1996.

[96] T. Skauli, K. L. Vodopyanov, T. J. Pinguet, A. Schober, O. Levi, L. A. Eyres, M. M. Fejer, J. S. Harris, B. Gerard, L. Becouarn, E. Lallier, and G. Arisholm, "Measurement of the nonlinear coefficient of orientation-patterned GaAs and demonstration of highly efficient second-harmonic generation," Opt. Lett. **27**, 628-630, 2002.

[97] M. Jütte, H. Stolz, and W. von der Osten, "Linear and nonlinear pulse propagation at bound excitons in CdS," J. Opt. Soc. Am. B **13**, 1205-1210, 1996.

[98] J. M. Gérard, B. Sermage, B. Gayral, B. Legrand, E. Costard, and V. Thierry-Mieg, "Enhanced spontaneous emission by quantum boxes in a monolithic optical microcavity," Phys. Rev. Lett. **81**, 1110-1113, 1998.

[99] H. Giessen, A. Knorr, S. Haas, S. W. Koch, S. Linden, J. Kuhl, M. Hetterich, M. Grün, and C. Klingshirn, "Self-induced transmission on a free exciton resonance in a semiconductor," Phys. Rev. Lett. **81**, 4260-4263, 1998.

[100] P. Borri, W. Langbein, S. Schneider, and U. Woggon, "Ultralong dephasing time in InGaAs quantum dots," Phys. Rev. Lett. **87**, 157401-157404, 2001.

[101] J. Diels and W. Rudolph, *Ultrashort laser pulse phenomena* (Academic Press, USA, 2006).

[102] A. V. Buryak, Y. S. Kivshar, and S. Trillo,"Optical solitons supported by competing nonlinearities," Opt. Lett. **20**, 19611963, 1995.

[103] G. Chuang, H. G. Winful, A. Galvanuaskas, and T. B. Norris, "Self-similar parabolic beam generation and propagation," Phys. Rev. E **72**, 016609, 2005.

[104] V. N. Serkin and A. Hasegawa, "Exactly integrable nonlinear Schrödinger equation models with varying dispersion, nonlinearity and gain: Application for soliton dispersion managements," IEEE J. Sel. Top. Quantum Electron **8**, 418-431, 2002.

[105] A. L. Gaeta, "Collapsing light really shines," Science **301** 54-55, 2003.

[106] R. Y. Chiao, E. Garmire, and C.H. Townes, "Self-trapping of optical beams," Phys. Rev. Lett. **13**, 479-482, 1964.

[107] K. Watanabe, H. Nakano, A. Honold, and Y. Yamamoto, "Optical nonlinearities of excitonic self-induced-transparency solitons: Toward ultimate realization of squeezed states and quantum nondemolition measurement," Phys. Rev. Lett. **62**, 2257-2260, 1989.

[108] This point was discussed in A. W. Snyder and D. J. Mitchell, " Spatial solitons of the power-law nonlinearity," Opt. Lett. **18**, 101-103, 1993.

[109] J. Moses, B. A. Malomed, and F. W. Wise, "Self-steepening of ultrashort optical pulses without self-phase-modulation," Phys. Rev. A **76**, 021802(R), 2007.

[110] V. I. Kruglov, D. Mechin, and J. D. Harvey, "Self-similar solutions of the generalized Schrödinger equation with distributed coefficients," Opt. Express **12**, 6198-6207, 2004.

[111] D. Mechin, S. H. Im, V. I. Kruglov, and J. D. Harvey, "Experimental demonstration of similariton pulse compression in a comblike dispersion-decreasing fiber amplifier," Opt. Lett. **31**, 2106-2108, 2006.

[112] C. Finot and G. Millot, "Collisions between similaritons in optical fiber amplifiers," Opt. Express **13**, 7653-7665, 2005.

[113] C. Finot, L. Provost, P. Petropoulos, and D.J. Richardson, " Parabolic pulse generation through passive nonlinear pulse reshaping in a normally dispersive two segment fiber device," Opt. Express **15**, 852-864, 2007.

[114] J. Limpert, T. Schreiber, T. Clausnitzer, K. Zöllner, H. -J. Fuchs, E. -B Bley, H. Zellmer, and A. Tünnermann, "High-power femtosecond Yb-doped fiber amplifier," Opt. Express **10**, 628-638, 2002.

[115] A. Malinowski, A. Piper, J. H. V. Price, K. Furusawa, Y. Jeong, J. Nilsson, and D. J. Richardson, "Ultrashort-pulse $Yb^{3+}$-fiber-based laser and amplifier system producing $>$ 25-W average power," Opt. Lett. **29**, 2073-2075, 2004.

[116] C. Finot and G. Millot, "Synthesis of optical pulses by use of similaritons," Opt. Express **12**, 5104-5109, 2004.

[117] F. Parmigiani, C. Finot, K. Mukasa, M. Ibsen, M. A. Roelens, P. Petropoulos, and D. J. Richardson, "Ultra-flat SPM-broadened spectra in a highly nonlinear fiber using parabolic pulses formed in a fiber Bragg grating," Opt. Express **14**, 7617-7622, 2006.

[118] Y. Ozeki, Y. Takushima, K. Aiso, K. Taira, and K. Kikuchi, "Generation of 10 GHz similariton pulse trains from 1.2 km-long erbium-doped fibre amplifier for application to multi-wavelength pulse sources," Electron. Lett. **40**, 1103-1104, 2004.

[119] C. Finot, S. Pitois, and G. Millot, "Regenerative 40 Gbit/s wavelength converter based on similariton generation," Opt. Lett. **30**, 1776-1778, 2005.

## Appendix A: Numerical Codes for Solving Maxwell-Bloch Equations

```
%main
clc;
clear;
T=400;                                  % time window (period)
nt=2^12;                                % number of points
dt=T/nt;                                % timestep (dt)
t=((0:nt)')*dt;                         % time vector
z=10;                                   % total distance
nz=300;                                 % total number of steps
nplot=10;                       % number of plots to make
n1=round(nz/nplot);           % number of steps per plot
nz=n1*nplot;              % total number of steps (revised)
dz=z/nz;                                % step-size
zv=(z/nplot)*(0:nplot);                 % space vector
z=zv';
omega=zeros(length(t),length(zv));
sigma=zeros(length(t),length(zv));
output1=zeros(length(t),length(zv));    %#ok<NASGU>
PW=zeros(length(t),length(zv));
Energy=zeros(1,length(zv));
RMS=zeros(1,length(zv));
PW1=zeros(length(t),length(zv));
RMS1=zeros(1,length(zv));
Gain=zeros(1,length(zv));
out=zeros(length(t),length(zv));        %#ok<NASGU>
omega(:,1)=InitCond(1,t);               %define initial pulse profile

%find Bloch vector at z=0
```

```
sigma(1,:)=0;                          %initial Bloch vector

%for nonlinear case, w(1,:)=-1 should be added.
y1=bloch(omega(:,1),sigma(:,1),nt,dt);
%y1=bloch(omega(:,1),sigma(:,1),w(:,1),nt,dt); for %nonlinear case.
sigma(:,1)=y1;
%sigma(:,1)=y1(:,1); %for nonlinear case.
%w(:,1)=y1(:,2); %for nonlinear case.

%find Bloch vector and optical field for different z
for i=1:nplot
  y1=maxwell(omega(:,i),sigma(:,i),dz,n1,dt,nt);
%y1=maxwell(omega(:,i),sigma(:,i),w(:,i),dz,n1,dt,nt);
%for nonlinear case.
      omega(:,i+1)=y1(:,1);
      sigma(:,i+1)=y1(:,2);
%      w(:,i+1)=y1(:,3); %for nonlinear case.
end
output1=abs(omega).^2;

%normalizing intensity
output=0;
for ii=1:(length(t)-1)
    output=output+((output1(ii+1,1)+output1(ii,1)).*dt)/2;
end
out=output1/output;
for l=1:(length(t)-1)
    Energy=Energy+((output1(l+1,:)+output1(l,:)).*dt)/2;
end
```

```
%display results
graph(out,zv,t);

%find RMS width
for k=1:(length(t))
    PW1(k,:)=t(k)*output1(k,:);
end
for iii=1:(length(t)-1)
    RMS1=RMS1+((PW1(iii+1,:)+PW1(iii,:)).*dt)/2;
end
Width1=RMS1./Energy;
Width1=Width1-0.25;          %fix the error function
E=t.^2;
for k=1:(length(t))
    PW(k,:)=E(k)*output1(k,:);
end
for iii=1:(length(t)-1)
    RMS=RMS+((PW(iii+1,:)+PW(iii,:)).*dt)/2;
end
Width2=RMS./Energy;
Width=sqrt(Width2-(Width1.^2));
% plot(z,Width);

%find gain factor
for iii=1:(length(t)-1)
    Gain=Gain+((output1(iii+1,:)+output1(iii,:)).*dt)/2;
end
asymptotic=z/2;
f=0:0.01:100;
asymwidth=0.5*sqrt(3*z);
% plot(z,asymwidth);
%************************************************************************
```

```
%This function defines the initial pulse profile.
function y=InitCond(type,t)

if type==1                                      %Exponential Iniatil Condition
        y=theta(t).*exp(-2*t);
elseif type==2                                  %Guassian Intial Conditon
        y=theta(t).*exp(-4*(t.^2));
elseif type==3
        y=theta(t).*(((t.^2)+1).\1);            %Lorentzian Intial Conditon
else
        y=theta(t).*sech(2*t);                  %Hyperbolic Intial Conditon
end
%*************************************************************************
%This function estimates step function
function theta = theta(x)

N=10;%100
theta=(1+tanh(N*x))/2;
%*************************************************************************
%This function finds Bloch vector for each step of z
function sigma=bloch(omega,sigma,nt,dt)

     for i=1:nt-1
          k1=derivatives(omega(i),sigma(i));
          sigma1=sigma(i)+dt*k1/2;
          k2=derivatives(omega(i),sigma1);
          sigma1=sigma(i)+dt*k2/2;
          k3=derivatives(omega(i),sigma1);
          sigma1=sigma(i)+dt*k3;
          k4=derivatives(omega(i),sigma1);
          nextstep=(dt*(k1+2*k2+2*k3+k4))/6;
          sigma(i+1)=sigma(i)+nextstep;
```

```
    end
%************************************************************************
%This function defines the Bloch equations. Based on the corresponding regime
%and considering inhomogeneous broadening, and linear and nonlinear cases,
%this function has different forms.

function dy=derivatives(omega,sigma,w,DELTA)
%In the case of inhomogeneous broadening,
% Delta should be defined in bloch function.
%Otherwise, it is zero.

%General form of Bloch equation.
dy(1)=-(1+1i*DELTA)*sigma-1i*omega*w;
dy(2)=-gamapaperp*(w+1)+real(omega)*imag(sigma)-imag(omega)*(real(sigma));
%w(eq)=-1;

%1) This function when neglecting damping and considering inhomogeneous
%broadening in nonlinear case (for example in quadratic solitons) has the form:

%function dy=derivatives(omega,sigma,w,DELTA)

%dy(1)=-1i*DELTA*sigma-1i*omega*w;
%dy(2)=real(omega)*imag(sigma)-imag(omega)*(real(sigma));

%2) This function when considering damping and no inhomogeneous
%broadening in nonlinear case (for example in self-similar kinks) has the form:

%function dy=derivatives(omega,v,w)

%gamapaperp=0.0001;
%dy(1)=-v+omega*w;
%dy(2)=-omega*v-gamapaperp*(w+1);
```

```
%3) This function when considering damping and no inhomogeneous
%broadening in linear case (for example in self-similar pulses in
%linear amplifiers) has the form:

%function dy=derivatives(omega,sigma)

%dy=-sigma-1i*omega; %dy=-sigma+1i*omega for linear absorbers
%**************************************************************************
%This function defines the Maxwell equation and finds the electric
%field for each step of z
function y=maxwell(omega,sigma,dz,nz,dt,nt)

r1=dz*1i/2;

for iz=1:nz
          y1=omega+r1*sigma;
          omega=y1;
          y1=bloch(omega,sigma,nt,dt);
          sigma=y1;
end

y(:,1)=omega;
y(:,2)=sigma;
%**************************************************************************
%This function displays the results
function graph(output,zv,t)

hold on
h = mesh(zv,t,output,...
         'MeshStyle', 'col', 'EdgeColor', 'black');
set(gca,'YDir','reverse');
```

```
hidden off;
xlim([0 max(zv)]);
ylim([0 max(t)]);
xlabel ('Z');
ylabel ('X');
zlabel ('|u(z,x)|^2');
```

## Appendix B: Numerical Codes for Split-Step Fourier Method

```
%main
clc
clear

%define initial parameters
xg0=1;
xc0=100;

X = 200;                                    % X window (period)
nx = 2*(2^12);                                  % number of points
dx = X/nx;                                  % xstep (dt)
x = ((1:nx)'-(nx+1)/2)*dx;                  % x vector
x1=[(0:nx/2-1),(-nx/2:-1)]';
f=[(0:nx/2-1),(-nx/2:-1)]'/(dx*nx);          %frequency vector
x2 = ((1:nx)'-(nx+1)/2)*dx;                  % x vector

z = 50;%100;                                    % total distance
nz = 25000;%50000;                                 % total number of steps
nplot = 5;%10; % number of plots to make
n1 = round(nz/nplot); % number of steps per plot
nz = n1*nplot; % total number of steps (revised)
dz = z/nz;                                  % step-size

%define iniatial condition
u0 = Initial(x,xg0,xc0,0.01);

zv = (z/nplot)*(0:nplot);
u = zeros(length(x),length(zv));
```

```
u(:,1) = u0;


%for each z find output
for ii = 1:nplot,
    ii
    u(:,ii+1) = Splitstep(u(:,ii),dx,dz,n1,200);
end


%sketch the output
output=abs(u).^2;
mesh(zv,x,output, ...
     'MeshStyle', 'col', 'EdgeColor', 'black');
set(gca,'YDir','reverse');
hidden off;
xlim([0 max(zv)]);
ylim([-max(x) max(x)]);
xlabel ('Z');
ylabel ('X');
zlabel ('|u(Z,X)|^2');
%************************************************************************
%This function defines the initial beam profile.
function u = Initial(x,xg0,xc0,C)

if (nargin<4)
  C = 0;
end
```

```
if (nargin<3)
  xc0 = 0;
end
if (nargin<2)
  xg0 = 0;
end

Amp_Signal=sqrt((sqrt(3/8))*(sech(x-xg0)));
Phase_Signal=-(C)*((x-xc0).^2)/(2);
u=(Amp_Signal).*exp(1i*(Phase_Signal));
%************************************************************************
%This function finds the solution of final equation by split-step method.
function u1 = Splitstep(u0,dx,dz,nz,maxiter,tol)

if (nargin<6)
    tol = 1e-5;
end
if (nargin<5)
    maxiter = 4;
end

nx = length(u0);

w = 2*pi*[(0:nx/2-1),(-nx/2:-1)]'/(dx*nx);
halfstep = 0;
halfstep = halfstep - 1i*(w).^2/factorial(2);
halfstep = exp(halfstep*dz/2);

u1 = u0;
% ufft = fft(u0);
for iz = 1:nz,
    ufft = fft(u0);
```

```
    uhalf = ifft(halfstep.*ufft);
    for ii = 1:maxiter,
        uv = uhalf .* exp(+1i*(abs(u1).^4 + abs(u0).^4)*dz/2);
        uv = fft(uv);
        ufft = halfstep.*uv;
        uv = ifft(ufft);
        if (norm(uv-u1,2)/norm(u1,2) < tol)
            u1 = uv;
            break;
        else
            u1=uv;
        end
    end
    if (ii == maxiter)
        warning(sprintf('Failed to converge to %f in %d iterations',...
            tol,maxiter));
    end
    u0 = u1;
end
%*************************************************************************
```

## Appendix C: Analytical Analysis for Self-Similar Pulses in Coherent Linear Amplifiers

Self-similar pulse width

RMS width: $\Delta T = \sqrt{< T^2 > - < T >^2}$

$$< T^2 >= \frac{\int_0^\infty dT T^2 |\Omega(Z,T)|^2}{\int_0^\infty dT |\Omega(Z,T)|^2}$$

$Z >> 1$: $\Omega(T,Z) \simeq \frac{e^{\sqrt{2TZ}}}{\sqrt{2\pi\sqrt{2TZ}}} e^{-T}$

$$|\Omega|^2 \simeq \frac{e^{2\sqrt{2TZ}}}{2\pi\sqrt{2TZ}} e^{-2T}$$

$$< T^2 >= \frac{\int_0^\infty dT T^2 \frac{e^{2\sqrt{2TZ}}}{\sqrt{T}} e^{-2T}}{\int_0^\infty dT \frac{e^{2\sqrt{2TZ}}}{\sqrt{T}} e^{-2T}}$$

$$< T^2 >= \frac{\frac{d^2}{d\alpha^2} \int_0^\infty \frac{dT}{\sqrt{T}} e^{2\sqrt{2TZ}} e^{-\alpha T}|_{\alpha=2}}{\int_0^\infty \frac{dT}{\sqrt{T}} e^{2\sqrt{2TZ}} e^{-2T}}$$

$$J(\alpha) = \int_0^\infty \frac{dT}{\sqrt{T}} e^{2\sqrt{2TZ}} e^{-\alpha T}$$

$$\Rightarrow < T^2 >= \frac{1}{J(2)} \frac{d^2}{d\alpha^2} J(\alpha)|_{\alpha=2}$$

$$< T >= -\frac{d}{d\alpha} \ln J(\alpha)|_{\alpha=2}$$

$$J(\alpha) = \int_0^\infty \frac{dT}{\sqrt{T}} e^{2\sqrt{2TZ}} e^{-\alpha T} |X = \sqrt{T}|$$

$$J(\alpha) = 2\int_0^\infty dX e^{2\sqrt{2Z}X} e^{-\alpha X^2}$$

$$J(\alpha) = 2\int_0^\infty dX exp[-\alpha(X^2 - 2\frac{\sqrt{2Z}}{\alpha}X)]$$

$$s = \sqrt{\alpha}(X - \frac{\sqrt{2Z}}{\alpha})$$

$$J(\alpha)=\frac{2}{\sqrt{\alpha}}e^{2Z/\alpha}\int_{-\sqrt{2Z}/\sqrt{\alpha}}^{\infty}dse^{-s^2}\simeq\frac{2}{\sqrt{\alpha}}e^{2Z/\alpha}\underbrace{\int_{-\infty}^{\infty}dse^{-s^2}}_{\sqrt{\pi}}$$

$$J(\alpha)=2\sqrt{\frac{\pi}{\alpha}}e^{2Z/\alpha}$$

$$1)<T>=-\frac{d}{d\alpha}\ln J(\alpha)|_{\alpha=2}$$

$$\ln J(\alpha)=-\frac{1}{2}\ln\alpha+\frac{2Z}{\alpha}+const$$

$$<T>=\frac{1}{2\alpha}+\frac{2Z}{\alpha^2}|_{\alpha=2}\simeq Z/2,\ Z>>1$$

$$2)<T^2>=\frac{1}{J(2)}\frac{d^2}{d\alpha^2}J(\alpha)$$

$$Z>>1:\ \frac{d^2J}{d\alpha^2}\simeq\frac{2\sqrt{\pi}}{\sqrt{\alpha}}\frac{d^2}{d\alpha^2}e^{2Z/\alpha}+4\frac{d}{d\alpha}(\sqrt{\frac{\pi}{\alpha}})\frac{d}{d\alpha}(e^{2Z/\alpha})$$

$$J''\simeq 2\sqrt{\frac{\pi}{\alpha}}\frac{d}{d\alpha}(-\frac{2Z}{\alpha^2}e^{2Z/\alpha})+2\sqrt{\frac{\pi}{\alpha}}\frac{1}{\alpha}\frac{2Z}{\alpha^2}e^{2Z/\alpha}$$

$$J''\simeq[2\sqrt{\frac{\pi}{\alpha}}(\frac{4Z}{\alpha^3}+\frac{2Z}{\alpha^2}\frac{2Z}{\alpha^2})+2\sqrt{\frac{\pi}{\alpha}}\frac{2Z}{\alpha^3}]e^{2Z/\alpha}$$

$$J''(\alpha)=2\sqrt{\frac{\pi}{\alpha}}e^{2Z/\alpha}[\frac{4Z}{\alpha^3}+\frac{4Z^2}{\alpha^4}+\frac{2Z}{\alpha^3}]$$

$$\Rightarrow J''(\alpha)=2\sqrt{\frac{\pi}{\alpha}}e^{2Z/\alpha}[\frac{6Z}{\alpha^3}+\frac{4Z^2}{\alpha^4}]$$

$$\alpha=2:\ J''(2)=2\sqrt{\frac{\pi}{2}}e^ZZ(\frac{6}{8}+\frac{4Z}{16})=2\sqrt{\frac{\pi}{2}}Ze^Z\times\frac{1}{4}(3+Z)$$

$$\Rightarrow<T^2>=\frac{1}{J(2)}J''(2)=\frac{Z}{4}(3+Z)=\frac{3Z}{4}+\frac{Z^2}{4}$$

$$\Delta T^2=<T^2>-<T>^2=\frac{3Z}{4}+\frac{Z^2}{4}-\frac{Z^2}{4}=\frac{3Z}{4}$$

$$\Rightarrow\Delta T=\sqrt{3Z}/2$$

## Appendix D: Analytical Analysis for Self-Similarity and Optical Kinks in Resonant Nonlinear Media

Coherent limit, $\frac{1}{T_P} \geq \gamma_\perp \gg \gamma_\parallel$.

a) Perfect resonance, $\gamma_\perp \gg \delta$: neglect inhomogeneous broadening. The Maxwell-Bloch equations (MBE) have the general form

$$\begin{cases} \partial_\zeta \Omega = \frac{kN|d_{ge}|^2}{\varepsilon_0 \hbar} v \\ \partial_\tau v = -\gamma_\perp v + \Omega w \\ \partial_\tau w = -\Omega v. \end{cases}$$

The Rabi frequency is unchirped, $\Omega^* = \Omega$.

Define: $\frac{\alpha}{2} = \frac{kN|d_{ge}|^2}{\gamma_\perp \varepsilon_0 \hbar}$, the MBE has the form

$$\begin{cases} \partial_\zeta \Omega = \frac{\gamma_\perp \alpha}{2} v \\ \partial_\tau v = -\gamma_\perp v + \Omega w \\ \partial_\tau w = -\Omega v. \end{cases} \tag{D-1}$$

Looking for self-similar solution, and define the similarity variable as $\eta = \alpha \zeta e^{-\gamma_\perp \tau}$, the self-similar solutions for Rabi frequency is revealed as

$$\Omega = \gamma_\perp \overline{\Omega}(\alpha \zeta e^{-\gamma_\perp \tau}), \tag{D-2}$$

and for the atomic variables as

$$v = e^{-\gamma_\perp \tau} \overline{v}(\alpha \zeta e^{-\gamma_\perp \tau}), \tag{D-3}$$

$$w = e^{-\gamma_\perp \tau} \overline{w}(\alpha \zeta e^{-\gamma_\perp \tau}). \tag{D-4}$$

Finding derivatives with respect to $\eta$

$$\partial_\zeta = \alpha e^{-\gamma_\perp \tau} d_\eta, \tag{D-5}$$

$$\partial_\tau = -\gamma_\perp \eta d_\eta. \tag{D-6}$$

Taking derivatives of (D-2) with respect to $\zeta$, and (D-3) and (D-4) with respect to $\tau$ by using (D-5) and (D-6) to obtain derivatives with respect to $\eta$

$$\partial_\zeta \Omega = \alpha\gamma_\perp e^{-\gamma_\perp \tau}\overline{\Omega}', \tag{D-7}$$

$$\partial_\tau v = -\gamma_\perp e^{-\gamma_\perp \tau}\overline{v} - \gamma_\perp e^{-\gamma_\perp \tau}\eta\overline{v}', \tag{D-8}$$

$$\partial_\tau w = -\gamma_\perp e^{-\gamma_\perp \tau}\overline{w} - \gamma_\perp e^{-\gamma_\perp \tau}\eta\overline{w}'. \tag{D-9}$$

Substituting (D-7)-(D-9) into (D-1)

$$\Longrightarrow \begin{cases} \alpha\gamma_\perp e^{-\gamma_\perp \tau}\overline{\Omega}' = \frac{\gamma_\perp \alpha}{2} e^{-\gamma_\perp \tau}\overline{v} \\ -\gamma_\perp e^{-\gamma_\perp \tau}(\overline{v} + \eta\overline{v}') = -\gamma_\perp e^{-\gamma_\perp \tau}\overline{v} + \gamma_\perp e^{-\gamma_\perp \tau}\overline{\Omega}\overline{w} \\ -\gamma_\perp e^{-\gamma_\perp \tau}(\overline{w} + \eta\overline{w}') = -\gamma_\perp e^{-\gamma_\perp \tau}\overline{\Omega}\overline{v}. \end{cases}$$

Find the set of ODE

$$\Longrightarrow \begin{cases} \overline{\Omega}' = \frac{1}{2}\overline{v} \\ \eta\overline{v}' = -\overline{\Omega}\overline{w} \\ (\eta\overline{w})' = \overline{\Omega}\overline{v}. \end{cases}$$

Combining these equations

$$\Longrightarrow \begin{cases} \overline{v} = 2\overline{\Omega}' \\ \eta\overline{v}' = -\overline{\Omega}\overline{w} \\ (\eta\overline{w})' = 2\overline{\Omega}\overline{\Omega}' \Longrightarrow \eta\overline{w} = \overline{\Omega}^2 + const. \end{cases}$$

Integrating with the aid of the asymptotic condition: $\eta \to 0$, $\overline{\Omega} \to \overline{\Omega}_\infty$, the one-atom inversion can be expressed as

$$\Longrightarrow \overline{w} = \frac{1}{\eta}(\overline{\Omega}^2 - \overline{\Omega}_\infty^2).$$

$$\overline{v} = 2\overline{\Omega}',$$

$$2\eta\overline{\Omega}'' = -\frac{\overline{\Omega}}{\eta}(\overline{\Omega}^2 - \overline{\Omega}_\infty^2).$$

ODE for a kink profile $\Longrightarrow \eta^2\overline{\Omega}'' = -\frac{\overline{\Omega}}{2}(\overline{\Omega}^2 - \overline{\Omega}_\infty^2)$.

Asymptotic analysis reveals that

a) $\eta \to 0$, $\Longleftrightarrow \tau \to +\infty$ (leading edge of the pulse): $\overline{\Omega} = \overline{\Omega}_\infty + \delta\overline{\Omega}$, $\delta\overline{\Omega} \ll \overline{\Omega}_\infty$ as $\eta \to 0$

$$\eta^2\delta\overline{\Omega}'' = -\frac{\overline{\Omega}_\infty}{2}\underbrace{(\overline{\Omega} - \overline{\Omega}_\infty)}_{\delta\overline{\Omega}}\underbrace{(\overline{\Omega}_\infty - \overline{\Omega}_\infty)}_{2\overline{\Omega}_\infty},$$

$$\eta^2\delta\overline{\Omega}'' = -\overline{\Omega}_\infty^2\delta\overline{\Omega},$$

look for $\delta\overline{\Omega} \sim \eta^s$, $s > 0$

$$\Rightarrow s(s-1) = -\overline{\Omega}_\infty^2,$$

$$s^2 - s + \overline{\Omega}_\infty^2 = 0,$$

$$\Rightarrow s = \frac{1 \pm \sqrt{1 - 4\overline{\Omega}_\infty^2}}{2},$$

choose "+" because as $\overline{\Omega}_\infty \to 0$, $s \to 1$, $\overline{\Omega} \to 0$ works

$$s = \frac{1 + \sqrt{1 - 4\overline{\Omega}_\infty^2}}{2},$$

Note: $\overline{\Omega}_\infty \leq 1/2 \Longleftrightarrow \Omega_\infty \leq \gamma_\perp/2$,

the system must be in an "overdamped" regime (no Rabi flopping): $\eta \to 0$: $\overline{\Omega} = \overline{\Omega}_\infty - |C|\eta^s$

$$s = \frac{1 + \sqrt{1 - 4\overline{\Omega}_\infty^2}}{2},$$

b) $\eta \to \infty$, $\overline{\Omega} \to 0$, consider $\eta \to \infty \Longleftrightarrow \tau \Longrightarrow -\infty$ (leading edge)

$$\overline{\Omega} \sim \eta^{-q}, q \geq 0$$

$\eta^2\overline{\Omega}'' = \frac{\overline{\Omega}\overline{\Omega}_\infty^2}{2}$ as $\eta \to \infty$

$$-q(-q-1) = \frac{\overline{\Omega}_\infty}{2},$$

$$q^2 + q - \overline{\Omega}_\infty/2 = 0,$$

$$q = \frac{-1+\sqrt{1+2\overline{\Omega}_\infty^2}}{2}, q \geq 0,$$

$\eta \to \infty$: $\overline{\Omega} \sim \eta^{-q}$,

$$\Rightarrow q = \frac{-1+\sqrt{1+2\overline{\Omega}_\infty^2}}{2}.$$

## Appendix E: Analytical Analysis for Spatial Optical Similaritons in Conservative Nonintegrable Systems

Ordinary differential equation for the similariton envelope has the form

$$\frac{1}{2}R''_{\eta\eta} + (\sigma R^4 \pm \frac{\beta^2}{8})R = 0. \tag{E-1}$$

We look for a self-similar solution in the form

$$R = \sqrt{\beta}\overline{R}(\beta\eta), \tag{E-2}$$

with the similarity variable

$$X = \beta\eta. \tag{E-3}$$

Substituting (E-2) and (E-3) into (E-1), we obtain

$$\frac{\beta^2}{2}\overline{R}''_{XX} + \beta^2(s\overline{R}^4 \pm \frac{1}{8})\overline{R} = 0,$$

or

$$\overline{R}''_{XX} + 2(s\overline{R}^4 \pm \frac{1}{8})\overline{R} = 0. \tag{E-4}$$

Integrating once (E-4)

$$\frac{1}{2}{R'_X}^2 + \frac{s\overline{R}^6}{3} \pm \frac{\overline{R}^2}{8} = \frac{1}{2}C,$$

$$R'_X = \sqrt{C - \frac{2\overline{R}^6}{3}s \pm \frac{\overline{R}^2}{4}}. \tag{E-5}$$

Integrating (E-5), we obtain

$$X = \int \frac{d\overline{R}}{\sqrt{C - \frac{2s}{3}\overline{R}^6 \pm \frac{1}{4}\overline{R}^2}},$$

$$X = -\int \frac{d(1/\overline{R}^2)}{2\sqrt{\frac{C}{\overline{R}^6} \pm \frac{1}{4\overline{R}^4} - \frac{2s}{3}}}.$$

Introducing the variable change

$$P = 1/\overline{R}^2,$$

we arrive at

$$X = -\int \frac{dP}{2\sqrt{CP^3 \pm \frac{P^2}{4} - \frac{2s}{3}}}.$$

Bright case, $s = +1$, choose "+".
$\overline{R} \to 0$, $\overline{R}'_X \to 0$, as $X \to \pm\infty \Rightarrow C = 0$.

$$X = -\int \frac{dP}{\sqrt{P^2 - \frac{8}{3}}},$$

$$P = \sqrt{\frac{8}{3}}\cosh s,$$

$$X = -\int \frac{\sqrt{\frac{8}{3}}\sinh s ds}{\sqrt{\frac{8}{3}}\sinh s} = -s,$$

$$P = \sqrt{\frac{8}{3}}\cosh X,$$

$$\overline{R} = \sqrt{\sqrt{\frac{3}{8}} sech X}.$$

# Appendix F: Copyright Permissions

## F.1 Permission From OSA

From: Soodeh [mailto:sd408131@dal.ca]
Sent: Wednesday, August 15, 2012 4:03 PM
To: pubscopyright
Subject: Permission

Dear Optical Society of America,

I am the first author of the following journals, while I was working toward my PhD degree. Now, I am preparing my PhD thesis for submission to the Faculty of Graduate Studies at Dalhousie University, Halifax, Nova Scotia, Canada. I am seeking your permission to include a manuscript version of the following paper(s) as a chapter in the thesis:

1. Soodeh Haghgoo and Sergey A. Ponomarenko, "Self-Induced Transparency Quadratic Solitons," Optics Express, Vol. 20, Issue 13, pp. 13988-13995 (2012).
2. Soodeh Haghgoo and Sergey A. Ponomarenko, "Shape-Invariant Pulses in Resonant Linear Absorbers," Optics Letters , Vol. 37, Issue 8, pp. 1328-1330 (2012).
3. Soodeh Haghgoo and Sergey A. Ponomarenko,, "Self-Similar Pulses in Coherent Linear Amplifiers," Optics Express, Vol. 19, Issue 10, pp. 9750-9758 (2011).

Full publication details and a copy of this permission letter will be included in the thesis.

Best Regards,

____

Soodeh Haghgoo

From: pubscopyright [copyright@osa.org]
To: pubscopyright
Cc:
Subject: RE: Permission

Dear Soodeh,

Thank you for contacting The Optical Society.

Because you are the author of the source papers which you wish to reproduce, OSA considers your requested use of its copyrighted materials to be permissible within the author rights granted in the Copyright Transfer Agreement submitted by the requester on acceptance for publication of his/her manuscript. It is requested that a complete citation of the original material be included in any publication. This permission assumes that the material was not reproduced from another source when published in the original publication.

Please let me know if you have any questions.

Best,

Hannah

Hannah Bembia
August 15, 2012
Authorized Agent, The Optical Society

### F.2 Permission From APS

From: ”Soodeh” [mailto:sd408131@dal.ca]
To: assocpub@aps.org
Sent: Wednesday, August 15, 2012 4:23:53 PM
Subject: Permission

Dear American Physical Society,

I am co- author of the following journals, while I was working toward my PhD degree. Now, I am preparing my PhD thesis for submission to the Faculty of Graduate Studies at Dalhousie University, Halifax, Nova Scotia, Canada. I would appreciate permission to include a manuscript version of the following paper(s) as a chapter in the thesis:

1. Sergey A. Ponomarenko and Soodeh Haghgoo, "Self-Similarity and Optical Kinks in Resonant Nonlinear Media," Phys. Rev. A, Rapid Communication, 82, 051801(R), (2010).
2. Sergey A. Ponomarenko and Soodeh Haghgoo, "Spatial Similaritons in Conservative Nonintegrable Systems," Phys. Rev. A, Rapid Communication, 81, 051801(R), (2010).

Full publication details and a copy of this permission letter will be included in the thesis. Thank you very much for your attention to this request.

Best Regards,

____

Soodeh Haghgoo

Dear Soodeh Haghgoo,

Thank you for your email. As the author, you have the right to use the article or a portion of the article in a thesis or dissertation without requesting permission from APS, provided the bibliographic citation and the APS copyright credit line are given on the appropriate pages.

Best wishes,

Melissa Overton
Publications Marketing Coordinator
American Physical Society

http://librarians.aps.org/

### F.3 Permission From Optics Communications

From: Soodeh [mailto:sd408131@dal.ca]
Sent: Wednesday, August 15, 2012 4:36 PM
To: customercare@copyright.com
Cc: Permissions Helpdesk
Subject: Permission

Dear Optics Communications,

I am the first author of the following journal, while I was working toward my PhD degree. Now, I am preparing my PhD thesis for submission to the Faculty of Graduate Studies at Dalhousie University, Halifax, Nova Scotia, Canada. I would appreciate permission to include a manuscript version of the following paper as a chapter in the thesis:

S. Haghgoo and S. A. Ponomarenko, "Optical Shocks in Resonant Media: The Role of Inhomogeneous Broadening," Submitted, Optics Communications (2012).

Full publication details and a copy of this permission letter will be included in the thesis. Thank you very much for your attention to this request.

Best Regards,

——

Soodeh Haghgoo

From: Permissions Helpdesk [permissionshelpdesk@elsevier.com]
To: Soodeh
Cc: customercare@copyright.com
Subject: RE: Permission

Dear Soodeh:

No written permission is required, as you retain the right to include the article in full or in part in a thesis or dissertation (provided that this is not to be published commercially) as an Elsevier journal author, as outlined at $http://support.elsevier.com/app/answers/detail/a_id/565$.

Please let us know whether you have any questions. Best of luck.

Regards,
Hop

Hop Wechsler
Permissions Helpdesk Manager
Global Rights Department
Elsevier
1600 John F. Kennedy Boulevard
Suite 1800
Philadelphia, PA 19103-2899
Tel: +1-215-239-3520
Mobile: +1-215-900-5674
Fax: +1-215-239-3805
E-mail: h.wechsler@elsevier.com
Questions about obtaining permission: whom to contact? What rights to request?
When is permission required? Contact the Permissions Helpdesk at:
+1-800-523-4069 x 3808 permissionshelpdesk@elsevier.com